Equivalent Circuit Programming

Submitted in partial fulfillment of the requirements for
the degree of
Doctor of Philosophy
in
Department of Electrical and Computer Engineering

Marko Jereminov
B.S., Electrical Engineering and Technology, South Carolina State University
M.S., Electrical and Computer Engineering, Carnegie Mellon University

Carnegie Mellon University
Pittsburgh, PA

August 2019

Acknowledgements

To my advisor, Larry Pileggi without whom this research project and my PhD career would not exist.

To my committee members, Jay Apt, Zico Kolter and Osman Yagan, for their guidance towards achieving the goals stipulated within this thesis.

To the funding agencies, National Science Foundation and Defense Advanced Research Projects Agency for their funding support toward this project.

To my colleges Amrit, David, Martin, Aayushya and Hui for being the most helpful collaborators and for enabling a productive working environment.

To my best friends, Ana, Matija, Dača, Aca and others for being the most amazing friends and a constant support.

To Kuzman, my friend, mentor and professor, for his guidance during the undergraduate studies in South Carolina.

To Vlada, Arnaud, Katarina, Betty and Jelena for being by my side throughout this whole journey in US and for uplifting my spirits when I needed it the most.

Finally, to my Grandma (Baki), Grandpa (Deki), Neci, Viti and to my Mom, to whom I owe everything I have achieved in my life so far. This thesis is for them.

Thesis Statement: Develop a generic framework and algorithms for continuous optimization of network steady-state operating point and apply it to the optimization of electrical power systems

Abstract

Optimal decision-making processes represent the key component of everyday life and can be found everywhere, from the atomic level in nature, to the emerging technologies that are becoming increasingly dependent on various Machine Learning algorithms and Artificial Intelligence. Consequently, finding the mathematical modeling formulations and algorithms for solving these decision-making problems now represents one of the significant, on-going research topics in science. Most importantly, after the publication of the so-called "No Free Lunch" (NFL) theorems that proves existence of no algorithm that can efficiently and robustly solve all classes of optimization problems, it became clear that the algorithms and mathematical modeling of the optimization problems have to take into the consideration all of the available domain specific knowledge in order to achieve the best efficiency, robustness and scalability.

The primary focus of this thesis is to develop a novel generic framework for continuous network optimization problems. Our approach, Equivalent Circuit Programming (ECP), incorporates all of the available domain knowledge and translates it into the efficient and robust simulation algorithms. Inspired by the NFL theory and circuit simulation algorithms developed around the state-of-art circuit simulator SPICE, we first address the key issues of applying the generic local optimization algorithms to network optimization problems. To that effect, we generalize the adjoint circuit theory to include the nonlinear network models and show that the complete set of optimality conditions of a network optimization problem can be represented by a combination of the network and its uniquely defined adjoint circuit. With the circuit representation of the considered class of optimization problems established, we next embed the domain-specific knowledge within the existing optimization heuristics to develop a completely new set of algorithms to ensure a more efficient, robust and scalable solution process.

To prove the concept and demonstrate the significant improvements in simulation efficiency, scalability and robustness, the proposed Equivalent Circuit Programming framework is applied to power system optimization problems. This is achieved by first introducing a generalized

methodology for modeling the power grid steady-state response in terms of equivalent circuit equations that further allows us to incorporate them within the ECP framework. The examined power system optimization problems include the newly introduced Power Flow Feasibility analyses, AC Optimal Power Flow (AC-OPF) and Security Constrained AC Optimal Power Flow (SC-OPF) problems. Optimization results are compared with the existing state-of-art local optimization algorithms for available network examples that include various realistic-size power system test cases of up to the 80k buses (nodes).

Table of Content

Contributions

1. *This thesis develops a novel Equivalent Circuit Programming (ECP) framework for continuous optimization of network steady-state operating point.*
2. *To that end, an important contribution represents the generalization of the adjoint network theory for nonlinear network elements and its extension to modeling the network optimization problems.*
3. *Furthermore, the thesis develops a set of novel heuristic algorithms for solving the ECP optimization problems based on an extension of both circuit simulation step-limiting algorithms and exact line search optimization approaches to ensure the robust and efficient convergence properties.*
4. *Finally, it introduces a generalized methodology for modeling of electrical power system simulation and optimization problems that facilitates their incorporation within the ECP framework.*

List of Figures

List of Tables

Chapter 1 Introduction and Motivation

An optimization is a systematic and quantitative process of searching for the best choice that satisfies the desired criterion among numerous possibilities, and as such, it represents an important component embedded almost everywhere in the world around us. Various processes governed by physical laws that continuously occur in nature can be explain in terms of optimization processes. For instance, as a molten metal cools, its particles tend to arrange in *low* energy states [1]. Similarly, the current flowing in an electric network (circuit) follows the path of the least resistance that *minimizes* the losses in the system [2]. Therefore, all of these processes can be classified in clusters corresponding to a particular law of physics, which can be now also seen as the "solution methodology" used to obtain an "optimal solution" for a respective cluster. From the perspective of science and engineering, all of the emerging technologies and experimental procedures are becoming increasingly dependent on various Machine Learning (ML) algorithms [3], [4] and Artificial Intelligence (AI) [5] that, again, represent nothing more but different frameworks that solve the optimization problems in their background. Most importantly, all of these processes can be defined in terms of mathematical models and further incorporated within the field of mathematical optimization, which consequently became one of the most important fields of study in engineering and science in general [3], and remains an on-going research topic.

Finding the algorithm that can efficiently and robustly solve a general mathematical optimization has been one of the most prominent problems since the early days of research in this area, particularly as the size of a problem increases. A closed form solution of a mathematical optimization does not exist in general [3], and hence an optimal solution has to be obtained through the use of some of the numerical methods [3],[6]-[7]. It is important to emphasize that most of the proposed and used numerical algorithms consider mimicking and embedding the knowledge of

natural optimization processes. Notably, all of the gradient based methods [3] use the idea that the fastest way to go down or up the hill, i.e. reach an optimal solution, is to take the steepest descent. Furthermore, some of the more recently introduced metaheuristics consider the more exact mimicking of the natural processes, such as the Simulated Annealing algorithm [1],[6] that is found in the heating and controlled cooling in metallurgy, while the Evolutionary algorithms (EA) [1],[8] use the idea of biological evolution and survival of the fittest as a base for finding the global optimal solution of a mathematical optimization problem. Interestingly, as it is the case in natural optimization processes where the "solution methodology" depends on a law of physics that governs the process, the fact that there doesn't exist an algorithm that can efficiently work for all of the mathematical optimization problems is proven by so-called "No Free Lunch" (NFL) theorems in [9]. Moreover, by examining the connection between the effective algorithms and problems they are solving, the authors from [9] demonstrated that if no domain-specific knowledge of a problem is incorporated within the algorithm, all of the algorithms should perform the same in average once applied to the complete spectrum of problems. Therefore, it became clear that in order to obtain an efficient and robust methodology for solving a particular class of optimization problems, all of the known domain specific information has to be taken into the account, particularly if we deal with the optimization of physical systems.

Utilizing the physical characteristics and domain specific knowledge of network analysis and simulation problems has been already shown to facilitate powerful theorem proofs and solution methodologies, long before the introduction of NFL theory. Namely, one of the main theorems that defines the conservation of energy within a network, Tellegen's Theorem [10], has been proven by the Kirchhoff Current and Voltage Laws (KCL and KVL), while the electronic circuit simulator SPICE [11]-[16] and its many derivatives have been shown to enable the simulation of the highly nonlinear circuit problems with even billions of variables [17]. Furthermore, it was recently demonstrated [18]-[30] that the same physics-based simulation methodology can be extended and applied to power system simulation problems, thereby enabling robust and efficient convergence properties for any size realistic power grid simulation problem [31]-[33].

Inspired by the NFL theorems and algorithms developed around the state-of-art circuit simulator SPICE, this thesis introduces a novel Equivalent Circuit Programming (ECP) framework for modeling and solving the continuous network optimization problems. The perspective of SPICE algorithms is first used to address the key components that prevent the efficiency,

scalability and robustness of a solution process, when generic heuristics implemented within the state-of-art optimization toolboxes is applied without utilizing any of the additional domain specific information provided by the problem itself. This lack of efficiency and robustness is further addressed and compared to the introduced ECP framework in all of the applications examined in the second part of the thesis. It is then demonstrated that the Adjoint Network theory that was first proposed for electrical circuit noise analysis [34]-[36] in SPICE, can be generalized and extended to nonlinear network models and further represents a fundamental connection between the network (circuit) simulation and optimization problems. Importantly, this extension of the Adjoint Network theory allows for representing the complete set of optimality conditions in terms of coupled system and adjoint networks, and further provides the additional domain specific knowledge needed to develop a new set of SPICE-like algorithms that now include all of the domain specific information embedded within the existing optimization heuristics. More importantly, it allows for the circuit simulation-like approach [14]-[15] for obtaining an optimal solution of an Equivalent Circuit Program that is demonstrated to result in robust and efficient convergence properties for large scale network optimization problems.

The second part of this thesis considers the application of the proposed ECP framework to power system simulation and optimization problems. It is important to emphasize that the scalable and reliable power dispatch and operation of an electrical power system is of the utmost importance to a country's economy and the well-being of its citizens [37]. In the U.S., the electricity-based services are considered an essential service [38], a lack of which can result in significant societal chaos [38]. Presently, the decisions on the electrical power dispatch and system operation are determined by a solution to a set of different power system simulation and optimization problems. In this thesis, we demonstrate that the proposed ECP framework can incorporate the existing problems required for the operation and planning of an electrical power system, as well as allows for introduction of new problems, such as the Feasibility Power Flow analysis discussed in Chapter 6. First, it is demonstrated that the generalized nonlinear network formulation introduced in Chapter 3 of the thesis can be applied to modeling the power grid steady-state response in terms of current, voltage and admittance state variables. With the equivalent circuit representation of a power grid established, its simulation and optimization can be included and solved as an ECP. The examined power system optimization problems include the newly introduced Power Flow Feasibility analyses, as well as AC Optimal Power Flow (AC-OPF) and Security Constrained AC

Optimal Power Flow (SC-OPF) problems discussed in Chapter 7. To validate the framework and demonstrate the efficiency, robustness and scalability, the optimization results obtained from the ECP framework are compared with the existing state-of-art local optimization algorithms for considered network examples that include various power system of up to the 80k buses, as well as real-life cases of transmission networks that include 75k+ nodes test cases representing the U.S. Eastern Interconnection high-voltage grid. Lastly, the thesis concludes with guidelines for the future work and provides ideas regarding possible extensions to the other power system optimization problems as well as other fields of engineering such as circuit design problems.

Chapter 2 Background

Inspired by the algorithms developed around the state-of-art circuit simulator SPICE [13]-[15] and results of NFL theorems [9], the main idea behind the Equivalent Circuit Programming (ECP) framework is that of embedding domain-specific knowledge of the network within the optimization framework in order to build the new set of algorithms that can ensure more robust and scalable solution processes. This chapter provides a background on important preliminaries and state-of-art algorithms related to the field of continuous mathematical optimizations, and discusses the state-of-art simulation algorithms and homotopy methods utilized within circuit simulation community. The chapter concludes with the drawbacks of the existing optimization algorithms from the perspective of circuit simulation problems.

2.1. Constrained Continuous Optimization Problem

A generalized continuous optimization problem can be defined as finding an optimization variable $\boldsymbol{x}$ that minimizes a smooth objective function:

$$\min_{\boldsymbol{x}\in C} \mathcal{F}(\boldsymbol{x}) \tag{2.1}$$

among all possible $\boldsymbol{x} \in \mathbb{R}^n$ that belong to the objective function domain and are further included within an additional continuous set of conditions, i.e. $\boldsymbol{x} \in C$:

$$C = \left\{\boldsymbol{x} \middle|\, g_i(\boldsymbol{x}) = 0, i = 1, \dots, m, h_j(\boldsymbol{x}) \leq 0, j = 1, \dots, k\right\} \tag{2.2}$$

Next, we provide basic definitions and preliminaries that will be used through the thesis.

2.1.1. Important Mathematical Definitions and Preliminaries

Definition 1. *Convex set* [3]. A set C is convex if the line segment between any two points that belong to the set C, lies in the set, i.e. if for any $x_1, x_2 \in C$ and any θ with $0 \leq \theta \leq 1$ we have

$$\theta x_1 + (1-\theta)x_2 \in C \tag{2.3}$$

In other words, as it can be seen from Figure 2.1., every point in a convex set can be seen by every other point along an unobstructed path between them that lies completely in the set.

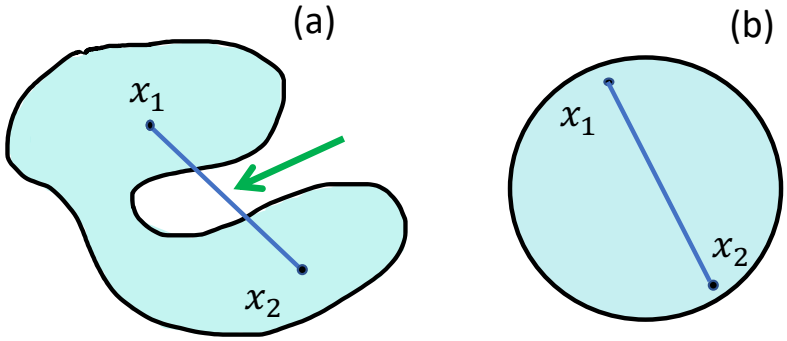

Figure 2.1. Examples of a nonconvex (a) and a convex (b) set.

Definition 2. *Convex function* [3]. A function $f: \mathbb{R}^n \longrightarrow \mathbb{R}$ is convex if **dom** f is a convex set and if for all $x_1, x_2 \in$ **dom** f, and θ with $0 \leq \theta \leq 1$ we have

$$f(x_1\theta + (1-\theta)x_2) \leq \theta f(x_1) + (1-\theta)f(x_2) \tag{2.4}$$

Geometrically, inequality in (2.4) implies that the line segment between two points, $(x_1, f(x_1))$ and $(x_2, f(x_2))$ lies above the graph of f, as shown in Figure 2.2., for a function $f_c(x)$. In contrast, an example of a nonconvex function is given by the function $f_{nc}(x)$.

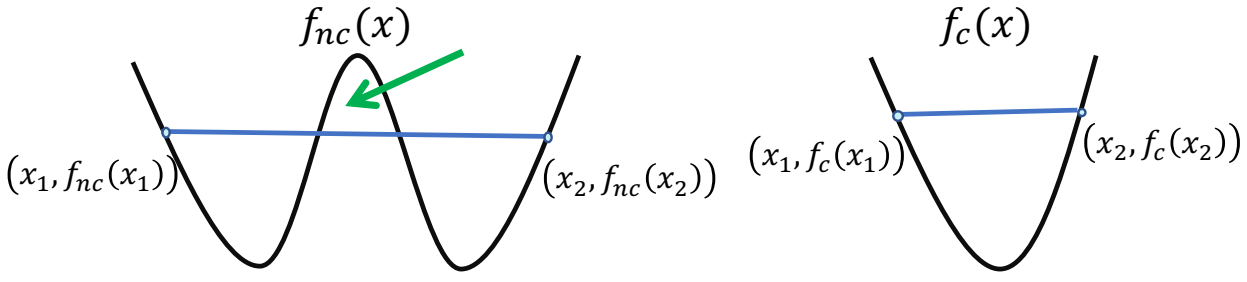

Figure 2.2. Examples of a nonconvex ($f_{nc}(x)$) and a convex ($f_c(x)$) function.

Definition 3. *The domain of an optimization problem* [3]. Consider a generalized optimization problem given by (2.1). The domain of an optimization problem represents the set of all points for which the objective function and all constraint functions given by the set C are defined.

$$\mathcal{D} = \mathbf{dom}\, \mathcal{F}(\boldsymbol{x}) \cap \bigcap_{i=1}^{m} \mathbf{dom}\, g_i(\boldsymbol{x}) \cap \bigcap_{j=1}^{k} \mathbf{dom}\, h_i(\boldsymbol{x}) \tag{2.5}$$

It is important to note that a solution to a problem (2.1) may not exist if there does not exist any point $\boldsymbol{x}$ that belongs to $\mathcal{D}$, i.e. $\mathcal{D} = \emptyset$, in which case the optimization problem is over-constrained and an optimal solution to the problem does not exist.

Definition 4. *An optimal solution* $\boldsymbol{x}^*$ [3]. An optimal solution to the optimization problem from (2.1) is a point in the domain $\mathcal{D}$ that minimizes the objective function $\mathcal{F}(\boldsymbol{x})$. Moreover, in general optimization problems there may exist more than one optimal solution. Hence, an optimal set X_{opt} [3] can be defined as a set that contains all optimal points:

$$X_{opt} = \{\boldsymbol{x} |\, \boldsymbol{x} \in C, \mathcal{F}(\boldsymbol{x}) = p^*\} \tag{2.6}$$

where p^* stands for an optimal objective function value that can be defined as:

$$p^* = \inf\{\mathcal{F}(\boldsymbol{x}) |\, \boldsymbol{x} \in C\} \tag{2.7}$$

One of the well-known approaches used to determine a point that minimizes the objective function $\mathcal{F}(\boldsymbol{x})$ while taking all of the additional constraints into the consideration, represents the augmentation of the objective function with a weighted sum of constrains within a Lagrangian function whose definition follows.

Definition 5. *Lagrangian Function* [3],[7]. Lagrangian, $\mathcal{L}$: $\mathbb{R}^n \times \mathbb{R}^m \times \mathbb{R}^k \to \mathbb{R}$ for the problem (2.1) is defined as:

$$\mathcal{L}(\boldsymbol{x}, \boldsymbol{\lambda}, \boldsymbol{\mu}) = \mathcal{F}(\boldsymbol{x}) + \boldsymbol{\lambda}^T g(\boldsymbol{x}) + \boldsymbol{\mu}^T h(\boldsymbol{x}) \tag{2.8}$$

where the vectors of dual variables or Lagrange multipliers $\boldsymbol{\lambda} \in \mathbb{R}^m$ and $\boldsymbol{\mu} \in \mathbb{R}^k$ represent "optimal weights" associated equality and inequality sets of constraints respectively, while the domain of $\mathcal{L}$ is defined by $\mathbf{dom}\, \mathcal{L} = \mathcal{D} \times \mathbb{R}^m \times \mathbb{R}^k$.

With the basic optimization problem definitions and terminology introduced and under the assumption of differentiable and continuous objective function and constraints as stated by (2.1), the reminder of the section discusses the optimality conditions that are required to be satisfied in order to ensure the optimality of the solution to the optimization problem.

2.1.1.1 First order Necessary optimality conditions (KKT conditions)

First order optimality or Karush-Kuhn-Tucker (KKT) conditions are usually postulated and proven from the Lagrange duality theorem, details of which can be found in [3],[7]. Moreover, for a given pair of primal and dual optimal points $(\boldsymbol{x}^*, \boldsymbol{\lambda}^*, \boldsymbol{\mu}^*)$, the final result can be expressed as a set of conditions derived from a gradient of Lagrangian function from (2.8) with respect to primal and dual variables that must vanish at an optimal point. Therefore, the KKT optimality conditions for a problem defined in (2.1) can be written as:

$$\nabla_x \mathcal{L}(\boldsymbol{x}^*, \boldsymbol{\lambda}^*, \boldsymbol{\mu}^*): \nabla_x \mathcal{F}(\boldsymbol{x}^*) + \nabla_x g(\boldsymbol{x}^*)^T \boldsymbol{\lambda}^* + \nabla_x h(\boldsymbol{x}^*)^T \boldsymbol{\mu}^* = \mathbf{0} \tag{2.9}$$

$$\nabla_\lambda \mathcal{L}(\boldsymbol{x}^*, \boldsymbol{\lambda}^*, \boldsymbol{\mu}^*): g(\boldsymbol{x}^*) = \mathbf{0} \tag{2.10}$$

$$\nabla_\mu \mathcal{L}(\boldsymbol{x}^*, \boldsymbol{\lambda}^*, \boldsymbol{\mu}^*): \boldsymbol{\mu}^* \odot h(\boldsymbol{x}^*) = \mathbf{0} \tag{2.11}$$

$$\boldsymbol{\mu}^* \geqslant \mathbf{0} \tag{2.12}$$

$$h(\boldsymbol{x}^*) \leqslant 0 \tag{2.13}$$

Notably, in addition to the gradient of Lagrangian function that defines the dual (2.9), primal (2.10) and complementary slackness (2.11) problems, the dual and primal feasibility conditions from (2.12)-(2.13) need to be satisfied as well [3]. Importantly, when the optimization problem is convex, i.e. defined by convex objective function and constraints, and the Slater's condition [3] is satisfied, the KKT conditions provide necessary and sufficient conditions to guarantee the optimality of the point for which they hold, and the point represents a global optimal solution. In the generalized case that can include nonconvex objective and/or constraints, the KKT conditions only represent necessary conditions and the second order sufficient condition has to be satisfied in order to claim the optimality of a point for which they hold.

2.1.1.2 Second order (Sufficient) optimality conditions

In contrast to the convex optimization problems for which the hold of KKT conditions represents a sufficient condition for a global optimality of the obtained point, a generalized optimization problem, as the one defined in (2.1), can have many local minima, maxima and even non-optimal saddle points. Therefore, in order to ensure the optimality of a point for which the KKT conditions hold, the Hessian of the Lagrangian function, $\nabla^2_{xx}\mathcal{L}(\boldsymbol{x}^*, \boldsymbol{\lambda}^*, \boldsymbol{\mu}^*)$ evaluated at that point has to be positive-definite on a step size $\boldsymbol{\tau}$:

$$\boldsymbol{\tau}^T \nabla^2_{xx}\mathcal{L}(\boldsymbol{x}^*, \boldsymbol{\lambda}^*, \boldsymbol{\mu}^*)\boldsymbol{\tau} > 0, \forall(\boldsymbol{\tau} \neq \mathbf{0}) \in T_{X^*} \tag{2.14}$$

where T_{V^*} represents the tangent linear sub-space at $\boldsymbol{x}^*$[7].

However, the hold of second order condition from (2.14) does not provide the information about global optimality of the point, but rather guarantees its optimality that can be local and is sometimes as valuable information to have particularly in real-life problems. Furthermore, the second order conditions can be only verified *posteriori*, and cannot be directly used within the solution process, as is the case with KKT conditions that are in general numerically solved in order to obtain the point candidate for an optimal solution. Lastly, it should be emphasized that many algorithms for optimization can be interpreted or are conceived as methods for solving the KKT optimality conditions, as it is discussed in the following sections.

2.1.2. Solving continuous mathematical optimization problems

One of the most common approaches for finding a solution to a continuous constrained optimization problem consists of formulating and solving its set of first order KKT optimality conditions for an optimal point candidate. However, finding an analytical solution to a set of optimality conditions can be only done in rare cases, and the different numerical methods need to be utilized to iteratively obtain a solution. This situation has served as an inspiration for developing the numerical algorithms from the early days of research in mathematical optimizations [3],[6]. Next, we provide a discussion on different state-of-art approaches for handling the constrained optimization problems.

2.1.2.1. Generalized Equality Constrained optimization problem

Consider a generalized continuous optimization problem of minimizing an objective function over a set of equality constraints C_E:

$$\begin{aligned} &\min_{\boldsymbol{x}\in C_E} \mathcal{F}(\boldsymbol{x}) \\ &C_E = \{\boldsymbol{x} |\, g(\boldsymbol{x}) = 0\} \end{aligned} \tag{2.15}$$

In order to obtain the KKT optimality conditions that can be used to find a candidate for an optimal point, the Lagrangian function is defined

$$\mathcal{L}(\boldsymbol{x}, \boldsymbol{\lambda}) = \mathcal{F}(\boldsymbol{x}) + \boldsymbol{\lambda}^T g(\boldsymbol{x}) \tag{2.16}$$

and further differentiated as:

$$\theta(\boldsymbol{y}) = \begin{cases} \nabla_x \mathcal{F}(\boldsymbol{x}) + \nabla_x g(\boldsymbol{x})^{\boldsymbol{T}} \boldsymbol{\lambda} \\ g(\boldsymbol{x}) \end{cases} = \mathbf{0} \tag{2.17}$$

where a new vector of respective primal and dual variables is introduced as $\boldsymbol{y} = [\boldsymbol{x}^{\boldsymbol{T}}, \boldsymbol{\lambda}^{\boldsymbol{T}}]$.

Note that the convexity of the problem in (2.15) is not assumed, and the set of equations $\theta(\boldsymbol{y})$ can be nonlinear and non-convex in general. Therefore, as one of the methods with local quadratic convergence, Newton Raphson (NR) method, whose infeasible start version [3] is presented in Algorithm 2.1., can be applied in order to find a solution to a system of nonlinear equation from (2.17) numerically.

The main idea behind the Newton Raphson method is to linearize the nonlinear set of equations by means of first order Taylor expansion:

$$\theta(\boldsymbol{y}^{k+1}) = \theta(\boldsymbol{y}^k) + \nabla_y \theta(\boldsymbol{y}^k) \Delta \boldsymbol{y} \approx \mathbf{0} \tag{2.18}$$

From Algorithm 2.1., the set of equations linearized at a given initial starting point $(\boldsymbol{x}^{\mathbf{0}}, \boldsymbol{\lambda}^{\mathbf{0}})$ is iteratively solved for NR-steps $\Delta \boldsymbol{y}$ that are further used to update the gradient of the problem $\nabla_y \theta(\boldsymbol{y}^k)$ and its residual $\theta(\boldsymbol{y}^k)$ in the next iteration, until the desired convergence criterion is satisfied. Moreover, due to the line search algorithm based on residual norm from step 2, this version of NR doesn't require feasibility of dual variables initial guess [3], which can be

sometimes challenging to determine due to the nonlinearity of the problem [3]. However, it can be shown that in comparison to the "feasible start" NR, frequently used in solving the convex optimization problems [3], the NR method discussed here has very similar performance [3], and only differs in the form of applied line search in step 2. of the algorithm.

Algorithm 2.1. *NR method for solving an equality constrained optimization problem.*

Initialize: starting point $\boldsymbol{x^0} \in \mathbf{dom}\, \mathcal{F}(\boldsymbol{x})$, $\boldsymbol{\lambda^0}$, tolerance $\epsilon > 0$, counter $k = 0$

Repeat:

1. Compute primal and dual Newton Raphson steps
2. **Apply a form of line search on** $\|\theta(\boldsymbol{y}^k + t\boldsymbol{\Delta y})\|_2$
3. Update NR step: $\boldsymbol{x}^{k+1} = \boldsymbol{x}^k + t\boldsymbol{\Delta x}$, $\boldsymbol{\lambda}^{k+1} = \boldsymbol{\lambda}^k + t\boldsymbol{\Delta\lambda}$
4. Increase counter $k \to k + 1$

Until: $\left\|\theta\left(\boldsymbol{y^{k+1}}\right)\right\|_2 \leq \epsilon$

2.1.2.2. Solution to a line search problem

From the NR algorithm discussed above, as well as most of the other iterative algorithms used in mathematical optimizations, solving a line search problem represents an important component of an algorithm, applied to determine a constant t that limits the obtained step size such that the desired norm of the residual or the objective function value is sufficiently decreased. Importantly, this feature is also used to ensure the global convergence of algorithms for certain class of problems, such as the ones in convex optimizations [3]. Considering the criterion given in the step 2 of the Algorithm 2.1. herein, we discuss the two ways of solving the line search problem, namely a Backtracking and Exact line search approaches.

Solving an Exact Line search problem corresponds to finding a step limiting factor t that attains the minimum of the following one-dimensional optimization problem.

$$t = \underset{t\in[0,1]}{\operatorname{argmin}} \|\theta(\boldsymbol{y}^k + t\boldsymbol{\Delta y})\|_2^2 \tag{2.19}$$

Moreover, due to the nonlinearities of the system $\theta(\boldsymbol{y})$, this problem can be as challenging to solve as the original problem, and hence this version of line search algorithm is currently preferred

only when the cost of computing the constant factor t from (2.19) is low; i.e. can be either solved analytically or efficiently, comparing to computing the search direction itself [3].

To circumvent the problem of computational cost introduced by the exact line search, most line searches used in practice are inexact, such that the step length constant t is chosen to approximately minimize the desired criterion or even just reduce it "enough" to keep going [3]. One of the algorithms represents the Backtracking line search that is presented in Algorithm 2.2. As it can be seen, for a given set of tuning parameters α and β, the value of step length t is iteratively decreased until the required condition of problem residual is decreased "enough."

Algorithm 2.2. *Backtracking Line search algorithm*.

Given: $\boldsymbol{x}^k, \boldsymbol{\Delta x}, \boldsymbol{\lambda}^k, \boldsymbol{\Delta \lambda}$, $\alpha \in (0,0.5)$ and $\beta \in (0,1)$

$t = 1$

while $\|\theta(\boldsymbol{x}^k + t\Delta \boldsymbol{x}, \boldsymbol{\lambda}^k + t\Delta \boldsymbol{\lambda})\|_2 > (1 - \alpha t)\|\theta(\boldsymbol{x}^k, \boldsymbol{\lambda}^k)\|_2$

$t \to \beta t$

In general, however, for problems that are not convex, not every iterative step of the convergence process will provide a positive definite $\nabla_y \theta(\boldsymbol{y}^k)$ matrix [3],[7], which can result in saturation and failing of line search algorithms. Specifically, there may not exist a constant t that decreases the desired condition from the step 2 of Algorithm 2.1. This scenario particularly amplifies with the introduction of inequality constraints within the nonlinear optimization problem.

2.1.2.3. Generalized Constrained optimization problem

The last piece of continuous mathematical optimization "algorithmic puzzle" represents the addition of inequality constraints within the optimization problem. Therefore, herein we discuss a set of algorithms needed for solving the generalized optimization problem from (2.1).

As it can be seen from the first order KKT optimality conditions (2.9)-(2.13), the addition of inequality constraints within the optimization problem significantly increases the complexity of solving the KKT conditions to obtain an optimal solution candidate. This impediment is mainly introduced by the set of complementary slackness (CS) conditions (2.11) that represent the

nonsmooth disjunctive functions that are not differentiable and thereby prevent the use of derivative based algorithms (such as those discussed in the previous section).

Handling the problem of non-smoothness of complementary slackness condition and its incorporation within the existing derivative based algorithms has paved the way to the new class of algorithms, namely Interior Point Method (IPM) algorithms [3],[7], [39]-[42]. It should be emphasized that the main idea behind IMP methods is the approximation of complementary slackness conditions by the addition of a small constant ε that now corresponds to the allowed complementary slackness violation, as shown in (2.20). Most importantly, the conditions are now differentiable, and the existing derivative based methods can be applied without loss of generality.

$$\boldsymbol{\mu} \odot h(\boldsymbol{x}) = -\varepsilon \tag{2.20}$$

Note, however, that as the CS violation parameter approaches zero, the problem becomes more and more steep, as it can be seen from Figure 2.3, and hence is prone to cause the numerical instability issues of an iterative methods [43].

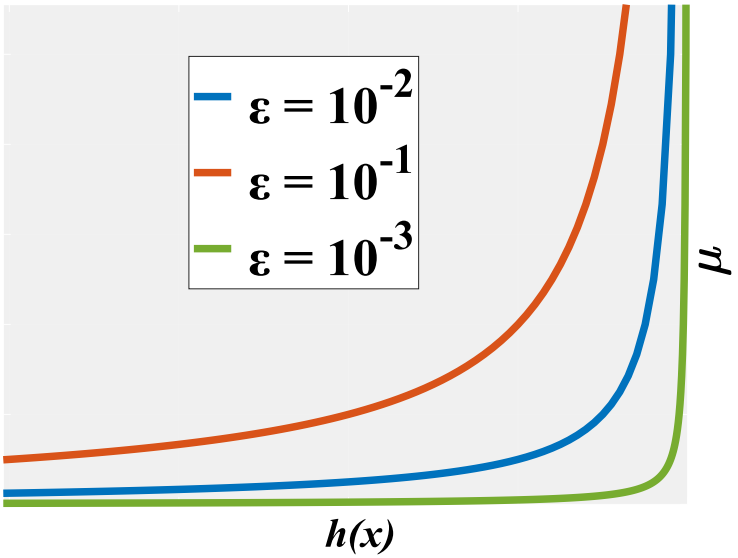

Figure 2.3. Improving the exactness of complementary slackness approximation by decreasing the ε parameter.

To that end, the IPM algorithms can be classified into two main categories [3],[7] based on the approach of handling the decreasing of ε parameter within the solution process.

1. Long-step IPMs – Barrier or Path Following Methods [3]-[7]
2. Short-step IPMs – Primal-Dual Interior Point Methods [39]-[42]

Consider the Lagrangian function of a generalized optimization problem from (2.8), and the respective set KKT optimality conditions with introduced complementary slackness approximation given as:

$$\theta\big(\boldsymbol{z}(\varepsilon)\big) = \begin{cases} \nabla_x \mathcal{F}(\boldsymbol{x}) + \nabla_x g(\boldsymbol{x})^T \boldsymbol{\lambda} \\ g(\boldsymbol{x}) \\ \boldsymbol{\mu} \odot h(\boldsymbol{x}) + \varepsilon \end{cases} = \mathbf{0} \tag{2.21}$$

where vector $\boldsymbol{z}(\varepsilon)$ represents $\boldsymbol{z}(\varepsilon) = [\boldsymbol{x}(\varepsilon)^T, \boldsymbol{\lambda}(\varepsilon)^T, \boldsymbol{\mu}(\varepsilon)^T]$ that is also a function of complementary slackness violation parameter ε.

To highlight the main difference between the long and short step IPMs in solving the set of equations from (2.21), refer to the Algorithm 2.3. and Algorithm 2.4. respectively. As it can be seen, the Long-step IPM, homotopically varies the complementary slackness violation parameter ε. Namely, for a fixed initial $\varepsilon^{\{0\}}$, the set of $\theta\big(\boldsymbol{z}(\varepsilon)\big)$ is solved on the same way as described in the Algorithm 2.1, while *additionally* ensuring the strict feasibility of iterates, as defined by (2.12)-(2.13). The ε parameter is then decreased, and the problem is resolved by using an optimal solution from the problem with previous ε as an initial starting point. The algorithm is terminated once the ε is decreased sufficiently enough, as prespecified by the tolerance parameter ϵ.

Algorithm 2.3. *Basic Long-step Interior Point Method (Path Following Method).*

Given: strictly feasible $\boldsymbol{z^0}$, $\kappa = 0$, $\varepsilon = \varepsilon^{\{0\}} > 0$, $0 < \sigma < 1$and tolerance $\epsilon > 0$

Repeat:

1. Centering step: Solving the set of $\theta\left(\boldsymbol{z}\left(\varepsilon^{\{\kappa\}}\right)\right)$ equations according to Algorithm 2.1.
2. Update: $\boldsymbol{z^{\kappa+1}} = \boldsymbol{z}^*\left(\varepsilon^{\{\kappa\}}\right)$
3. Stopping criterion. **Quit** if $\varepsilon^{\{\kappa\}} < \epsilon$
4. Decrease ε: $\varepsilon^{\{\kappa+1\}} \rightarrow \sigma\varepsilon^{\{\kappa\}}$
5. Increase counter: $\kappa \rightarrow \kappa + 1$

On the other side, the Short-step IPMs handle the decreasing of ε parameter within the inner Newton Raphson loop that is described in Algorithm 2.1, and there is no distinction between the inner and outer loop as in the Long-step IMPs.

Algorithm 2.4. *Basic Short-step Interior Point Method (Primal-Dual IPM).*

Given: $\boldsymbol{x^0}$ that satisfies $h(\boldsymbol{x}) < \boldsymbol{0}$, $\boldsymbol{\mu} > \boldsymbol{0}$, $0 < \sigma < 1$ and tolerance $\epsilon > 0$, $\alpha \in (0,0.5)$ and $\beta \in (0,1)$

Repeat:

1. Determine ε. Set $\varepsilon = -\sigma h\left(\boldsymbol{x^k}\right)^T \boldsymbol{\mu^k}$
2. Compute primal and dual Newton Raphson steps, $\Delta \boldsymbol{z}$
3. **Apply a form of line search on** $\left\|\theta\left(\boldsymbol{z}^k + t_{pd}\boldsymbol{\Delta z}\right)\right\|_2$
   - Compute the largest positive t_{pd}^{max}, not exceeding 1 that ensures $\boldsymbol{\mu > 0}$**:** $t_{pd}^{max} = \min\left\{1, \min\left\{-\frac{\mu_i^k}{\Delta\mu} \mid \Delta\mu_i < 0\right\}\right\}$
   - Start backtracking with $t_{pd} \rightarrow 0.99t_{pd}^{max}$ as described in Algorithm 2.2. by $t_{pd} \rightarrow \beta t_{pd}$ until all of the inequality constraints are satisfied, i.e. $h\left(\boldsymbol{x}^k + t_{pd}\boldsymbol{\Delta x}\right) < \boldsymbol{0}$
   - Continue Line search algorithm until the residual condition is satisfied.
4. Update NR step: $\boldsymbol{x}^{k+1} = \boldsymbol{x}^k + t_{pd}\boldsymbol{\Delta x}$**,** $\boldsymbol{\lambda}^{k+1} = \boldsymbol{\lambda}^k + t_{pd}\boldsymbol{\Delta\lambda}$**,** $\boldsymbol{\mu}^{k+1} = \boldsymbol{\mu}^k + t_{pd}\boldsymbol{\Delta\mu}$
5. Increase counter: $k \rightarrow k + 1$

Until: $\left\|\theta\left(\boldsymbol{z^{k+1}}\right)\right\|_2 \leq \epsilon$ and $\varepsilon \leq \epsilon$

Lastly, it is extremely important to emphasize that all of the algorithms based on a solution of some version of line search problems use a single factor for limiting the complete NR vector step size. In the following sections, it will be shown from circuit simulation perspective that this represent the major drawback of the existing state-of-art algorithms, particularly as the size of the formulated nonlinear problems increases.

2.2. Circuit (Network) simulation problem

The second main ingredient that is embedded within the Equivalent Circuit Programming framework represents the circuit simulation approach towards solving the network problems, as well as the algorithms behind the state-of-art circuit simulator SPICE [11]-[16]. Therefore, this part of chapter provides a definition of a steady-state circuit simulation problem and discusses the algorithms and homotopy methods that facilitate efficient and robust large-scale simulations within SPICE.

Representation of a complex system by an equivalent circuit (network) has been utilized throughout the fields of science and engineering. For example, other than in electrical engineering, equivalent circuits have been used to represent mechanical systems [44], as well as biological [45] and chemical processes [46]. Specifically, such representation can apply for any system governed by the properties that ensure the conservation of energy, also defined by Tellegen's Theorem [10]:

1. There exists a conservation of flow of extensive quantity (Kirchhoff Current Law-KCL)
2. There exists a uniqueness of potentials at the network nodes (Kirchhoff Voltage Law-KVL)
3. The effect of radiation doesn't exist or is not significant and can be neglected

Consider an equivalent circuit defined by the set of nodes $\mathcal{V}$ and the set of branches $\mathcal{E}$, such that each branch is identified with a pair of nodes (v_i, v_j). One of the well-known ways of formulating a set of governing equivalent circuit equations is by expressing them in terms of KCL and voltage state variables at each of the circuit nodes, as done in Modified Nodal Analysis (MNA) [15]. Moreover, current state variables are added [15] if required to define the additional KVL relationships between the circuit nodes or other dependencies or nonlinearities within the circuit.

In general, a set of equivalent circuit governing equations that further define its steady-state operating point (response) can be expressed in terms of a set of algebraic MNA equations with voltage and current state variables $\boldsymbol{V_N}$ and $\boldsymbol{I_B}$ as follows:

$$\begin{aligned} I_{KCL}(\boldsymbol{V_N}, \boldsymbol{I_B}) &= \mathbf{0} \\ F(\boldsymbol{V_N}, \boldsymbol{I_B}) &= \mathbf{0} \end{aligned} \tag{2.22}$$

where the first set (I_{KCL}) of equations correspond to KCL defined at each node of the circuit, while the second set of equations stands for the additional constraints on the circuit branch voltages or other nonlinearities that can be introduced by various network device models. To provide more detailed definitions corresponding to the set of equivalent circuit equations defined in (2.22), we next introduce a definition of a steady-state network response as well as discuss the different types of circuit steady-state analyses.

2.2.1. Steady-state circuit response and the linear AC analysis

The steady-state response of an equivalent circuit (network) defines its behavior after an external excitation (turning ON/OFF, disturbance, etc.) occurs and when the network reaches its steady condition. In general, due to the independence of time, the steady-state is often modeled and analyzed in the frequency domain.

- Linear AC Steady-State response

Linear AC analysis considers the networks whose response remains of the same harmonic frequency as its excitation input, but changes in magnitude and phase. Such networks can be exactly modeled in terms of complex sources and admittances obtained by the application of Fourier transformation to the time domain governing equations for each of the linear circuit elements, as shown in (2.23)-(2.27).

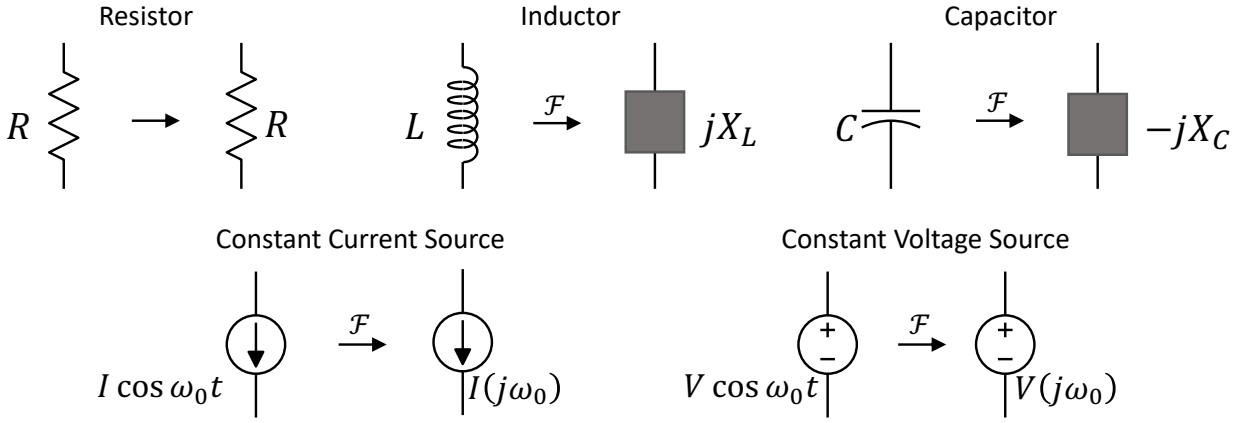

Figure 2.4. Mapping of linear circuit elements from time to frequency domain.

$$i_R(t) = \frac{1}{R} v_R(t) \quad \overset{\mathcal{F}}{\rightarrow} \quad I_R(j\omega) = \frac{1}{R} V_R(j\omega) \tag{2.23}$$

$$v_L(t) = L\frac{di_L(t)}{dt} \quad \overset{\mathcal{F}}{\rightarrow} \quad V_L(j\omega) = j\omega L I_L(j\omega) \equiv jX_L I_L(j\omega) \tag{2.24}$$

$$i_C(t) = C\frac{dv_C(t)}{dt} \quad \overset{\mathcal{F}}{\rightarrow} \quad I_C(j\omega) = j\omega C V_C(j\omega) \equiv jX_C V_C(j\omega) \tag{2.25}$$

$$v_S(t) \quad \overset{\mathcal{F}}{\rightarrow} \quad V_S(j\omega) = \tilde{V}_S \tag{2.26}$$

$$i_S(t) \quad \overset{\mathcal{F}}{\rightarrow} \quad I_S(j\omega) = \tilde{I}_S \tag{2.27}$$

Where $i_X(t)$, $v_X(t)$, $I_X(j\omega)$ and $V_X(j\omega)$ stand for the time and frequency domain element currents and voltages respectively, while the placeholder $X \in \{R, L, C, S\}$ indicates the type of linear circuit element.

The generalized set of linear circuit equations that defines a steady-state response of a linear RLC network as the one presented in Figure 2.5 can be then written as:

$$\begin{aligned} Y_{RLC}^{N}(j\omega)\tilde{\boldsymbol{V}}_N + \tilde{\boldsymbol{I}}_{\boldsymbol{S}} + E_N\tilde{\boldsymbol{I}} &= \mathbf{0} \\ E_N\tilde{\boldsymbol{V}}_{\boldsymbol{N}} - \tilde{\boldsymbol{V}}_{\boldsymbol{S}} &= \mathbf{0} \end{aligned} \tag{2.28}$$

where $Y_{RLC}^{N}(j\omega)$ represent the linear node admittance matrix defining the RLC circuit elements, while E_N corresponds to the matrix that "connects" current variables to the respective circuit nodes whose voltage is to be controlled.

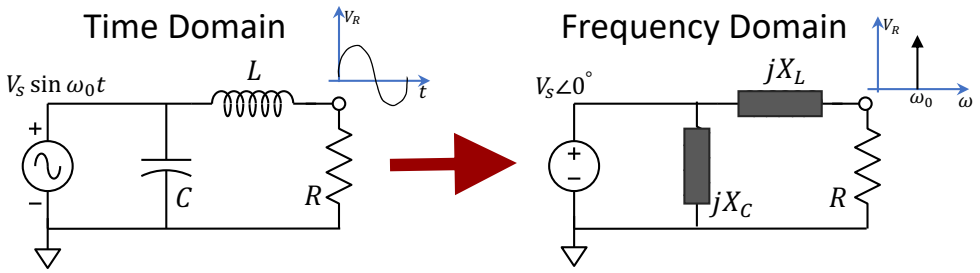

Figure 2.5. RLC circuit example. Note that the linear complex admittances can only cause the magnitude and angle change of the voltage across R.

2.2.1.1. Linear Adjoint Network Theory

With the introduction of linear AC network response and its circuit representation in the frequency domain, it is important to mention the notion of adjoint networks that was first proposed for electrical circuit noise analysis [34]-[36] in SPICE. Moreover, as it will be shown in the following chapters, the adjoint networks serve as a fundamental link between network governing equations and equivalent circuit representation of the ECP optimality conditions. Hence, herein we discuss mapping from the original linear network elements to the respective adjoint equivalents that can be derived and are governed by Tellegen's Theorem [10].

For a given a network η and its topologically equivalent adjoint $\hat{\eta}$ in steady-state with $\tilde{\boldsymbol{I}}_{\boldsymbol{B}}$, $\tilde{\boldsymbol{V}}_{\boldsymbol{B}}$, $\tilde{\mathfrak{T}}$ and $\tilde{\boldsymbol{\lambda}}$ representing network and adjoint network complex branch currents and voltages

respectively, the Tellegen's Theorem implies that the conservation of energy within both networks has to hold, i.e.

$$\begin{aligned} \tilde{\boldsymbol{I}}_{\boldsymbol{B}}^{H}\tilde{\boldsymbol{V}}_{\boldsymbol{B}} &= 0 \\ \tilde{\boldsymbol{\lambda}}^{H}\tilde{\boldsymbol{\mathfrak{T}}} &= 0 \end{aligned} \tag{2.29}$$

where H represents a complex transpose operator.

Due to the topological equivalence of two networks, it can be further shown [14] that the Tellegen's Theorem also implies the following relationship:

$$\tilde{\boldsymbol{\lambda}}^{H}\tilde{\boldsymbol{I}}_{\boldsymbol{B}} - \tilde{\boldsymbol{\mathfrak{T}}}^{H}\tilde{\boldsymbol{V}}_{\boldsymbol{B}} = 0 \tag{2.30}$$

Next, let the original network governing steady-state equations have a form of KCL equations given in (2.28). To establish the relationship between the original and adjoint network elements, we perturb the admittance in each network branch $Y_{RLC} \to Y_{RLC} + \delta Y_{RLC}$ such that the network response is perturbed; i.e. $\tilde{\boldsymbol{V}}_{\boldsymbol{B}} \to \tilde{\boldsymbol{V}}_{\boldsymbol{B}} + \delta\tilde{\boldsymbol{V}}_{\boldsymbol{B}}$,$\tilde{\boldsymbol{I}}_{\boldsymbol{B}} \to \tilde{\boldsymbol{I}}_{\boldsymbol{B}} + \delta\tilde{\boldsymbol{I}}_{\boldsymbol{B}}$ and $\tilde{\boldsymbol{I}} \to \tilde{\boldsymbol{I}} + \delta\tilde{\boldsymbol{I}}$. Hence, the vector that defines currents in each branch of the network from (2.28), as well as Tellegen's Theorem expression from (2.30) have a form of:

$$\begin{aligned} (Y_{RLC} + \delta Y_{RLC})\left(\tilde{\boldsymbol{V}}_{\boldsymbol{B}} + \delta\tilde{\boldsymbol{V}}_{\boldsymbol{B}}\right) + E_B\left(\tilde{\boldsymbol{I}} + \delta\tilde{\boldsymbol{I}}\right) + \tilde{\boldsymbol{I}}_{\boldsymbol{S}} &= \tilde{\boldsymbol{I}}_{\boldsymbol{B}} + \delta\tilde{\boldsymbol{I}}_{\boldsymbol{B}} \\ E_B\left(\tilde{\boldsymbol{V}}_{\boldsymbol{B}} + \delta\tilde{\boldsymbol{V}}_{\boldsymbol{B}}\right) - \tilde{\boldsymbol{V}}_{\boldsymbol{S}} &= \boldsymbol{0} \end{aligned} \tag{2.31}$$

$$\tilde{\boldsymbol{\lambda}}^{H}\left(\tilde{\boldsymbol{I}}_{\boldsymbol{B}} + \delta\tilde{\boldsymbol{I}}_{\boldsymbol{B}}\right) - \tilde{\boldsymbol{\mathfrak{T}}}^{H}\left(\tilde{\boldsymbol{V}}_{\boldsymbol{B}} + \delta\tilde{\boldsymbol{V}}_{\boldsymbol{B}}\right) = 0 \tag{2.32}$$

Equations (2.31) and (2.32) can be then further simplified with the assumption that the terms $\delta Y_{RLC}\delta\tilde{\boldsymbol{V}}_{\boldsymbol{B}}$ are negligibly small:

$$\begin{aligned} \delta Y_{RLC}\tilde{\boldsymbol{V}}_{\boldsymbol{B}} + Y_{RLC}\delta\tilde{\boldsymbol{V}}_{\boldsymbol{B}} + E_B\delta\tilde{\boldsymbol{I}} &= \delta\tilde{\boldsymbol{I}}_{\boldsymbol{B}} + \tilde{\boldsymbol{I}}_{\boldsymbol{B}} - \left(Y_{RLC}\tilde{\boldsymbol{V}}_{\boldsymbol{B}} + E_B\tilde{\boldsymbol{I}} + \tilde{\boldsymbol{I}}_{\boldsymbol{S}} + \delta Y_{RLC}\delta\tilde{\boldsymbol{V}}_{\boldsymbol{B}}\right) \approx \delta\tilde{\boldsymbol{I}}_{\boldsymbol{B}} \\ E_B\delta\tilde{\boldsymbol{V}}_{\boldsymbol{B}} = \tilde{\boldsymbol{V}}_{\boldsymbol{S}} - E_B\tilde{\boldsymbol{V}}_{\boldsymbol{B}} &= \boldsymbol{0} \end{aligned} \tag{2.33}$$

$$\tilde{\boldsymbol{\lambda}}^{H}\delta\tilde{\boldsymbol{I}}_{\boldsymbol{B}} - \tilde{\boldsymbol{\mathfrak{T}}}^{H}\delta\tilde{\boldsymbol{V}}_{\boldsymbol{B}} = -\tilde{\boldsymbol{\lambda}}^{H}\tilde{\boldsymbol{I}}_{\boldsymbol{B}} + \tilde{\boldsymbol{\mathfrak{T}}}^{H}\tilde{\boldsymbol{V}}_{\boldsymbol{B}} = 0 \tag{2.34}$$

Note that constant sources within the network, e.g. $\tilde{\boldsymbol{I}}_{\boldsymbol{S}}$, as well as the voltage perturbations of the branches corresponding to a voltage source are not affected by the admittance perturbation within the network, and hence their contributions do not affect the further derivations.

By substituting the expression for $\delta\tilde{\boldsymbol{I}}_{\boldsymbol{B}}$ from (2.33) to (2.34) we obtain:

$$\tilde{\boldsymbol{\lambda}}^{H}\delta Y_{RLC}\tilde{\boldsymbol{V}}_{\boldsymbol{B}} + \left(\tilde{\boldsymbol{\lambda}}^{H}Y_{RLC} - \tilde{\mathfrak{T}}^{H}\right)\delta\tilde{\boldsymbol{V}}_{\boldsymbol{B}} + \tilde{\boldsymbol{\lambda}}^{H}E_{B}\delta\tilde{\boldsymbol{I}} = 0 \tag{2.35}$$

Therefore, for Tellegen's Theorem to remain satisfied, the adjoint branch currents $\tilde{\mathfrak{T}}$, as well as the adjoint voltages related to a network branch defined by a voltage source have to correspond to:

$$\begin{aligned} \tilde{\mathfrak{T}} &= Y_{RLC}^{H}\tilde{\boldsymbol{\lambda}} \\ \tilde{\boldsymbol{\lambda}}^{H}E_{B} &= 0 \end{aligned} \tag{2.36}$$

which indicates that the adjoint branch current is proportional to the Hermitian of the network admittance, while the adjoint voltages that correspond to a network branches governed by a voltage source are shorted. Element-wise, it is implied that an admittance is defined by its complex conjugate in the adjoint network. Lastly, the excitation sources of the original network do not affect its adjoint equivalent, and therefore, are turned off in the adjoint network. The generalized relationship between the original and adjoint network elements is given in Table 2.1:

Table 2.1:Defining the mapping from an original to the adjoint network elements

Original Network		Adjoint Network
Independent current source	→	open
Independent voltage source	→	short
Capacitor	→	Inductor
Resistor	→	Resistor
Inductor	→	Capacitor

2.2.1.2 Nonlinear circuit elements

Similar to the case of solving the nonlinear equations that arise from formulating the optimization problem optimality conditions, Newton Raphson method represents one of the frequently used numerical algorithms utilized for solving circuit simulation problems. Herein, we show that once applied to a circuit problem, each of the terms from generalized NR formulation, as the one presented in Algorithm 2.1., can be mapped to the linearized equivalent circuit, thereby

providing the additional knowledge of problem physical characteristics. This domain-specific knowledge can be now utilized to develop the set of algorithms that replace the line search problem in step 2 of the Algorithm 2.1., which represents the most important difference between the generalized optimization solver that uses the NR and the circuit simulator. In other words, a constant damping factor t obtained by solving the line search problem is now replaced by a vector of limiting factors for each of the circuit variables obtained based on the understanding of physical characteristics of the problem.

To demonstrate the mapping of Newton Raphson method to an equivalent circuit, consider a nonlinear diode model from Figure 2.6 (a), whose governing equation is given by:

$$I(V) = I_{sat}\left(e^{\frac{V}{V_T}} - 1\right) \tag{2.37}$$

where I_{sat} represents a diode saturation current while a constant V_T represents the diode thermal voltage.

As it is the case in (2.18), the first order Taylor expansion is applied to linearize the nonlinear diode current, $I(V)$ around the $(k+1)^{th}$ iteration as:

$$I(V^{k+1}) = I(V^k) - \left.\frac{dI(V)}{dV}\right|_k V^k + \left.\frac{dI(V)}{dV}\right|_k V^{k+1} \equiv I_{EQ}^k + G_{EQ}V^{k+1} \tag{2.38}$$

Next, by grouping the constant terms known from previous iteration (I_{EQ}^k), it can be seen that diode current at next NR iteration $I(V^{k+1})$ represents sum of a constant term and the term proportional to its voltage sensitivity. Hence it can be mapped to a constant current source I_{EQ}^k and a conductance G_{EQ} as shown in Figure 2.6 (b).

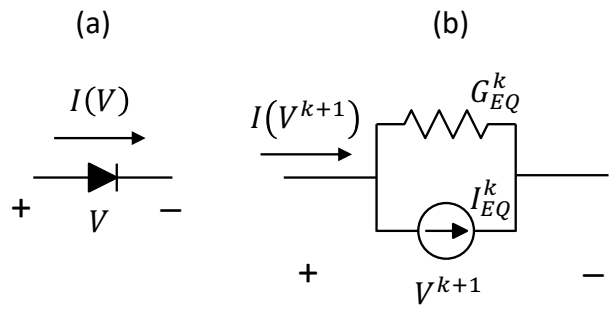

Figure 2.6: Nonlinear Diode model (a) and the linearized equivalent circuit model of a diode (b).

2.2.2. Solving a circuit simulation problem

As it can be seen from the previous section, each of the nonlinear circuit devices can be linearized with the first order Taylor expansion and mapped to an equivalent circuit model of a device by following the same methodology as presented on a diode example. The complete equivalent circuit representation of a problem is then obtained by hierarchically combining (connecting) the derived linear and linearized equivalent circuit models, as defined by the circuit (network) topology. Importantly, the hierarchical building of the circuit representation, also called stamping [15], corresponds to an efficient, modular construction of the Jacobian matrix and constant vector that defines the Newton-Raphson (NR) values during the iteration process.

Once the complete equivalent circuit is built, its set of governing circuit equations correspond to the linearized set of equations that are updated at each step of NR, as it is presented in Algorithm 2.5. For the equivalent circuit approach to NR, only circuit elements (Jacobian terms) that are dependent on the values from the previous iteration are recomputed, while the linear parts are only computed and stamped once at the beginning of the simulation. This approach was shown to represent an extremely efficient formulation and solution method for solving the nonlinear circuit problems [15]. As emphasized above, the main difference between the circuit simulation and traditional NR method, however, is the domain-specific knowledge obtained from the circuit representation of the problem. This provides important information that allows for developing efficient heuristics for limiting the Newton step, thereby ensuring robust and efficient convergence properties [11],[14]-[15],[43].

Algorithm 2.5. *Newton Raphson method for solving a circuit simulation problem*

Initialize: starting point $\boldsymbol{V^0}$, tolerance $\epsilon > 0$, counter $k = 0$

Stamp Linear circuit elements

Repeat:

1. Stamp linearized circuit elements evaluated at $\boldsymbol{V^k}$and compute NR step $\boldsymbol{\Delta V}$ by solving a linearized circuit
2. **Apply circuit simulation NR-step limiting heuristics**
3. Update NR step: $\boldsymbol{V^{k+1} = V^k + T \odot \Delta V}$
4. Increase counter $k \rightarrow k + 1$

Until: $\|\boldsymbol{\Delta V}\|_\infty \leq \epsilon$

2.2.2.1 NR-step limiting circuit simulation methods

As a major and most important difference between the generic NR algorithm and the one applied in circuit simulations, herein we discuss three well-known NR-step limiting approaches, all of which were inspired by limiting the voltage step of a diode model, and further generalized to the complete domain of circuit simulation problems.

1. Fixed step junction limiting heuristics [11]-[12],[14]-[15]

One of the simplest and yet most effective step-limiting heuristics is based on placing a fixed bound on the NR-step size depending on the physical regions of a device model, as introduced by Nagel in [12], and summarized in Algorithm 2.6. As can be seen, for the given vectors of voltages from previous NR iteration $\boldsymbol{V^k}$ and newly obtained ones $\widehat{\boldsymbol{V}}$, as well as a set of bounding parameters, α_D and β_D, for the voltage less than β_D, no step limiting is used, while for voltages greater than β_D, the NR steps are limited to $\boldsymbol{V^k} \pm \alpha_D$. It should be noted that the set of parameters α_D and β_D is determined from the characteristics of a model, where for instance $\alpha_D = 2V_T$ and $\beta_D = 10V_T$ are chosen for the diode model discussed above. Most importantly it was found that the general value for β_D can be near optimally picked as the value of a maximum curvature point of the nonlinear device model, which is for diode model from (2.37) approximately equal to $10V_T$. Lastly, the graphical representation of the NR convergence on a diode model as well as the fixed step junction limiting which inspired the generalization of this heuristics is presented in Figure 2.7.

Algorithm 2.6. *Fixed step junction limiting heuristics*

Given: $\boldsymbol{V^k}, \widehat{\boldsymbol{V}}$, α_D and β_D

For each pointwise element of $\boldsymbol{V^k}$ and $\widehat{\boldsymbol{V}}$:

Condition (if):	**Action:**
$\left\|\hat{V}_i - V_i^k\right\| \le \alpha_D$	$V_i^{k+1} = \hat{V}_i$
$\hat{V}_i \le \beta_D$ & $V^k \le \beta_D$	$V_i^{k+1} = \hat{V}_i$
$\hat{V}_i \le V_i^k$ & $V_i^k \ge \beta_D$	$V_i^{k+1} = V_i^k - \alpha_D$
$V_i^k \le \hat{V}_i$ & $\hat{V}_i \ge \beta_D$	$V_i^{k+1} = \max\left[\beta_D, V_i^k + \alpha_D\right]$

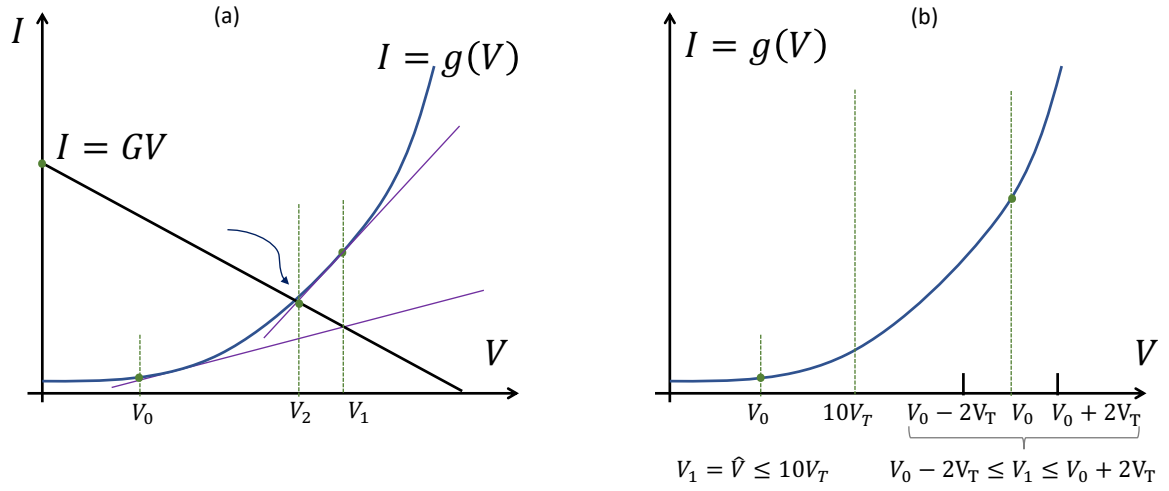

Figure 2.7. graphical representation of NR iterations on a diode model (a), and representation of a fixed step junction limiting heuristics.

2. Hyperbolic tangent fixed bound diode limiting

The second fixed bound approach proposed in [14],[43] uses the hyperbolic tangent function to limit the voltage step as:

$$V^{k+1} = V^k + \beta_D \tanh\left[\frac{\hat{V} - V^k}{\beta_D}\right] \tag{2.39}$$

Moreover, the hyperbolic tangent function ranges from -1 to $+1$, and hence the maximum voltage step is limited by β_D, whereas for the small steps $V^{k+1} = \hat{V}$, since the slope of the function for a small argument approaches 1. In contrast, as the magnitude of a step approaches β_D, it becomes more and more damped. Lastly, the limiting is embedded within the continuous function and hence no special cases need to be considered as in the previously discussed step limiting.

3. Alternating basis auxiliary function diode limiting

Contrary to the fixed step size heuristics, the last considered NR step limiting heuristic is based on introduction of auxiliary function proposed by Colon and Nagel in [13]. The expression for alternating basis updates is obtained by equating the nonlinear diode function evaluated at V^{k+1}

$$I(V^{k+1}) = I_{sat}\left(e^{\frac{V^{k+1}}{V_T}} - 1\right) \tag{2.40}$$

with the current obtained from the linearized diode equations from (2.38):

$$I(\hat{V}) = I(V^k) - \left.\frac{dI(V)}{dV}\right|_k V^k + \left.\frac{dI(V)}{dV}\right|_k \hat{V} \tag{2.41}$$

Then solving the obtained expression for V^{k+1}, which consequently results in:

$$V^{k+1} = V^k + V_T \log\left[\frac{\hat{V} - V^k}{V_T} - 1\right] \tag{2.42}$$

The voltage update from (2.42) is only applied if the NR step is positive as well as if $\hat{V}$ exceedes the value of the critical curvature point of the nonlinear function, which for the diode model above is precisely:

$$V_{CRIT} = V_T \log\left[\frac{V_T}{\sqrt{2} I_{sat}}\right] \tag{2.43}$$

Lastly, as it can be seen from the step limiting techniques discussed above, the circuit simulation problems replace the line search optimization solved within the generalized NR algorithm by the step limiting heuristics whose parameters are tuned depending on the characteristics of the nonlinear models. More importantly, even though none of them ensures that the residual of the problem is decreased at every iteration, these approximated trust region techniques based on the "physics" of the problem were shown to work quite effectively for nonlinear circuit simulations. One of the reasons supporting this is the nonconvex nature of most of the circuit simulation problems that could most likely cause the line search algorithms with a constant step length parameter t to saturate, and hence preventing the monotonic decrease of residual throughout the simulation. However, the aforementioned step limiting techniques may not be sufficient to enable the robust convergence properties of the extremely large-scale circuit simulations, and homotopy methods were subsequently developed.

2.2.2.2 Homotopy methods to improve simulation robustness

Exploring and applying path tracing homotopy methods for solving nonlinear circuit problems has been attracting research interest from the early days of circuit simulation research. In general, a homotopy method can be mathematically defined as:

$$H(\boldsymbol{x}, \lambda_H) = (1 - \lambda_H)F(\boldsymbol{x}) + \lambda_H G(\boldsymbol{x}), \quad \lambda_H \in [0,1] \tag{2.44}$$

where $F(\boldsymbol{x})$ is an original nonlinear problem defined in terms of a vector of state variables $\boldsymbol{x}$, while $G(\boldsymbol{x})$ represent the initial homotopy problem for which the solution can be trivially obtained. The λ_H is a homotopy factor that is varied, usually dynamically [43], in discrete steps from 1 to 0 while the homotopy problem $H(\boldsymbol{x}, \lambda_H)$ is iteratively resolved by using the solution from the previous homotopy step as an initial guess.

It is important to emphasize that all of the circuit simulation homotopy methods are developed from the physical perspective, namely, by embedding homotopy factor within the circuit elements. Therefore, the three well known circuit simulation homotopy methods are:

1. **Source/Power stepping** [15],[43]: Embeds the homotopy factor within the circuit excitation sources. The initial homotopy problem then represents a circuit with all of the sources turned OFF and its solution is trivial, namely equal to zero. The solution to the original problem is then obtain by homotopically turning ON the excitation sources, while using the previously obtained homotopy solution as an initial start.
2. **G-min stepping** [47]: Shorts the complete circuit by connecting a large conductance from each node to the ground. The initially shorted operating point is then trivial, and the solution of the original circuit is obtained by gradually relaxing these added conductances.
3. **Artificial Source homotopy** [48]: Connects a voltage source through a small source resistor at every node of the circuit. Therefore, the initial homotopy solution is trivially obtained, and is governed by the voltage sources. Next, the sources are sequentially disconnected by embedding the homotopy factor within the source resistances, and the problem is continuously resolved until the “artificially” added voltage sources are completely removed. The authors in [48] also provide the sufficient conditions for which this homotopy method is globally convergent.

2.3. Drawbacks of existing optimization algorithms from the perspective of circuit simulations

Solving a nonlinear constrained optimization problem can be a very challenging task that is prone to divergence, very slow convergence or convergence to a nonoptimal saddle points. With the employed commercial optimization toolboxes, formulating and solving an optimization problem sometimes represents more an art in tuning the correct solver parameters than the technology [3]. These challenges can arise due to:

1. The initial starting point that is crucial and can greatly affect the efficiency and the quality of the obtained solution.
2. Inefficiency of handling the problem nonlinearities.
3. Modeling of inequality constraints that introduces an additional level of complexity; i.e. requires the use of Interior Point Methods and additional damping of NR step.

It is important to emphasize that from the perspective of solving a circuit simulation problem, which, as it will be shown in the following chapters, a network optimization problem can be represented as, the three major challenges mentioned above have one thing in common. That is a constant step length parameter obtained as a solution to some form of a line search problem. Moreover, since the first introduction of the SPICE-like simulators [11]-[13], it has been shown that damping the complete solution vector of a nonlinear simulation has two serious drawbacks [11]. First, if the iterative solutions are in vicinity of the correct solution, the convergence process can be unnecessarily slowed down. Second, if the solutions of two consecutive iterations differ widely, the problem may diverge or oscillate.

Returning back to the three main sources of challenges emphasized above. First, with a single step limiting factor, a bad initial starting point amplified with the nonlinearities introduced by problem constraints can cause the line search problem to allow only a very small NR step size that can barely reduce the residual of the function. Moreover, due to the nonlinearities of the problem, the line search may not even have a feasible solution, in which case it saturates, and only the increase of residual can allow for the future convergence of the iterative process. The problem of small step sizes is amplified even more with the introduction of inequality constraints that require the additional damping of a step size with a factor that ensures the primal and dual feasibility of each constraint in the problem. This means that the bigger problem gets in terms of

variable count, the worse the result, since one step size can possibly affect and saturate the whole solution vector. Finally, and most importantly, this unnecessary damping of certain variables from a complete solution vector can force the iteration process to remain stuck in the local area, thereby increasing the chances of converging to a local solution or a saddle point, as demonstrated from the drawing in Figure 2.8.

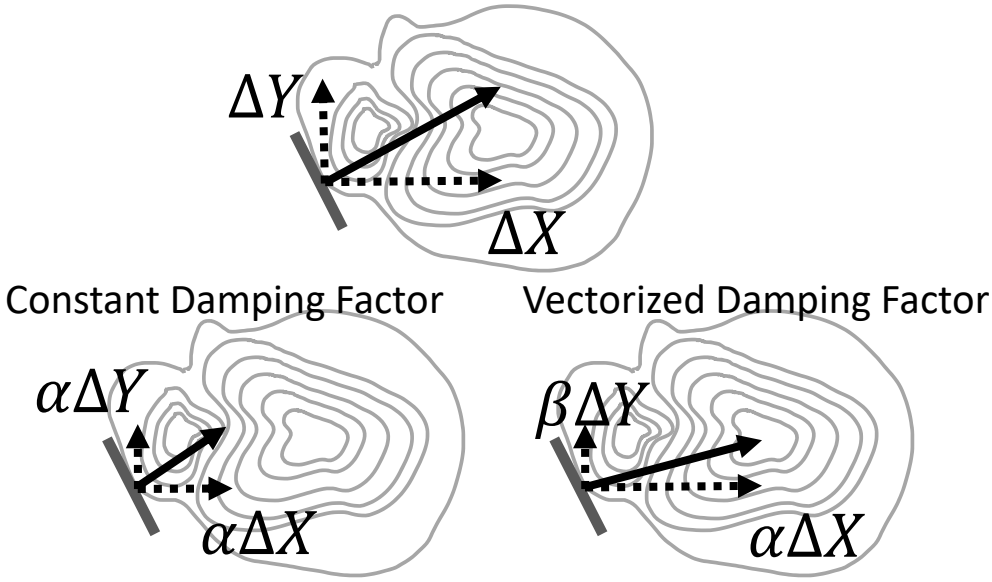

Figure 2.8. Emphasizing the drawbacks of a single step limiting factor within the optimization solution space.

Conversely, the circuit simulation techniques and algorithms employ the knowledge of the problem's physical characteristics in order to limit NR step size, which means that each of the variables is treated and limited separately. However, this may not necessarily decrease the residual at every iteration, which can be a blessing as well as a curse. If not limited properly, the convergence process can take a step from which it cannot recover, causing the future divergence. Hence, the drawing from Figure 2.8 highlights the best case for vectorizing the step size limiting factors, assuming that they are obtained purely from the knowledge of physical characteristics of the problem. Therefore, *this thesis focuses on utilizing the equivalent circuit representation of the ECP problem in order to merge the best of the two approaches together* and develop a new set of heuristics that can allow more scalable and efficient solution process. Furthermore, this approach can potentially improve the solution quality by ensuring that the vectorized damping of a NR step ensures more optimal residual decrement at each iteration.

Chapter 3 Generalization of Steady-State Network Modeling and Nonlinear Adjoint Network Theory

Presently, network theory recognizes four well-established types of modeling the network steady-state response, namely responses defined by Linear and Nonlinear DC and AC analyses in terms of voltage and current state variables. While the modeling of first three network responses is covered in Chapter 2, the fourth one, Nonlinear AC or Harmonic Balance analysis [49], defines an AC network for which the response is distorted due to the device nonlinearities, and hence is not of the same harmonic frequency as its excitation input. This type of analysis is mostly used in radio frequency (RF) circuit simulations [50] and is represented in the frequency domain in terms of n coupled harmonic circuits, one for each harmonic defined by Discrete Fourier transformation to approximate the distorted time domain response at the steady-state. Herein, we only mention it for completion and emphasize that it can be incorporated within the ECP framework without any loss of generality.

In order to obtain the modeling framework that is differentiable and compatible with any network steady-state optimization problem, this chapter generalizes the network response modeling to include the Nonlinear AC analysis at the fixed frequency, by introducing the additional set of admittance state variables. It is shown that the nonlinearities within this type of AC analysis do not introduce the distortion to the time domain response, as in the case of Harmonic Balance analysis, but rather represent the additional constraints on the linear AC network steady-state response. Moreover, in order to enable the analyticity of the network models, we further introduce the equivalent split-circuit approach for handling the nonlinear systems in frequency domain. Lastly, the chapter is concluded by extending the nonlinear AC analysis at the fixed frequency to generalize the Adjoint circuit theory, by providing the mapping of admittance state variables to the adjoint domain.

3.1 Constraining the linear network AC response by introduction of admittance state variables

Consider a linear AC network with excitation sources of a single frequency defined by the set of nodes $\mathcal{V}$ and the set of branches $\mathcal{E}$, such that each branch is identified with a pair of nodes (v_i, v_j), and whose set of complex governing equations characterizes its steady-state response in terms of phasor branch currents and voltages given for the input excitation frequency. Moreover, as it could be seen from Chapter 2, an additional phasor current variable is added to the set of KCL equations (2.28) in order to constrain the phasor voltage across a particular branch. In general, however, the constraints on a steady-state response can be nonlinearly related, and even non-analytically related, to the network phasor currents and voltages. For instance, it could be required to constrain the voltage magnitude of a particular node but not its angle, or a magnitude of current flowing in a circuit branch, in which case the addition of a complex variable to control a particular magnitude or phase within the network may not be sufficient and is even not analytic since it doesn't satisfy the Cauchy-Riemann conditions [51]. Therefore, in addition to phasor current state variables, it is required to introduce a new set of variables that can be compatible with constraining only a certain component of another phasor.

Herein, it is important to emphasize the notion of a driving point admittance [52], which can perfectly characterize the phasor relationship between the current and voltage signals at a specific frequency, as the ones presented in Figure 3.1. Additionally, by Ohm's Law, an admittance can also affect magnitude and angle of current and voltage signals by changing its real and imaginary components, namely conductance (G) and susceptance (B), which is exactly the characteristic of a variable needed in order to constrain only a specific component of a signal in phasor domain.

Therefore, we generalize the linear AC steady-state network modeling by adding a set of admittance (conductance and susceptance) state variables in order to ensure the capability of modeling the generalized constraints on its response. Furthermore, as it was the case with addition of phasor current variables, the newly introduce conductance and susceptance variables also provide an intuitive physical explanation behind them. For instance, adding a susceptance variable to constrain the voltage magnitude of a particular circuit node can be seen as solving for a capacitor susceptance that maintains the voltage magnitude level at a given set point specified by the network

design, etc. Hence, the definition of linear AC network governing equations from (2.28) can be extended to include the admittance state variables, $\boldsymbol{Y_{GB}} = \boldsymbol{G} + j\boldsymbol{B}$, for which an additional set of network steady-state response constraints, $f\left(\tilde{\boldsymbol{V}}, \tilde{\boldsymbol{I}}_{\boldsymbol{V}}, \boldsymbol{Y_{GB}}\right)$, can be included.

$$\begin{gathered} \left(Y_{RLC} + \mathrm{Tdiag}(\boldsymbol{Y_{GB}})\right)\tilde{\boldsymbol{V}} + \tilde{\boldsymbol{I}}_{\boldsymbol{S}} + E_N\tilde{\boldsymbol{I}}_{\boldsymbol{V}} = \boldsymbol{0} \\ E_N\tilde{\boldsymbol{V}} - \tilde{\boldsymbol{V}}_{\boldsymbol{S}} = \boldsymbol{0} \\ f(\tilde{\boldsymbol{V}}, \tilde{\boldsymbol{I}}_{\boldsymbol{V}}, \boldsymbol{Y_{GB}}) = \boldsymbol{0} \end{gathered} \tag{3.1}$$

Where $\tilde{\boldsymbol{I}}_{\boldsymbol{V}}$ represents a set of current variables added to constrain the respective node voltages and matrix T relates the introduced admittance variables to the corresponding network branches.

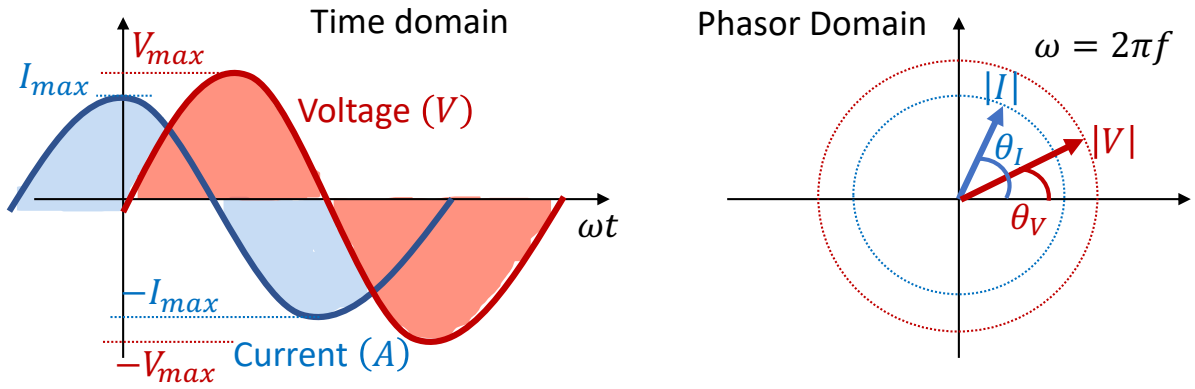

Figure 3.1. Current and voltage signals in time and phasor domain.

Notably, the introduction of admittance state variables also represents an introduction of nonlinearities within the previously linear set of equations that do not cause the distortion in a network signal, but rather enforce the desired constraints on its response while maintaining network feasibility (satisfied KCL and KVL). Even though the bilinear terms are analytic, and their derivative exists in complex domain [51], the additional constraints on a network response may not be in general. Therefore, we next discuss the methodology behind the split-circuit concept [18]-[22] and demonstrate that the challenges introduced by the nonanalyticity of complex functions can be successfully overcome by splitting the complex network into two mutually coupled real and imaginary sub-networks.

3.2. Splitting the nonlinear complex circuit to ensure problem analyticity

In order to remove the nonanalyticity of nonlinear complex functions that constrain the network steady-state response, the main idea behind the split-circuit approach is to separate the complex governing network equations into their real and imaginary components and further represent them in terms of the two mutually coupled sub-circuits, namely real and imaginary circuits. Recalling that each of the complex current, voltage and admittance state variables, as well as the network admittances can be defined in cartesian coordinates, we first rewrite the set of governing network equations in terms of respective real and imaginary components:

$$\begin{gathered}\left[G_{RLC}+\mathrm{Tdiag}(\boldsymbol{G})+j\left(B_{RLC}+\mathrm{Tdiag}(\boldsymbol{B})\right)\right](\boldsymbol{V_R}+j\boldsymbol{V_I})+\boldsymbol{I_{SR}}+E_N\boldsymbol{I_{VR}}+j(\boldsymbol{I_{SI}}+E_N\boldsymbol{I_{VI}})=\boldsymbol{0} \\ E_N\boldsymbol{V_R}-\boldsymbol{V_{SR}}+j(E_N\boldsymbol{V_I}-\boldsymbol{V_{SI}})=\boldsymbol{0} \\ f_G(\boldsymbol{V_R},\boldsymbol{V_I},\boldsymbol{I_{VR}},\boldsymbol{I_{VI}},\boldsymbol{G},\boldsymbol{B})=\boldsymbol{0} \\ f_B(\boldsymbol{V_R},\boldsymbol{V_I},\boldsymbol{I_{VR}},\boldsymbol{I_{VI}},\boldsymbol{G},\boldsymbol{B})=\boldsymbol{0}\end{gathered} \tag{3.2}$$

The real-valued set of algebraic equations from (3.3) that governs a split-circuit equivalent of an original problem is then obtained by separating the respective complex governing equations to their real and imaginary components. Most importantly, the split-circuit equations are now differentiable, and the NR can be applied without loss of generality.

$$\begin{gathered}[G_{RLC}+\mathrm{Tdiag}(\boldsymbol{G})]\boldsymbol{V_R}-[B_{RLC}+\mathrm{Tdiag}(\boldsymbol{B})]\boldsymbol{V_I}+\boldsymbol{I_{SR}}+E_N\boldsymbol{I_{VR}}=\boldsymbol{0} \\ [G_{RLC}+\mathrm{Tdiag}(\boldsymbol{G})]\boldsymbol{V_I}+[B_{RLC}+\mathrm{Tdiag}(\boldsymbol{B})]\boldsymbol{V_R}+\boldsymbol{I_{SI}}+E_N\boldsymbol{I_{VI}}=\boldsymbol{0} \\ E_N\boldsymbol{V_R}-\boldsymbol{V_{SR}}=\boldsymbol{0} \\ E_N\boldsymbol{V_I}-\boldsymbol{V_{SI}}=\boldsymbol{0} \\ f_G(\boldsymbol{V_R},\boldsymbol{V_I},\boldsymbol{I_{VR}},\boldsymbol{I_{VI}},\boldsymbol{G},\boldsymbol{B})=\boldsymbol{0} \\ f_B(\boldsymbol{V_R},\boldsymbol{V_I},\boldsymbol{I_{VR}},\boldsymbol{I_{VI}},\boldsymbol{G},\boldsymbol{B})=\boldsymbol{0}\end{gathered} \tag{3.3}$$

Next, to map a set of equations from (3.3) to an equivalent circuit that is iteratively solved as discussed in Chapter 2, we consider each of the network elements separately, map their governing equations to the respective split-circuit models, linearize them if needed, and then

hierarchically combine them in order to build a set of network equations that now correspond to a linearized problem from (3.3).

Consider a network admittance element ($G + jB$), whose governing equation is defined by Ohm's Law in terms of phasor current ($I_{GB,R} + jI_{GB,I}$) and voltage ($V_{GB,R} + jV_{GB,I}$) variables given in rectangular coordinates as:

$$I_{GB,R} + jI_{GB,I} = (G + jB)\left(V_{GB,R} + jV_{GB,I}\right) \tag{3.4}$$

The equations that govern a split-circuit representation of an admittance are then obtained by splitting (3.4) to its real and imaginary current components as:

$$\begin{aligned} I_{GB,R} &= GV_{GB,R} - BV_{GB,I} \\ I_{GB,I} &= GV_{GB,I} + BV_{GB,R} \end{aligned} \tag{3.5}$$

As it can be seen from (3.5), the terms where the real and imaginary admittance currents are proportional to the respective real and imaginary voltages can be, by Ohm's Law, mapped to conductances, while the terms that relate the real current to the imaginary voltage as well as imaginary current to the real voltage represent the coupling between the two sub-circuits and govern the voltage controlled current sources. Therefore, the split-circuit representation of an admittance from (3.4) corresponds to a conductance (G) in parallel with a voltage controlled current source, as shown in Figure 3.2. Additionally, all of the remaining network models that can be encountered in defining the linear AC network response represent linear current and voltage sources that can be trivially mapped to the split-circuit domain (separating real and imaginary components), as it is presented in Figure 3.2.

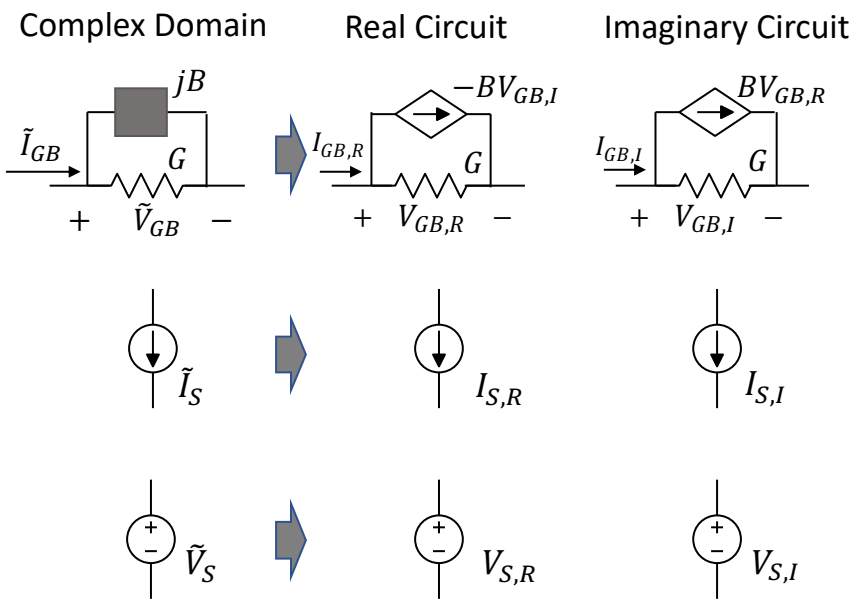

Figure 3.2. Mapping the network models defining the linear AC response to the split-circuit domain.

It should be noted that the unknown admittance variables introduce the bilinear nonlinearities to the split-circuit governing equations from (3.5) and, therefore, have to be linearized by means of first order Taylor expansion around the $(k+1)^{th}$ iteration, together with the additional constraint functions. The linearized unknown admittance currents and the respective constraints added can then be simplified to obtain:

$$
\begin{aligned}
I_{GB,R}^{k+1} &= G^k V_{GB,R}^{k+1} - B^k V_{GB,I}^{k+1} + G^{k+1} V_{GB,R}^{k} - B^{k+1} V_{GB,I}^{k} - G^k V_{GB,R}^{k} + B^k V_{GB,I}^{k} \\
I_{GB,I}^{k+1} &= G^k V_{GB,I}^{k+1} + B^k V_{GB,R}^{k+1} + G^{k+1} V_{GB,I}^{k} + B^{k+1} V_{GB,R}^{k} - G^k V_{GB,I}^{k} - B^k V_{GB,R}^{k} \\
f_G\left(X_G^k\right) &+ \nabla f_G^T\left(X_G^k\right)\left(X_G^{k+1} - X_G^k\right) = 0 \\
f_B\left(X_B^k\right) &+ \nabla f_B^T\left(X_B^k\right)\left(X_B^{k+1} - X_B^k\right) = 0
\end{aligned}
\tag{3.6}
$$

Referring to the linearized real and imaginary currents from (3.6), the terms where the real and imaginary currents ($I_{GB,R}^{k+1}$ and $I_{GB,I}^{k+1}$) are proportional to the real and imaginary voltages ($V_{GB,R}^{k+1}$ and $V_{GB,I}^{k+1}$) by Ohm's Law, and represent conductance. In this case the G^k from previous NR iteration, while the legacy terms known from the previous NR iteration represent a constant current source. All other components correspond to the coupling terms and can be mapped to the controlled current sources, as presented in Figure 3.3. Furthermore, the additional linearized constraints are added directly to the set of circuit equations for the introduced admittance state variables.

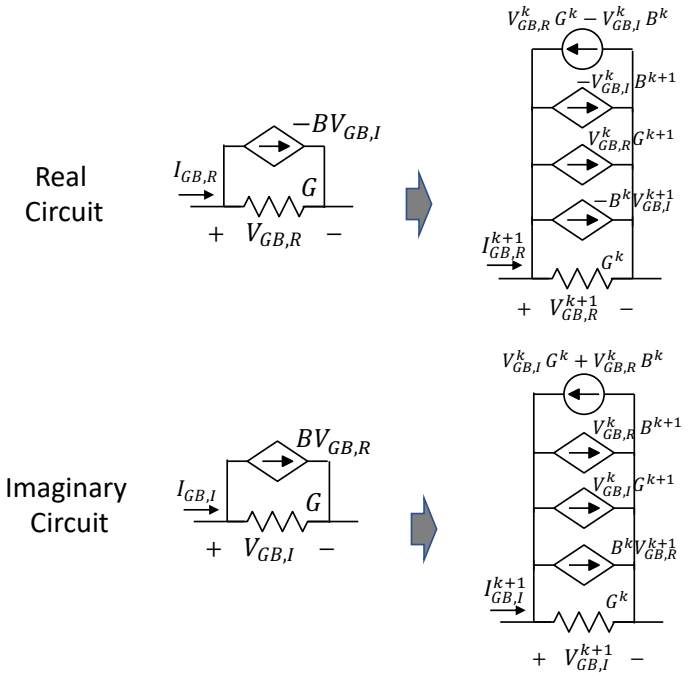

Figure 3.3. Linearized split-circuit representation of an unknown admittance.

The derivation of the linearized split-circuit model of an admittance allows for the additional constraints on a linear AC response, and concludes the generalized split-circuit modeling and its extension to the adjoint domain follows in the next section.

3.3. Generalization of Adjoint Circuit theory

Consider a network γ modeled in terms of the generalized formulation for defining its steady-state response and its topologically equivalent adjoint $\widehat{\gamma}$, with $\tilde{\boldsymbol{I}}$, $\tilde{\boldsymbol{V}}$, $\tilde{\boldsymbol{\mathfrak{T}}}$ and $\tilde{\boldsymbol{\lambda}}$ representing network and adjoint network steady-state branch currents and voltages in phasor domain respectively. Since the network state is now also represented in terms of admittance state variables, i.e. $\boldsymbol{Y_{GB}} = \boldsymbol{G} + j\boldsymbol{B}$, let $\boldsymbol{\lambda_Y}$ be a new set of *adjoint admittance* variables $\boldsymbol{\lambda_Y} \in [\boldsymbol{\lambda_G}, \boldsymbol{\lambda_B}]$ that are introduced for each of the additional constraints on the network steady state response, $f_G(\cdot)$ and $f_B(\cdot)$.

As is the case with the linear network model discussed in Chapter 2, Tellegen's Theorem defined by (2.29)-(2.30) must hold. However, due to the nonlinearities within the generalized modeling formulation, Tellegen's Theorem only holds at the operating point (solution), and it is further expected that the nonlinearities introduced in the original network γ also translate to its

adjoint. Moreover, inspired by Tellegen's Theorem and under the assumption that the set of additional constraints on network response is defined in terms of differentiable real valued functions, namely $\boldsymbol{f_Y}(\cdot)$, we can additionally define a third equation that relates the adjoint admittance variables with the respective constraints as:

$$\begin{gathered}\tilde{\boldsymbol{\lambda}}^H\tilde{\boldsymbol{I}} = 0 \\ \tilde{\mathfrak{T}}^H\tilde{\boldsymbol{V}} = 0 \\ \boldsymbol{\lambda}_{\boldsymbol{Y}}^T\boldsymbol{f_Y}(\cdot) = 0\end{gathered} \tag{3.7}$$

Notably, since $\boldsymbol{f_Y}(\cdot)$ vanishes at the solution, the third equation from (3.7) holds without loss of generality. Moreover, prior to perturbing the network admittances $Y_{RLC} \to Y_{RLC} + \delta Y_{RLC}$ and admittance states $\boldsymbol{Y_{GB}} \to \boldsymbol{Y_{GB}} + \delta\boldsymbol{Y_{GB}}$ to establish the generalized relationship between the original and adjoint network elements, we first obtain the small-signal model [14]-[15] for the additional set of constraints on network steady state response. Namely, for a small network perturbance, the set of equations $\bar{\boldsymbol{f}}_{\boldsymbol{Y}}(\boldsymbol{X} + \delta\boldsymbol{X})$ follows:

$$\bar{\boldsymbol{f}}_{\boldsymbol{Y}}(\boldsymbol{X} + \delta\boldsymbol{X}) = \boldsymbol{f_Y}(\boldsymbol{X}) + \nabla^T\boldsymbol{f_Y}\delta\boldsymbol{X} \equiv \nabla^T\boldsymbol{f_Y}\delta\boldsymbol{X} \tag{3.8}$$

where $\boldsymbol{X}$ defines a vector of network split circuit state variables, i.e. $\boldsymbol{X} = [\boldsymbol{V_R^T}\ \boldsymbol{V_I^T}\ \boldsymbol{G}^T\ \boldsymbol{B}^T]$.

The network is then perturbed; i.e. $\tilde{\boldsymbol{V}} \to \tilde{\boldsymbol{V}} + \delta\tilde{\boldsymbol{V}}$ and $\tilde{\boldsymbol{I}} \to \tilde{\boldsymbol{I}} + \delta\tilde{\boldsymbol{I}}$, in order to obtain a governing equation for each of the network branch currents as the ones given in (3.9), where $\Upsilon = Y_{RLC} + \mathrm{Tdiag}(\boldsymbol{Y_{GB}})$, $\delta\Upsilon = \delta Y_{RLC} + \mathrm{Tdiag}(\delta\boldsymbol{Y_{GB}})$ and $\Upsilon = \Upsilon_{\mathrm{G}} + j\Upsilon_{\mathrm{B}}$. It is important to note that as in the case of independent current sources $\tilde{\boldsymbol{I}}_{\boldsymbol{S}}$, relating the linear voltage sources to the adjoint domain is trivial, namely turning OFF, and hence they are omitted from the further derivations.

$$\begin{gathered}[\Upsilon + \delta\Upsilon](\tilde{\boldsymbol{V}} + \delta\tilde{\boldsymbol{V}}) + \tilde{\boldsymbol{I}}_{\boldsymbol{S}} = \tilde{\boldsymbol{I}} + \delta\tilde{\boldsymbol{I}} \Longrightarrow \\ \Upsilon\delta\tilde{\boldsymbol{V}} + \delta\Upsilon\tilde{\boldsymbol{V}} \approx \delta\tilde{\boldsymbol{I}} \Longrightarrow \\ \Upsilon_{\mathrm{G}}\delta\boldsymbol{V_R} - \Upsilon_B\delta\boldsymbol{V_I} + \delta\Upsilon_{\mathrm{G}}\boldsymbol{V_R} - \delta\Upsilon_B\boldsymbol{V_I} = \delta\boldsymbol{I_R} \\ \Upsilon_{\mathrm{G}}\delta\boldsymbol{V_I} + \Upsilon_B\delta\boldsymbol{V_R} + \delta\Upsilon_{\mathrm{G}}\boldsymbol{V_I} + \delta\Upsilon_B\boldsymbol{V_R} = \delta\boldsymbol{I_I}\end{gathered} \tag{3.9}$$

The perturbed expressions obtained from Tellegen's Theorem are then given in complex and split-circuit domains as:

$$\begin{aligned}
\tilde{\boldsymbol{\lambda}}^H\left(\tilde{\boldsymbol{I}}+\delta\tilde{\boldsymbol{I}}\right) &\equiv \tilde{\boldsymbol{\lambda}}^H\delta\tilde{\boldsymbol{I}} \equiv \boldsymbol{\lambda}_{\boldsymbol{R}}^T\delta\boldsymbol{I}_{\boldsymbol{R}} + \boldsymbol{\lambda}_{\boldsymbol{I}}^T\delta\boldsymbol{I}_{\boldsymbol{I}} = 0 \\
\tilde{\mathfrak{T}}^H\left(\tilde{\boldsymbol{V}}+\delta\tilde{\boldsymbol{V}}\right) &\equiv \tilde{\mathfrak{T}}^H\delta\tilde{\boldsymbol{V}} \equiv \mathfrak{T}_{\boldsymbol{R}}^T\delta\boldsymbol{V}_{\boldsymbol{R}} + \mathfrak{T}_{\boldsymbol{I}}^T\delta\boldsymbol{V}_{\boldsymbol{I}} = 0 \\
\boldsymbol{\lambda}_{\boldsymbol{Y}}^T[\boldsymbol{f}_{\boldsymbol{Y}}(\boldsymbol{X}) + \nabla\boldsymbol{f}_{\boldsymbol{Y}}\delta\boldsymbol{X}] &\equiv \boldsymbol{\lambda}_{\boldsymbol{Y}}^T\nabla^T\boldsymbol{f}_{\boldsymbol{Y}}\delta\boldsymbol{X} = 0
\end{aligned} \tag{3.10}$$

Furthermore, since all three equations from (3.10) hold at the perturbed solution, the following should also be true:

$$\boldsymbol{\lambda}_{\boldsymbol{R}}^T\delta\boldsymbol{I}_{\boldsymbol{R}} + \boldsymbol{\lambda}_{\boldsymbol{I}}^T\delta\boldsymbol{I}_{\boldsymbol{I}} - \mathfrak{T}_{\boldsymbol{R}}^T\delta\boldsymbol{V}_{\boldsymbol{R}} - \mathfrak{T}_{\boldsymbol{I}}^T\delta\boldsymbol{V}_{\boldsymbol{I}} + \boldsymbol{\lambda}_{\boldsymbol{Y}}^T\nabla^T\boldsymbol{f}_{\boldsymbol{Y}}\delta\boldsymbol{X} = 0 \tag{3.11}$$

which represents a basis for obtaining the elementwise mapping of the original generalized network elements to the respective adjoint ones.

Next, by substituting the real and imaginary current sensitivities from (3.9) to (3.11), expanding the last term of (3.11) and further grouping the similar sensitivities, the expression from (3.11) translates to:

$$\begin{aligned}
&\left[\boldsymbol{\lambda}_{\boldsymbol{R}}^T\Upsilon_{\mathrm{G}} + \boldsymbol{\lambda}_{\boldsymbol{I}}^T\Upsilon_B + \boldsymbol{\lambda}_{\boldsymbol{G}}^T\nabla_{\boldsymbol{V}_{\boldsymbol{R}}}^T\boldsymbol{f}_{\boldsymbol{G}} + \boldsymbol{\lambda}_{\boldsymbol{B}}^T\nabla_{\boldsymbol{V}_{\boldsymbol{R}}}^T\boldsymbol{f}_{\boldsymbol{B}} - \mathfrak{T}_{\boldsymbol{R}}^T\right]\delta\boldsymbol{V}_{\boldsymbol{R}} \\
&\quad + \left[\boldsymbol{\lambda}_{\boldsymbol{I}}^T\Upsilon_{\mathrm{G}} - \boldsymbol{\lambda}_{\boldsymbol{R}}^T\Upsilon_B + \boldsymbol{\lambda}_{\boldsymbol{G}}^T\nabla_{\boldsymbol{V}_{\boldsymbol{I}}}^T\boldsymbol{f}_{\boldsymbol{G}} + \boldsymbol{\lambda}_{\boldsymbol{B}}^T\nabla_{\boldsymbol{V}_{\boldsymbol{I}}}^T\boldsymbol{f}_{\boldsymbol{B}} - \mathfrak{T}_{\boldsymbol{I}}^T\right]\delta\boldsymbol{V}_{\boldsymbol{I}} \\
&\quad + [\boldsymbol{\lambda}_{\boldsymbol{R}}^T\delta\Upsilon_{\mathrm{G}} + \boldsymbol{\lambda}_{\boldsymbol{I}}^T\delta\Upsilon_B]\boldsymbol{V}_{\boldsymbol{R}} + [\boldsymbol{\lambda}_{\boldsymbol{I}}^T\delta\Upsilon_{\mathrm{G}} - \boldsymbol{\lambda}_{\boldsymbol{R}}^T\delta\Upsilon_B]\boldsymbol{V}_{\boldsymbol{I}} \\
&\quad + [\boldsymbol{\lambda}_{\boldsymbol{G}}^T\nabla_{\boldsymbol{G}}^T\boldsymbol{f}_{\boldsymbol{G}} + \boldsymbol{\lambda}_{\boldsymbol{B}}^T\nabla_{\boldsymbol{G}}^T\boldsymbol{f}_{\boldsymbol{B}}]\delta\boldsymbol{G} + [\boldsymbol{\lambda}_{\boldsymbol{G}}^T\nabla_{\boldsymbol{B}}^T\boldsymbol{f}_{\boldsymbol{G}} + \boldsymbol{\lambda}_{\boldsymbol{B}}^T\nabla_{\boldsymbol{B}}^T\boldsymbol{f}_{\boldsymbol{B}}]\delta\boldsymbol{B} = 0
\end{aligned} \tag{3.12}$$

A simplification to the expression in (3.12) is then made by factoring the real and imaginary adjoint currents ($\mathfrak{T}_{\boldsymbol{R}}, \mathfrak{T}_{\boldsymbol{I}}$) in terms of sum of branch current vectors that correspond to the network admittance elements ($\mathfrak{T}_{\boldsymbol{RL}}, \mathfrak{T}_{\boldsymbol{IL}}$) and the vectors that define the current flow through the real and imaginary branches of admittance states $\mathfrak{T}_{\boldsymbol{RY}}, \mathfrak{T}_{\boldsymbol{IY}}$. Furthermore, we enforce the relationships obtained in Chapter 2 for network admittances, i.e. (2.36).

$$\begin{aligned}
&\left[\text{diag}(\boldsymbol{G})T^T\boldsymbol{\lambda_R} + \text{diag}(\boldsymbol{B})T^T\boldsymbol{\lambda_I} + \nabla_{\boldsymbol{V_R}}\boldsymbol{f_G}\boldsymbol{\lambda_G} + \nabla_{\boldsymbol{V_R}}\boldsymbol{f_B}\boldsymbol{\lambda_B} - \boldsymbol{\mathfrak{T}_{RY}}\right]^T \delta\boldsymbol{V_R} \\
&\quad + \left[\text{diag}(\boldsymbol{G})T^T\boldsymbol{\lambda_I} - \text{diag}(\boldsymbol{B})T^T\boldsymbol{\lambda_R} + \nabla_{\boldsymbol{V_I}}\boldsymbol{f_G}\boldsymbol{\lambda_G} + \nabla_{\boldsymbol{V_I}}\boldsymbol{f_B}\boldsymbol{\lambda_B} - \boldsymbol{\mathfrak{T}_{IY}}\right]^T \delta\boldsymbol{V_I} \\
&\quad + \left[\text{diag}(\boldsymbol{V_R})T^T\boldsymbol{\lambda_R} + \text{diag}(\boldsymbol{V_I})T^T\boldsymbol{\lambda_I} + \nabla_{\boldsymbol{G}}\boldsymbol{f_G}\boldsymbol{\lambda_G} + \nabla_{\boldsymbol{G}}\boldsymbol{f_B}\boldsymbol{\lambda_B}\right]^T \delta\boldsymbol{G} \\
&\quad + \left[\text{diag}(\boldsymbol{V_R})T^T\boldsymbol{\lambda_I} - \text{diag}(\boldsymbol{V_I})T^T\boldsymbol{\lambda_R} + \nabla_{\boldsymbol{B}}\boldsymbol{f_G}\boldsymbol{\lambda_G} + \nabla_{\boldsymbol{B}}\boldsymbol{f_B}\boldsymbol{\lambda_B}\right]^T \delta\boldsymbol{B} = 0
\end{aligned} \tag{3.13}$$

In order for Tellegen's Theorem defined in (3.13) to remain satisfied, the following four relationships that govern the mapping of the admittance states and respective constraints on network steady-state response to the adjoint domain have to hold:

$$\begin{aligned}
\boldsymbol{\mathfrak{T}_{RY}} &= \text{diag}(\boldsymbol{G})T^T\boldsymbol{\lambda_R} + \text{diag}(\boldsymbol{B})T^T\boldsymbol{\lambda_I} + \nabla_{\boldsymbol{V_R}}\boldsymbol{f_G}\boldsymbol{\lambda_G} + \nabla_{\boldsymbol{V_R}}\boldsymbol{f_B}\boldsymbol{\lambda_B} \\
\boldsymbol{\mathfrak{T}_{IY}} &= \text{diag}(\boldsymbol{G})T^T\boldsymbol{\lambda_I} - \text{diag}(\boldsymbol{B})T^T\boldsymbol{\lambda_R} + \nabla_{\boldsymbol{V_I}}\boldsymbol{f_G}\boldsymbol{\lambda_G} + \nabla_{\boldsymbol{V_I}}\boldsymbol{f_B}\boldsymbol{\lambda_B} \\
\text{diag}(\boldsymbol{V_R})T^T\boldsymbol{\lambda_R} &+ \text{diag}(\boldsymbol{V_I})T^T\boldsymbol{\lambda_I} + \nabla_{\boldsymbol{G}}\boldsymbol{f_G}\boldsymbol{\lambda_G} + \nabla_{\boldsymbol{G}}\boldsymbol{f_B}\boldsymbol{\lambda_B} = \boldsymbol{0} \\
\text{diag}(\boldsymbol{V_R})T^T\boldsymbol{\lambda_I} &- \text{diag}(\boldsymbol{V_I})T^T\boldsymbol{\lambda_R} + \nabla_{\boldsymbol{B}}\boldsymbol{f_G}\boldsymbol{\lambda_G} + \nabla_{\boldsymbol{B}}^T\boldsymbol{f_B}\boldsymbol{\lambda_B} = \boldsymbol{0}
\end{aligned} \tag{3.14}$$

By examining the adjoint split-circuit governing equations from (3.14), it can be shown that as it was the case with network admittance derived in Chapter 2, an admittance state is defined by its complex conjugate translated to the adjoint split-circuit domain; i.e., first two terms of the real and imaginary adjoint current equations. Interestingly, in addition to the complex conjugate admittance, the second part of the adjoint current governing equations represents adjoint conductance and susceptance controlled by the gradient of the additional constraints on network steady-state response. Elementwise, governing equations for mapping an admittance state variable to adjoint split-circuit domain, as shown in Figure 3.4, can be written as:

$$\begin{aligned}
\mathfrak{T}_{RY} &= G\lambda_R + B\lambda_I + \sum_{i=1}^{|f_G|}\frac{\partial f_{G,i}}{\partial V_R}\lambda_{G,i} + \sum_{i=1}^{|f_B|}\frac{\partial f_{B,i}}{\partial V_R}\lambda_{B,i} \\
\mathfrak{T}_{IY} &= G\lambda_I - B\lambda_R + \sum_{i=1}^{|f_G|}\frac{\partial f_{G,i}}{\partial V_I}\lambda_{G,i} + \sum_{i=1}^{|f_B|}\frac{\partial f_{B,i}}{\partial V_I}\lambda_{B,i}
\end{aligned} \tag{3.15}$$

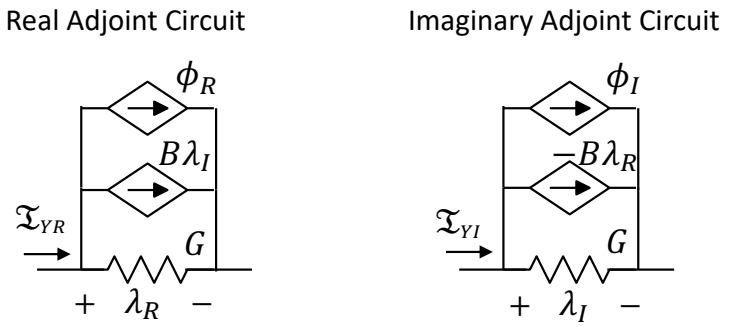

Figure 3.4. Adjoint split-circuit of an admittance state variable with respective constraints on network response.

Additionally, the second two equations from (3.14) correspond to the equations added for adjoint conductance and susceptance variables, and are elementwise given as:

$$\begin{aligned} f_{\lambda_G}(\cdot) &\equiv V_R\lambda_R + V_I\lambda_I + \sum_{i=1}^{|f_G|} \frac{\partial f_{G,i}}{\partial G} \lambda_{G,i} + \sum_{i=1}^{|f_B|} \frac{\partial f_{B,i}}{\partial G} \lambda_{B,i} = 0 \\ f_{\lambda_B}(\cdot) &\equiv V_R\lambda_I - V_I\lambda_R + \sum_{i=1}^{|f_G|} \frac{\partial f_{G,i}}{\partial B} \lambda_{G,i} + \sum_{i=1}^{|f_B|} \frac{\partial f_{B,i}}{\partial B} \lambda_{B,i} = 0 \end{aligned} \tag{3.16}$$

With the mapping of generalized steady-state network modeling to the adjoint domain established, Table 2.1 from Chapter 2 can be extended to include the relationship between the original and adjoint circuit representation of a conductance and susceptance state variables as presented in Table 3.1:

Table 3.1:Generalizing the mapping from an original to the adjoint network elements

Original Network		Adjoint Network
Independent current source ^{L}	→	open ^{L}
Independent voltage source ^{L}	→	short ^{L}
Network Conductance ^{L}	→	Network Conductance ^{L}
Network Susceptance ^{L}	→	Conjugate Network Susceptance ^{L}
Conductance State + $\boldsymbol{f_G}$ ^{NL}	→	Conductance State + Controlled Adjoint admittance ^{NL}
Susceptance State + $\boldsymbol{f_B}$ ^{NL}	→	Conjugate Susceptance + Controlled Adjoint admittance ^{NL}

*Where superscript (L) stands for linear models, while (NL) marks models that introduce nonlinearities within the generalized formulation

It is important to note from Table 3.1 that the excitation sources of the original network are turned off in the adjoint circuit, and hence its response will still be trivial, namely zero.

Lastly, as expected from the beginning, the nonlinearities introduced in the original network γ also translate to its adjoint, and hence need to be linearized as it was previously done in Section 3.2. with the bilinear nonlinearities introduced by admittance state variables. Therefore, we first linearize the adjoint real and imaginary currents from (3.15) as:

$$\begin{aligned}\mathfrak{T}_{RY}^{k+1} &= G^k\lambda_R^{k+1} + B^k\lambda_I^{k+1} + G^{k+1}\lambda_R^k + B^{k+1}\lambda_I^k + \nabla\phi_{R,k}^T\xi^{k+1} + i_{RY}^k \\ \mathfrak{T}_{IY}^{k+1} &= G^k\lambda_I^{k+1} - B^k\lambda_R^{k+1} + G^{k+1}\lambda_I^k - B^{k+1}\lambda_R^k + \nabla\phi_{I,k}^T\xi^{k+1} + i_{IY}^k\end{aligned} \tag{3.17}$$

where i_{RY}^k and i_{IY}^k correspond to the constant historic terms known from previous NR iteration, while ξ is a vector placeholder for state variable defining network and adjoint network responses, i.e. $\boldsymbol{\xi} = [V_R\ V_I\ G\ B\ \lambda_G\ \lambda_B]^T$.

Referring to (3.17), the terms that relate the real and adjoint imaginary currents ($\mathfrak{T}_{RY}^{k+1}$ and $\mathfrak{T}_{IY}^{k+1}$) to the real and imaginary voltages (λ_R^{k+1} and λ_I^{k+1}) by Ohm's Law represent conductance, while the legacy terms known from the previous NR iteration represent a constant current source. All other components correspond to the coupling terms and can be mapped to the controlled current sources as presented in Figure 3.5.

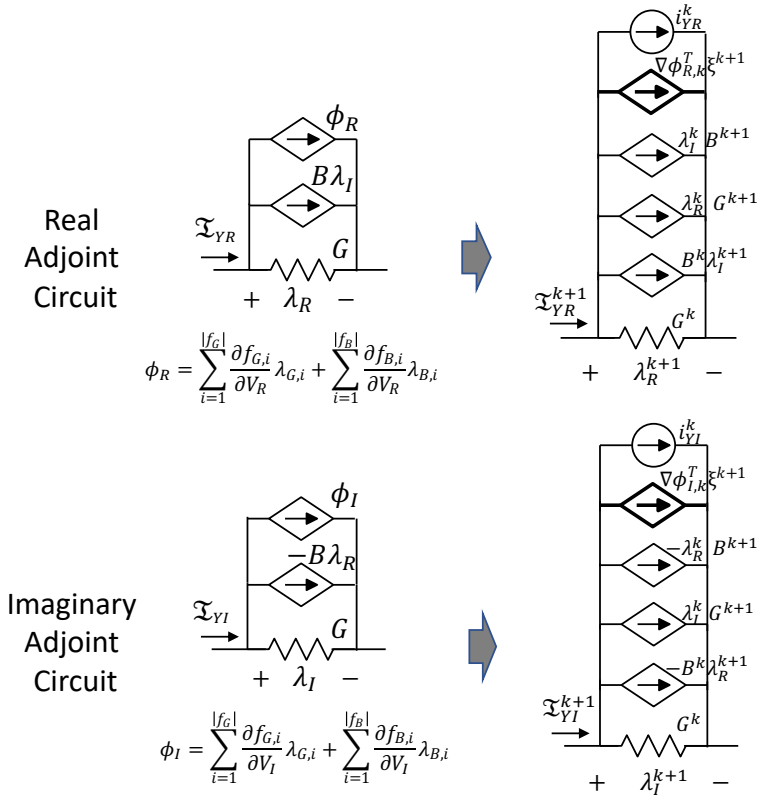

Figure 3.5. Linearized adjoint split-circuit representation of an admittance state.

The remaining two equations that correspond to the adjoint conductance and susceptance variables from (3.16) are expanded by means of first order Taylor expansion, and are directly included within the set of linearized split-circuit equations for the introduced adjoint admittance variables:

$$\begin{aligned} f_{\lambda_G}(\boldsymbol{\xi^k}) + \nabla f_{\lambda_G}^T(\boldsymbol{\xi^k})(\boldsymbol{\xi^{k+1}} - \boldsymbol{\xi^k}) = 0 \\ f_{\lambda_B}(\boldsymbol{\xi^k}) + \nabla f_{\lambda_B}^T(\boldsymbol{\xi^k})(\boldsymbol{\xi^{k+1}} - \boldsymbol{\xi^k}) = 0 \end{aligned} \tag{3.18}$$

In conclusion, with developed generalized and differentiable framework for modeling the linear AC network response and its unique mapping to the corresponding elements within the adjoint domain, all of the components required for the introduction of an Equivalent Circuit Program and its circuit representation are established. Therefore, the next chapter addresses the importance of further introduction of coupling between the original and its adjoint network, as well as the addition of new excitation sources within the adjoint circuit whose response is, as shown in this chapter, otherwise trivial.

Chapter 4 Equivalent Circuit Programming

Throughout the years, researchers and scientists have developed various different perspectives of interpreting the duality theory and the respective optimality conditions, which range from geometric to game-and-price interpretations, as discussed in [3]. Thus far, we have addressed the most important optimization and circuit simulation concepts, as well as introduced the generalized and differentiable framework for modeling the linear AC steady-state response, all of which represent fundamental components that further lead to our Equivalent Circuit Programming (ECP) problem.

This chapter provides an interpretation for optimality conditions of a network optimization problem from the perspective of equivalent circuits and conservation of energy within a system. It is demonstrated that for a given network and its uniquely defined adjoint, the additional excitation of adjoint network corresponds to embedding the optimization objective to the circuit problem, whose simulation now coincides with solving the KKT optimality conditions to obtain a candidate for an optimal solution. Most importantly, understanding the physical characteristics of dual problem from the equivalent circuit perspective is shown to provide a new insight regarding ECP problem feasibility and allows for introduction of new algorithms, such as the one discussed at the end of this chapter that is inspired by LASSO regularization. We further show that this formulation can be now applied to efficiently localize the infeasibilities within an ECP problem.

4.1. Defining an Equivalent Circuit Program (ECP)

Consider a network γ modeled in terms of the generalized formulation for defining its steady-state response within a split-circuit domain as given by (3.3), and let $\boldsymbol{X_L}$ and $\boldsymbol{X_U}$ represent the vectors of predefined network operational and performance upper and lower limits corresponding to each of the state variables as well as the additional constraints; i.e. $f_G(\cdot)$ and

$f_B(\cdot)$. Moreover, since each of the additional constraints define a particular physical quantity within the network, namely voltage or current magnitude, power, etc., for simplicity we can further introduce a set of slack variables $\boldsymbol{p_s}$ and $\boldsymbol{q_s}$ such that:

$$\begin{aligned} f_G(\cdot) - \boldsymbol{p_s} &= \mathbf{0} \\ f_B(\cdot) - \boldsymbol{q_s} &= \mathbf{0} \end{aligned} \tag{4.1}$$

It is important to emphasize that the slack variables now correspond to the constrained physical quantities and can be bounded instead of $f_G(\cdot)$ and $f_B(\cdot)$, without loss of generality. Finally, let $\mathcal{C}_{ckt}$ represent a set of network governing equations from (3.3) with additional slack variables as given in (4.2).

$$\mathcal{C}_{ckt}(\boldsymbol{x_s}) = \begin{bmatrix} \mathcal{I}_R \\ \mathcal{I}_I \\ \mathcal{V}_R \\ \mathcal{V}_I \\ \mathcal{P} \\ \mathcal{Q} \end{bmatrix} = \begin{cases} [G_{RLC} + \mathrm{Tdiag}(\boldsymbol{G})]\boldsymbol{V_R} - [B_{RLC} + \mathrm{Tdiag}(\boldsymbol{B})]\boldsymbol{V_I} + \boldsymbol{I_{SR}} + E_N\boldsymbol{I_R} \\ [B_{RLC} + \mathrm{Tdiag}(\boldsymbol{B})]\boldsymbol{V_R} + [G_{RLC} + \mathrm{Tdiag}(\boldsymbol{G})]\boldsymbol{V_I} + \boldsymbol{I_{SI}} + E_N\boldsymbol{I_I} \\ E_N\boldsymbol{V_R} - \boldsymbol{V_{SR}} \\ E_N\boldsymbol{V_I} - \boldsymbol{V_{SI}} \\ f_G(\boldsymbol{x}) - \boldsymbol{p_s} \\ f_B(\boldsymbol{x}) - \boldsymbol{q_s} \end{cases} = 0 \tag{4.2}$$

where $\boldsymbol{x} = \left[\boldsymbol{V_R^T}, \boldsymbol{V_I^T}, \boldsymbol{I_R^T}, \boldsymbol{I_I^T}, \boldsymbol{G^T}, \boldsymbol{B^T}\right]$, and $\boldsymbol{x_s} = [\boldsymbol{x^T}, \boldsymbol{p_s^T}, \boldsymbol{q_s^T}]$.

For the network γ whose steady-state response is modeled by (4.2), an Equivalent Circuit Program is defined as a problem of optimizing a network performance or operating condition:

$$\min_{\boldsymbol{x_S} \in C_{ECP}} \mathcal{F}(\boldsymbol{V_R}, \boldsymbol{V_I}, \boldsymbol{G}, \boldsymbol{B}, \boldsymbol{p_s}, \boldsymbol{q_s}) \tag{4.3}$$

subject to the set of network governing equations, as well as the operational and performance limits represented by a set C_{ECP}:

$$C_{ECP} = \{\boldsymbol{x_s} | \mathcal{C}_{ckt}(\boldsymbol{x_s}) = \mathbf{0}, \boldsymbol{X_L} < \boldsymbol{x_s} < \boldsymbol{X_U}\} \tag{4.4}$$

4.2. Equivalent Circuit Perspective for Interpreting ECP Optimality Conditions

With the generalized definition of an ECP introduced, we next analyze its set of necessary and sufficient optimality conditions and further demonstrate their relation to the equivalent split-circuit representation of a network and its respective adjoint circuit.

4.2.1. Necessary KKT optimality conditions

We start the derivation of necessary KKT optimality conditions by defining the Lagrangian function of an ECP problem from (4.3) as:

$$\begin{aligned}\mathcal{L}(\cdot) = \mathcal{F}(\cdot) + \boldsymbol{\lambda}_{\boldsymbol{R}}^{T}\mathcal{I}_R + \boldsymbol{\lambda}_{\boldsymbol{I}}^{T}\mathcal{I}_I + \boldsymbol{\mathfrak{T}}_{\boldsymbol{R}}^{T}\mathcal{V}_R + \boldsymbol{\mathfrak{T}}_{\boldsymbol{I}}^{T}\mathcal{V}_I + \boldsymbol{\lambda}_{\boldsymbol{G}}^{T}\,\mathcal{P} + \boldsymbol{\lambda}_{\boldsymbol{B}}^{T}\,\mathcal{Q} + \boldsymbol{\mu}_{\boldsymbol{L}}^{T}(\boldsymbol{X_L} - \boldsymbol{x_s}) \\ + \boldsymbol{\mu}_{\boldsymbol{U}}^{T}(\boldsymbol{x_s} - \boldsymbol{X_U})\end{aligned} \tag{4.5}$$

where $\boldsymbol{\lambda_R}$, $\boldsymbol{\lambda_I}$, $\boldsymbol{\mathfrak{T}_R}$, $\boldsymbol{\mathfrak{T}_I}$, $\boldsymbol{\lambda_G}$, $\boldsymbol{\lambda_B}$, $\boldsymbol{\mu_L}$ and $\boldsymbol{\mu_U}$ represent dual variables related to the respective network governing equations as well as upper and lower operational and performance bounds.

Prior to discussing each of the three components that define the set of KKT optimality conditions, namely, primal and dual problems as well as complementary slackness conditions, it is important to emphasize the resemblance of the terms related to the set of network constraints from (4.5), with the expression of Tellegen's Theorem that characterizes the conservation of energy within the network, as defined in Chapter 3 (3.11).

4.2.1.1. Primal problem – governing network split-circuit equations

As the first component of the KKT conditions, the primal problem that also corresponds to a set of network governing equations within the split-circuit domain, is obtained by differentiating the Lagrangian function from (4.5) with respect to dual variables related to the set of network equations, namely $\boldsymbol{\lambda_R}$, $\boldsymbol{\lambda_I}$, $\boldsymbol{\mathfrak{T}_R}$, $\boldsymbol{\mathfrak{T}_I}$, $\boldsymbol{\lambda_G}$, $\boldsymbol{\lambda_B}$:

$$\mathcal{C}_{ckt}(\boldsymbol{x_s}) = \mathbf{0} \tag{4.6}$$

Moreover, from the perspective of solving a circuit simulation problem, the primal problem from (4.6) can be obtained by elementwise linearization of the nonlinearities within the network

governing equations, as discussed in Chapter 3, and hierarchical building of linearized set of split-circuit equations that is now iteratively solved together with the other two components of KKT conditions.

4.2.1.2. Dual problem – Adjoint network split-circuit equations with additional excitations

Contrary to the primal problem that is trivially mapped to the equivalent split-circuit domain, an equivalent circuit representation of the dual problem is a little bit more interesting and is governed by the idea of the adjoint networks. To highlight this relationship, the governing equations of an ECP dual problem are obtained by differentiating the Lagrangian function from (4.5) with respect to the primal network state variables as:

$$\nabla_{\boldsymbol{V_R}}\mathcal{L}(\cdot) \equiv [G_{RLC} + \mathrm{diag}(\boldsymbol{G})T^T]\lambda_R + [B_{RLC} + \mathrm{diag}(\boldsymbol{B})T^T]\lambda_I + E_N^T\boldsymbol{\mathfrak{T}_R} + \nabla_{\boldsymbol{V_R}}f_G(\cdot)\boldsymbol{\lambda_G} + \nabla_{\boldsymbol{V_R}}f_B(\cdot)\boldsymbol{\lambda_B} + \nabla_{\boldsymbol{V_R}}\mathcal{F}(\cdot) + \boldsymbol{\mu_{U,V_R}} - \boldsymbol{\mu_{L,V_R}} = \mathbf{0} \tag{4.7}$$

$$\nabla_{\boldsymbol{V_I}}\mathcal{L}(\cdot) \equiv [G_{RLC} + \mathrm{diag}(\boldsymbol{G})T^T]\lambda_I - [B_{RLC} + \mathrm{diag}(\boldsymbol{B})T^T]\lambda_R + E_N^T\boldsymbol{\mathfrak{T}_I} + \nabla_{\boldsymbol{V_I}}f_G(\cdot)\boldsymbol{\lambda_G} + \nabla_{\boldsymbol{V_I}}f_B(\cdot)\boldsymbol{\lambda_B} + \nabla_{\boldsymbol{V_I}}\mathcal{F}(\cdot) + \boldsymbol{\mu_{U,V_I}} - \boldsymbol{\mu_{L,V_I}} = \mathbf{0} \tag{4.8}$$

$$\nabla_{\boldsymbol{G}}\mathcal{L}(\cdot) \equiv \mathrm{diag}(\boldsymbol{V_R})T^T\boldsymbol{\lambda_R} + \mathrm{diag}(\boldsymbol{V_I})T^T\boldsymbol{\lambda_I} + \nabla_{\boldsymbol{G}}\boldsymbol{f_G}\boldsymbol{\lambda_G} + \nabla_{\boldsymbol{G}}\boldsymbol{f_B}\boldsymbol{\lambda_B} + \nabla_{\boldsymbol{G}}\mathcal{F}(\cdot) + \boldsymbol{\mu_{U,G}} - \boldsymbol{\mu_{L,G}} = \mathbf{0} \tag{4.9}$$

$$\nabla_{\boldsymbol{B}}\mathcal{L}(\cdot) \equiv \mathrm{diag}(\boldsymbol{V_R})T^T\boldsymbol{\lambda_I} - \mathrm{diag}(\boldsymbol{V_I})T^T\boldsymbol{\lambda_R} + \nabla_{\boldsymbol{B}}\boldsymbol{f_G}\boldsymbol{\lambda_G} + \nabla_{\boldsymbol{B}}\boldsymbol{f_B}\boldsymbol{\lambda_B} + \nabla_{\boldsymbol{B}}\mathcal{F}(\cdot) + \boldsymbol{\mu_{U,B}} - \boldsymbol{\mu_{L,B}} = \mathbf{0} \tag{4.10}$$

$$\nabla_{\boldsymbol{I_R}}\mathcal{L}(\cdot) \equiv E_N^T\boldsymbol{\lambda_R} = \mathbf{0} \tag{4.11}$$

$$\nabla_{\boldsymbol{I_I}}\mathcal{L}(\cdot) \equiv E_N^T\boldsymbol{\lambda_I} = \mathbf{0} \tag{4.12}$$

$$\nabla_{\boldsymbol{p_s}}\mathcal{L}(\cdot) \equiv -\boldsymbol{\lambda_G} + \nabla_{\boldsymbol{p_s}}\mathcal{F}(\cdot) + \boldsymbol{\mu_{U,p_s}} - \boldsymbol{\mu_{L,p_s}} = \mathbf{0} \tag{4.13}$$

$$\nabla_{\boldsymbol{q_s}}\mathcal{L}(\cdot) \equiv -\boldsymbol{\lambda_B} + \nabla_{\boldsymbol{q_s}}\mathcal{F}(\cdot) + \boldsymbol{\mu_{U,q_s}} - \boldsymbol{\mu_{L,q_s}} = \mathbf{0} \tag{4.14}$$

After taking a closer look, particularly at (4.7)-(4.12), it can be seen that they exactly correspond to the adjoint split-circuit governing equations derived in Chapter 3 (3.14), with one

major difference. Namely, a given set of adjoint split-circuit equations from (3.14) that can be further written in the form of:

$$\mathcal{A}_{ckt}(\boldsymbol{x}, \boldsymbol{\lambda_R}, \boldsymbol{\lambda_I}, \mathfrak{T}_{\boldsymbol{R}}, \mathfrak{T}_{\boldsymbol{I}}, \boldsymbol{\lambda_G}, \boldsymbol{\lambda_B}) = \mathbf{0} \tag{4.15}$$

does not have excitation sources and hence its response is trivial. To that end, it should be noted that (4.11)-(4.12) constrain the adjoint voltages of a voltage source network branch to zero, thereby turning it OFF, as defined in Table 3.1. Contrary to (4.15), the adjoint circuit defined within the dual ECP problem is *excited by the gradient of objective function* and the additional set of dual (adjoint) variables related to the upper and lower operational and performance bounds, which only provides an additional excitation in the case a bound becomes active (bounded variable is at the limit). Moreover, (4.13)-(4.14) represent a set of equations that are added for the slack variables introduced to further control the additional constraints on the network steady-state response. Therefore, for the vector of excitation sources $\boldsymbol{\psi_S} = \nabla \mathcal{F}_{\boldsymbol{x_s}}(\boldsymbol{x_S}) + \boldsymbol{\mu_U} - \boldsymbol{\mu_L}$, we can further define a set of excited adjoint split-circuit equations as:

$$\bar{\mathcal{A}}_{ckt}(\cdot) = \mathcal{A}_{ckt}(\boldsymbol{x}, \boldsymbol{\lambda_R}, \boldsymbol{\lambda_I}, \mathfrak{T}_{\boldsymbol{R}}, \mathfrak{T}_{\boldsymbol{I}}, \boldsymbol{\lambda_G}, \boldsymbol{\lambda_B}) + \boldsymbol{\psi_S} = \mathbf{0} \tag{4.16}$$

Lastly, by following the same methodology used to derive the linearized adjoint split-circuit in Chapter 3, the linearized form of an adjoint network from (4.16) is hierarchically built by connecting the split-circuit models for each of the network devices and iteratively solving it together with the primal problem, while ensuring the primal and dual feasibility at each iteration.

4.2.1.3. Complementary Slackness (CS) conditions – Diode Controlled circuits

The third component of the KKT optimality conditions represent the complementary slackness equations that enforce the bounds on the respective network state variables. As is the case in the Interior Point methods discussed in Chapter 2, the CS conditions are approximated by introducing a vector of small constants $\boldsymbol{\varepsilon}$ such as:

$$\begin{aligned} \boldsymbol{\mu_L} \odot (\boldsymbol{X_L} - \boldsymbol{x_s}) &= -\boldsymbol{\varepsilon} \\ \boldsymbol{\mu_U} \odot (\boldsymbol{x_s} - \boldsymbol{X_U}) &= -\boldsymbol{\varepsilon} \end{aligned} \tag{4.17}$$

It is important to note that each of the CS equations from (4.17) represent the steep "switch-like" nonlinearities that resemble diodes in circuit simulation problems, as shown in Figure 4.1. Namely, after a certain voltage point across a diode is exceeded, it starts conducting current. Similarly, in the case of a CS condition, as the bounded state variable approaches its limit, an adjoint current $\boldsymbol{\mu_L}$ or $\boldsymbol{\mu_U}$ "activates" and becomes nonzero. These current values are precisely governed by the amount of current needed to excite the adjoint circuit such that a respective variable remains at the limit, while ensuring the problem feasibility (KCL and KVL in both network and its adjoint).

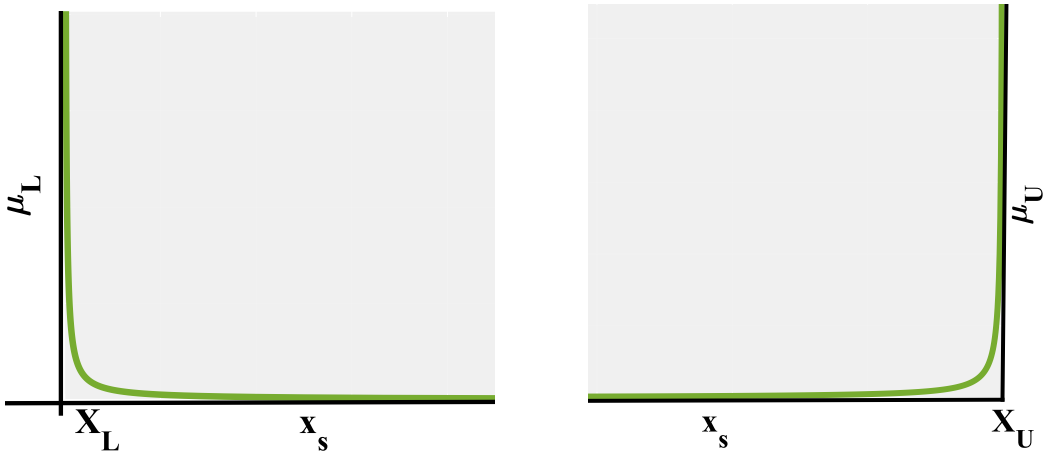

Figure 4.1. Representation of upper and lower CS conditions for a fixed small CS violation parameter ε.

Importantly, when it comes to algorithms applied to solving the problems with CS conditions, the traditional state-of-art Interior Point methods usually handle the steepness of CS nonlinearities by some form of a path tracing homotopy, which once combined with a single step limiting line-search algorithms, can significantly slow down the solution process as well as become stuck within the infeasible regions from which it cannot recover. In contrast, as discussed in Chapter 2, the circuit simulation community has developed several efficient diode-limiting techniques that when included with the other simulation methods allow for robust and efficient large-scale circuit simulations with millions of variables. Therefore, instead of homotopically varying the CS violation parameter ε, we fix it directly to the preset small value ranging from 10^{-6} to 10^{-12}. From a set of new algorithms developed based on physical characteristics of the ECP problem that is inspired by the idea of diode limiting, we have developed a new algorithm solely for the purpose of handling the CS constraints, whose detailed description is provided in the following chapter.

4.2.2. Second order Sufficient optimality conditions

Followed by simulating a circuit whose governing equations correspond to the first order KKT optimality condition of an ECP problem from (4.3), the obtained operating point represents an optimal solution to the problem in the local surrounding area only if the second order sufficient condition is met. Namely, there does not exist a small perturbation to the circuit operating point $\delta \boldsymbol{x_s}$ that will further decrease the value of objective function, or as given in Chapter 2, the second order sensitivity of the Lagrangian function evaluated at optimal solution, $\nabla^2_{xx}\mathcal{L}(*)$ has to be positive definite for small feasible perturbations around an optimal point given as:

$$\delta \boldsymbol{x}_s^T \nabla^2_{xx}\mathcal{L}(*)\delta \boldsymbol{x_s} > 0, \forall[\delta \boldsymbol{x_s} \neq \boldsymbol{0}] \in \text{Null}\left(\nabla_{\boldsymbol{x_s}} C_{ECP}\right) \tag{4.18}$$

To obtain a physical interpretation of the sufficient condition from (4.18), it is important to highlight the equivalence of its expression to the one defined in terms of perturbations of adjoint excitation sources (gradient of objective function), and the other primal network-controlled adjoint currents, $\boldsymbol{\mathfrak{T}_X}$:

$$\delta \boldsymbol{x}_s^T\left[\nabla_{\boldsymbol{x_s}} \boldsymbol{\psi_S}(*) + \nabla_{\boldsymbol{x_s}} \boldsymbol{\mathfrak{T}_X}(*)\right]\delta \boldsymbol{x_s} \equiv \delta \boldsymbol{x}_s^T[\delta \boldsymbol{\psi_S} + \delta \boldsymbol{\mathfrak{T}_X}] > 0 \tag{4.19}$$

Hence, we postulate the following Lemma to reformulate the sufficient condition from (4.18) in terms of conservation of energy within the adjoint circuit.

Lemma 4.1. *Passivity of the adjoint circuit.* An operating point of the coupled network and its respective additionally excited adjoint is said to be an optimal operating point and a solution to the ECP problem if the adjoint circuit remains passive [53] for all small feasible perturbations around its operating point.

Proof. Recall the Tellegen's Theorem defined for the adjoint circuit:

$$\boldsymbol{x}_s^T[\boldsymbol{\psi_S} + \boldsymbol{\mathfrak{T}_X} + \boldsymbol{\mathfrak{T}_L}] = 0 \tag{4.20}$$

where $\boldsymbol{\mathfrak{T}_L}$ correspond to the linear adjoint currents not dependent on primal network response (e.g. linear RLC network in adjoint domain).

After applying the small feasible perturbation from (4.18) to the network operating point $\boldsymbol{x_s} \rightarrow \boldsymbol{x_s} + \delta \boldsymbol{x_s}$, the adjoint circuit responds and the respective adjoint excitation and currents within the

adjoint network are perturbed, namely, $\boldsymbol{\psi_S} \rightarrow \boldsymbol{\psi_S} + \delta\boldsymbol{\psi_S}$, $\boldsymbol{\mathfrak{T}_X} \rightarrow \boldsymbol{\mathfrak{T}_X} + \delta\boldsymbol{\mathfrak{T}_X}$ and $\boldsymbol{\mathfrak{T}_L} \rightarrow \boldsymbol{\mathfrak{T}_L} + \delta\boldsymbol{\mathfrak{T}_L}$ such that the conservation of energy within a system holds and thus (4.20) can be rewritten and further simplified with enforcing the Tellegen's theorem as:

$$\begin{aligned}(\boldsymbol{x_s} + \delta\boldsymbol{x_s})^T[\boldsymbol{\psi_S} + \delta\boldsymbol{\psi_S} + \boldsymbol{\mathfrak{T}_X} + \delta\boldsymbol{\mathfrak{T}_X} + \boldsymbol{\mathfrak{T}_L} + \delta\boldsymbol{\mathfrak{T}_L}] \equiv \\ \delta\boldsymbol{x_s}^T[\delta\boldsymbol{\psi_S} + \delta\boldsymbol{\mathfrak{T}_X}] + \delta\boldsymbol{x_s}^T\delta\boldsymbol{\mathfrak{T}_L} = -\boldsymbol{x_s}^T[\delta\boldsymbol{\psi_S} + \delta\boldsymbol{\mathfrak{T}_X} + \delta\boldsymbol{\mathfrak{T}_L}]\end{aligned} \tag{4.21}$$

Finally, due to the passivity of linear network elements (absorb the power) $\delta\boldsymbol{x_s}^T\delta\boldsymbol{\mathfrak{T}_L} > 0$ and therefore the sufficient condition is met if and only if $\delta\boldsymbol{x_s}^T[\delta\boldsymbol{\psi_S} + \delta\boldsymbol{\mathfrak{T}_X}] > 0$ or from (4.21):

$$-\boldsymbol{x_s}^T\delta\boldsymbol{\psi_S} > \boldsymbol{x_s}^T[\delta\boldsymbol{\mathfrak{T}_X} + \delta\boldsymbol{\mathfrak{T}_L}] \tag{4.22}$$

Namely, for a given ECP problem such as the one from (4.3), and by following the reference or passive sign direction of current flows [15], the additional power supplied by the adjoint excitation sources due to the applied perturbation ($\boldsymbol{x_s}^T\delta\boldsymbol{\psi_S}$) has to be greater than the power supplied by the rest of adjoint circuit. Most importantly, this condition represents a well-defined characteristic in circuit theory and is known as passivity of the circuit [53]. ■

As it is demonstrated, an equivalent circuit perspective to the ECP problem and its respective optimality conditions provides the new intuition on understanding the physical characteristics of the problem. Moreover, *solving an ECP optimization corresponds to solving a circuit simulation problem of coupled network and its additionally excited adjoint, whose passivity around the operating point further guarantees its optimality*. Lastly, before introducing the set of algorithms and techniques for solving an ECP problem that are obtained by utilizing its physical characteristics, the last part of the chapter provides a discussion on the ECP problem feasibility.

4.3. On Feasibility of an ECP from the equivalent circuit perspective

So far, we have presented the equivalent circuit representation of the ECP problem KKT optimality conditions, as well as derived the sufficient conditions based on circuit theoretic principles that can be used as a check for the optimality of an operating point. However, the complete physical interpretation of the adjoint circuit variables in reference to the network steady-

state operating point is still to be discussed. To that end, this section provides an interpretation of the adjoint circuit variables from the perspective of analyzing an ECP problem feasibility and the conservation of energy within a system.

Notably, a completely defined equivalent circuit response governed by KCL and KVL equations represents a natural optimization problem, where the current follows the path of the least resistance that minimizes the losses in the system. As demonstrated in the previous chapter and under the assumption of no illegal connections that violate the conservation of energy within the circuit [15], a linear AC network response is always feasible and its uniquely defined adjoint exists with a trivial response, namely equal to zero. Most importantly, once incorporated within the optimization problem, the operating point of the completely defined circuit represents an optimal solution independently of the objective function. Such steady-state operating point can be then additionally constrained to enforce the specific performance conditions with the introduction of admittance state variables that are now controlled in order to prevent the violation of KCL and KVL within a circuit. However, the introduced nonlinearities in modeling the network can result in over-constraining of its response, for which there doesn't exist an operating point that satisfies the set of governing circuit equations while preserving the conservation of energy within a system as given by Tellegen's Theorem. It follows that, the corresponding adjoint circuit cannot be defined.

In order to demonstrate that the infeasibility of the network equations can be utilized and "redirected" as an excitation to the adjoint circuit, we consider the following ECP problem:

$$\min_{\boldsymbol{x_S}, \boldsymbol{\varphi_s} \in C_{ECP,f}} \frac{1}{2} \|\boldsymbol{w} \odot \boldsymbol{\varphi_s}\|_2^2 \tag{4.23}$$

where $\boldsymbol{w} = \left[\boldsymbol{w}_{\boldsymbol{I_R}}^T \; \boldsymbol{w}_{\boldsymbol{I_I}}^T \; \boldsymbol{w}_{\boldsymbol{V_R}}^T \; \boldsymbol{w}_{\boldsymbol{V_I}}^T \; \boldsymbol{w}_{\boldsymbol{p}}^T \; \boldsymbol{w}_{\boldsymbol{q}}^T\right]$ represents a vector of weights on the respective infeasibility variables $\boldsymbol{\varphi_s} = [\boldsymbol{I}_{\boldsymbol{\Delta R}}^T \; \boldsymbol{I}_{\boldsymbol{\Delta I}}^T \; \boldsymbol{V}_{\boldsymbol{\Delta R}}^T \; \boldsymbol{V}_{\boldsymbol{\Delta I}}^T \; \boldsymbol{p}_{\boldsymbol{\Delta}}^T \; \boldsymbol{q}_{\boldsymbol{\Delta}}^T]$ related to the network response modeled in terms governing equations and bounds $C_{ECP,f}$:

$$C_{ECP,f} = \{\boldsymbol{x_s}, \boldsymbol{\varphi_s} | \mathcal{C}_{ckt}(\boldsymbol{x_s}) + \boldsymbol{\varphi_s} = \boldsymbol{0}, \boldsymbol{X_L} < \boldsymbol{x_s} < \boldsymbol{X_U}\} \tag{4.24}$$

The KKT optimality conditions are then obtain by defining the Lagrangian function for $\boldsymbol{\lambda}$ being a vector of adjoint variables, i.e. $\boldsymbol{\lambda} = [\boldsymbol{\lambda}_{\boldsymbol{R}}^T \; \boldsymbol{\lambda}_{\boldsymbol{I}}^T \; \boldsymbol{\mathfrak{T}}_{\boldsymbol{R}}^T \; \boldsymbol{\mathfrak{T}}_{\boldsymbol{I}}^T \; \boldsymbol{\lambda}_{\boldsymbol{G}}^T \; \boldsymbol{\lambda}_{\boldsymbol{B}}^T]$:

$$\mathcal{L}(\cdot) = \frac{1}{2}\|\boldsymbol{w} \odot \boldsymbol{\varphi_s}\|_2^2 + \boldsymbol{\lambda}^T(\mathcal{C}_{ckt}(\boldsymbol{x_s}) + \boldsymbol{\varphi_s}) + \boldsymbol{\mu_L^T}(\boldsymbol{X_L} - \boldsymbol{x_s}) + \boldsymbol{\mu_U^T}(\boldsymbol{x_s} - \boldsymbol{X_U}) \tag{4.25}$$

and differentiating it to come up to the original and adjoint network governing equations as given by (4.6) and (4.16), as well as a set of CS conditions. Lastly, (4.26) represents the final set of additional KKT equations corresponding to the introduced vector of network infeasibility variables $\boldsymbol{\varphi_s}$, and will further provide with an interpretation of the relationship between the adjoint and the network state variables:

$$\boldsymbol{w} \odot \boldsymbol{\varphi_s} + \boldsymbol{\lambda} = \boldsymbol{0} \equiv \boldsymbol{\varphi_s} = -\boldsymbol{m} \odot \boldsymbol{\lambda} \tag{4.26}$$

Where $\boldsymbol{m}$ corresponds to a vector that is inversely proportional to the vector of weights in pointwise sense, $m_i = \frac{1}{w_i}, \forall i \in [1, |w_i|]$, and can be also written as $\boldsymbol{m} = \left[\boldsymbol{m_{I_R}^T}\ \boldsymbol{m_{I_I}^T}\ \boldsymbol{m_{V_R}^T}\ \boldsymbol{m_{V_I}^T}\ \boldsymbol{m_p^T}\ \boldsymbol{m_q^T}\right]$.

The set of equations from (4.26) can be also written in terms of the infeasibility variables related to each of the respective components of $\boldsymbol{\varphi_s}$, namely:

$$\begin{gathered}
\boldsymbol{I_{\Delta R}} = -\boldsymbol{m_{I_R}} \odot \boldsymbol{\lambda_R}, \boldsymbol{I_{\Delta I}} = -\boldsymbol{m_{I_I}} \odot \boldsymbol{\lambda_I} \\
\boldsymbol{V_{\Delta R}} = -\boldsymbol{m_{V_R}} \odot \boldsymbol{\mathfrak{T}_R}, \boldsymbol{V_{\Delta I}} = -\boldsymbol{m_{V_I}} \odot \boldsymbol{\mathfrak{T}_I} \\
\boldsymbol{p_\Delta} = -\boldsymbol{m_p} \odot \boldsymbol{\lambda_G} \\
\boldsymbol{q_\Delta} = -\boldsymbol{m}_q \odot \boldsymbol{\lambda_B}
\end{gathered} \tag{4.27}$$

and further used to eliminate the infeasibility variables by replacing them with the respective scaled adjoint ones, which now corresponds to introducing the coupling between the network and its adjoint circuit as:

$$\mathcal{C}_{ckt}(\boldsymbol{x_s}) - \boldsymbol{m} \odot \boldsymbol{\lambda} = \boldsymbol{0} \tag{4.28}$$

From the equivalent circuit perspective, this coupling corresponds to addition of new sources within the original network that are now controlled by the respective points from adjoint circuit. Moreover, considering that the adjoint network is still not excited, its response will remain trivial as long as the network is feasible. However, if the set of network governing equations

becomes over-constrained and there doesn't exist an operating point that preserves the conservation of energy within a system, the excess or deficiency of energy is redirected to the adjoint circuit, and now represents a source of adjoint excitations that will act in order to minimize the energy transfer between the network and its adjoint. This corresponds to minimizing the L2-norm of the problem infeasibilities as given by (4.23).

Next, by further examination of the relationships between the network and adjoint state variables from (4.27), it can be seen that they follow a quite interesting pattern. Namely, once connected to the network through the coupling sources as in (4.28), *adjoint voltages represent the additional current sources within the network KCL equations*. Therefore, it can be said that the voltages of the adjoint circuit provide the necessary information related to the current infeasibility of the network, the information that once additionally included within the network equations tends to decrease the adjoint voltage to zero. Oppositely, the coupled *adjoint currents "act" like the additional voltage sources within the network KVL equations*, thereby carrying the information about the voltage infeasibility of the network.

The relationship between adjoint admittance variables and their respective representation within the network is, however, dependent on the introduced constraints $f_G(\cdot)$ and $f_B(\cdot)$. For instance, if the additional constraints define the relationship between the power supplied/absorbed by the admittance state variables, then the adjoint admittances can be seen as "power sources", and hence contain the information about the power excess/deficiency within the network. Lastly, it can be shown that the same perspective also holds for adjoint variables introduced for the set of complementary slackness conditions ($\boldsymbol{\mu_L}$ and $\boldsymbol{\mu_U}$). If a controlled network state variable approaches its limit and the CS constraint becomes active, its respective adjoint variable μ_L or μ_U will be related to the quantity that carries the information about the network infeasibility due to the bounded variable. Namely, it is proportional to the difference of the bounded variable and its value for the unbounded network response.

4.4. Localizing ECP infeasibility inspired by L1-norm regularization (LASSO)

As it can be seen from the previous section, the network infeasibility, i.e. nodes where the laws of conservation of energy cannot be satisfied, can be captured and quantified by the addition

of extra coupling between the network and its adjoint. For a given network defined in terms of a set of nodes $\mathcal{V}$ and the set of branches $\mathcal{E}$, it can be shown that in the most of realistic scenarios, the sources of infeasibility are sparsely distributed within the network and are introduced by the additional constraints on one of the network steady-state variables. Hence, the coupling of the network with its adjoint uses this excess/deficiency of energy and turns it into the excitation of the adjoint network at its respective node, which now ensures that the infeasibility is optimally allocated corresponding to L2-norm minimization problem. However, since the adjoint circuit as well as its respective network represents an interconnected system, the excitation of a particular node within the adjoint circuit causes the current to flow in the area around, which can further provide the additional excitation to the network nodes/branches that are not truly infeasible. Therefore, in this concluding section we introduce an algorithm inspired by the L1-norm regularization (LASSO), and demonstrate that its application can be used to efficiently quantify the correct spots of the network infeasibility, while removing the ones that are not truly infeasible, and thereby increasing the sparsity of the infeasible locations within the network.

In order to obtain the intuition behind the application of traditional L1 regularization to our ECP problem, such as the one defined in (4.23), we introduce the L1 regularization term for the vector of infeasibility variables $\boldsymbol{\varphi_s}$ as given by the ECP problem below:

$$\min_{\boldsymbol{t_{L_1}},\boldsymbol{x_s},\boldsymbol{\varphi_s}\in C_L} \frac{1}{2}\|\boldsymbol{w}\odot\boldsymbol{\varphi_s}\|_2^2 + \boldsymbol{\beta}^T\boldsymbol{t_{L_1}} \tag{4.29}$$

Where the set C_L represent the extended set from (4.24) that now includes the additional constraints on the regularization vector $\boldsymbol{t_{L_1}}$ as:

$$C_L = \left\{\boldsymbol{t_{L_1}}, \boldsymbol{x_s}, \boldsymbol{\varphi_s} | \mathcal{C}_{ECP,f}(\boldsymbol{x_s}, \boldsymbol{\varphi_s}), -\boldsymbol{t_{L_1}} < \boldsymbol{\varphi_s} < \boldsymbol{t_{L_1}}\right\} \tag{4.30}$$

The additional regularization corresponds to adding the extra terms to the Lagrangian function from (4.25) that is now augmented:

$$\mathcal{L}_{L1}(\cdot) = \mathcal{L}(\cdot) + \boldsymbol{\beta}^T\boldsymbol{t_{L_1}} + \boldsymbol{\mu}_+^T\left(\boldsymbol{\varphi_s} - \boldsymbol{t_{L_1}}\right) + \boldsymbol{\mu}_-^T\left(-\boldsymbol{t_{L_1}} - \boldsymbol{\varphi_s}\right) \tag{4.31}$$

and the respective KKT conditions related to the vector of infeasibility variables $\boldsymbol{\varphi_s}$, as well as the additional set of equations for the regularization variable $\boldsymbol{t_{L_1}}$ can be obtained as:

$$\nabla_{\boldsymbol{\varphi_s}}\mathcal{L}_{L1}(\cdot) \equiv \boldsymbol{w} \odot \boldsymbol{\varphi_s} + \boldsymbol{\lambda} + \boldsymbol{\mu}_+ - \boldsymbol{\mu}_- = \boldsymbol{0} \Rightarrow \boldsymbol{\varphi_s} = -\boldsymbol{m} \odot \boldsymbol{\lambda} + \boldsymbol{\mu}_- - \boldsymbol{\mu}_+ = \boldsymbol{0}$$
$$\nabla_{\boldsymbol{t_{L_1}}}\mathcal{L}_{L1}(\cdot) \equiv \boldsymbol{\beta} - (\boldsymbol{\mu}_- + \boldsymbol{\mu}_+) = \boldsymbol{0} \tag{4.32}$$

As can be seen from (4.32), adding the L1 regularization of the $\boldsymbol{\varphi_s}$, contributes with the additional terms to the set of equations that defines the network infeasibility variables, which is an indicator that for a good choice of $\boldsymbol{\beta}$ the places of nonzero adjoint variables that correspond to the network nodes that are not truly infeasible can be corrected. However, the key word here is "a good choice of $\boldsymbol{\beta}$", which cannot be known in advance.

Therefore, instead of solving the traditional L1-regularization problem with the hope that a we can somehow correctly guess the $\boldsymbol{\beta}$, we first take a closer look at the conditions from (4.32) by solving for $\boldsymbol{\mu}_+$from the second set of equations and substituting it in the KKT conditions that define the infeasibility variables as:

$$\boldsymbol{\varphi_s} = -\boldsymbol{m} \odot \boldsymbol{\lambda} + 2\boldsymbol{\mu}_- - \boldsymbol{\beta} \tag{4.33}$$

Due to the dual feasibility conditions that have to be ensured, it can be shown that the values of now redefined vector of infeasibility variables can only be within the range of:

$$\boldsymbol{\varphi_s} = -\boldsymbol{m} \odot \boldsymbol{\lambda} \pm \boldsymbol{\beta} \tag{4.34}$$

This even more strongly highlights the importance of $\boldsymbol{\beta}$ vector. Since if the i^{th} component of $\boldsymbol{\varphi_s}$ corresponds to falsely quantified infeasibility, the optimal pick for β_i would be the value that cancels the corresponding infeasibility.

From the perspective of an equivalent circuit, and considering that (4.34) also defines the coupling sources between the network and its adjoint, the vector $\boldsymbol{\beta}$ represents a set of additional sources that are added to "correct" the respective falsely quantified infeasibilities within the network. Moreover, for the initial feasibility problem of solving the coupled network and its adjoint, the value of $\boldsymbol{\beta}$ is not known, and can be therefore initially set to zero. Next, depending on the predefined condition for quantifying and locating the infeasibilities within the network, e.g. only allowed at particular nodes, the respective components of $\boldsymbol{\beta}$ are chosen as the negative values of coupling infeasibility sources. These values are added to the system model that will now tend

to decrease the respective adjoint variables of a particular network node after resolving the ECP problem. The iterative process of this algorithm inspired by LASSO and presented in Algorithm 4.1. is then repeated until one of the predefined stopping criteria based on the increased sparsity of the $\boldsymbol{\varphi_s}$vector is met.

Algorithm 4.1. *Greedy LASSO algorithm for infeasibility sparsification within an ECP problem.*
Given: maximum iteration count k_{max}, infeasible ECP problem with existing network nodes whose infeasibility may be corrected, rounding tolerance indicating infeasibilities $\epsilon_{INF} \in \mathbb{Z}^1$

Initialize: counter $k = 0$, $\boldsymbol{\beta}^{\{k\}} = \mathbf{0}$

- Based on desired criterion determine the set of network nodes $\mathfrak{C}_{err}$ whose infeasibility may be corrected

Repeat:

1. For $i = 1{:}\,\mathrm{mod}(\boldsymbol{m})$
   If $i \in \mathfrak{C}_{err}$, **then** $\beta^{\{k+1\}}(i) = \boldsymbol{m} \odot \boldsymbol{\lambda}^{\{\boldsymbol{k}\}} - \beta^{\{k\}}(i)$
   Else $\beta^{\{k+1\}}(i) = \beta^{\{k\}}(i)$
2. **Resolve an ECP equivalent circuit** given by adjoint circuit from (4.16), respective CS conditions and the set of network equations coupled to the adjoint circuit as:
$$\mathcal{C}_{ckt}(\boldsymbol{x_s}) - \boldsymbol{m} \odot \boldsymbol{\lambda} + \boldsymbol{\beta}^{\{k+1\}} = \mathbf{0}$$
3. Compute new vector of infeasibilities: $\boldsymbol{\varphi}^{\{k+1\}} = \mathrm{round}\left(-\boldsymbol{m} \odot \boldsymbol{\lambda}^{\{\boldsymbol{k+1}\}} + \boldsymbol{\beta}^{\{k+1\}}, \epsilon_{INF}\right)$
4. Recompute the set of network nodes $\mathfrak{C}_{err}$, whose infeasibilities needs correction
5. Stopping criterion. **Quit if** $[\mathfrak{C}_{err} = \emptyset]$ or $\left[\left\|\boldsymbol{\varphi}^{\{k+1\}}\right\|_{\mathbf{0}} \geq \left\|\boldsymbol{\varphi}^{\{k\}}\right\|_{\mathbf{0}} \& \left\|\boldsymbol{\varphi}^{\{k+1\}}\right\|_{\mathbf{2}}^{\mathbf{2}} \geq \left\|\boldsymbol{\varphi}^{\{k+1\}}\right\|_{\mathbf{2}}^{\mathbf{2}}\right]$ or $[k = k_{max}]$
6. Increase counter: $k \to k + 1$

In conclusion, this chapter provides the new equivalent circuit perspective on understanding a network optimization problem and its optimality conditions, as well as further demonstrating the connection between the problem physical characteristics and the mathematical optimization theory. Moreover, the theoretic background behind the concept of ECP, which also represents the first part this thesis, is completed in the next chapter that introduces the newly developed circuit simulation techniques that can be applied to ensure the robust and efficient solution process of an ECP problem.

Chapter 5 Solving an Equivalent Circuit Program

From the physical perspective, solving an Equivalent Circuit Program for an optimal solution candidate corresponds to simulating the response of a circuit consisting of a joint split-circuit representation of the network and its additionally excited adjoint. The further introduction of coupling between them ensures the simulation feasibility and provides the sparse locations of infeasibilities within the network. Moreover, if the adjoint circuit remains passive for all small perturbations around the obtained operating point, the point also represents an optimal solution to the simulated ECP problem. Having this in mind, and further inspired by the advantages of optimization and circuit simulation methods, this chapter introduces a new set of ECP simulation techniques obtained by fully exploiting the physical representation of an ECP problem and further merging the best features of both optimization and circuit simulation techniques together. To that end, a set of developed algorithms includes:

1. Constant Diode limiting
2. Dynamical Diode Limiting
3. Voltage Pre-Filtering Technique
4. Optimal Limiting
5. Sequential Optimal Limiting
6. Variable Post-Filtering Technique

To start the discussion on simulating an ECP circuit, let C_{ECP} represents its set of governing equations defined by the three subsets, namely a set of split-circuit network equations $\mathcal{C}_{ckt}$, a set of additionally excited adjoint circuit equations $\bar{\mathcal{A}}_{ckt}$, as well as a set of complementary slackness conditions (diode control circuits) $\mathcal{D}_{ckt}$ given by (5.1)

$$\mathrm{C}_{ECP}(\boldsymbol{x_s}, \boldsymbol{\lambda}, \boldsymbol{\mu}) = \begin{cases} \mathcal{C}_{ckt}(\boldsymbol{x_s}, \boldsymbol{\lambda}) \\ \bar{\mathcal{A}}_{ckt}(\boldsymbol{x_s}, \boldsymbol{\lambda}, \boldsymbol{\mu}) = \mathbf{0} \\ \mathcal{D}_{ckt}(\boldsymbol{x_s}, \boldsymbol{\mu}) \end{cases} \tag{5.1}$$

Similarly, as in the case of other circuit simulation problems from Chapter 2, we can further formulate the NR algorithm as given in Algorithm 5.1. It is, however, important to note a that the main difference now represents the applied circuit heuristics in Step 2, whose flowchart is further presented in Figure 5.1, that represents the main topic covered in the rest of the chapter.

Algorithm 5.1. NR *solution process for simulating an ECP equivalent circuit.*

Initialize:

- Starting point $\boldsymbol{\Upsilon_{ECP}^{0}}$, tolerance $\epsilon > 0$, counter $k = 0$
- Apply constant diode limiting to ensure primal feasibility of bounded variables **only**

Stamp Linear circuit elements

Repeat:

5. Stamp linearized ECP - circuit elements evaluated at $\boldsymbol{\Upsilon_{ECP}^{k}}$ and compute NR step $\boldsymbol{\Delta\Upsilon_{ECP}}$ by solving a linearized circuit
6. **Apply ECP simulation techniques obtain a vectorized step-limit $\boldsymbol{T}$** (see Figure 5.1)
7. Update NR step: $\boldsymbol{\Upsilon_{ECP}^{k+1}} = \boldsymbol{\Upsilon_{ECP}^{k}} + \boldsymbol{T} \odot \boldsymbol{\Delta\Upsilon_{ECP}}$
8. Increase counter $k \rightarrow k + 1$

Until: $\|\boldsymbol{T} \odot \boldsymbol{\Delta\Upsilon_{ECP}}\|_\infty \leq \epsilon$ and $\|\mathrm{C}_{ECP}(\boldsymbol{x_s^k}, \boldsymbol{\lambda}^k, \boldsymbol{\mu}^k)\|_2^2 \leq \epsilon$

As can be seen from Algorithm 5.1, for a given initial starting point that *only needs to be feasible for the bounded primal and respective adjoint variables*, the linearized equivalent circuit is hierarchically built and iteratively solved while applying the ECP simulation techniques, until convergence. Moreover, in referring to the Figure 5.1, the diode-like CS conditions represent the steepest nonlinearities within the circuit, and hence a set of diode heuristics (1)-(2) plays an important role and is applied before any other developed technique. Next, followed by the application of diode limiting, the voltages of both network and its adjoint are pre-filtered (3). Namely, inspired by the fixed-step limiting from the circuit simulation community, the voltages below a certain threshold are passed to the next iteration and are not further affected by the following applied techniques. However, contrary to the fixed-step limiting approaches, the voltage steps that exceed the threshold are not set to a fixed point but are rather passed further to the

optimal limiting technique (4) that represents the 3D version of exact line search problem, which is generally allowed due to the nature of nonlinearities within the network.

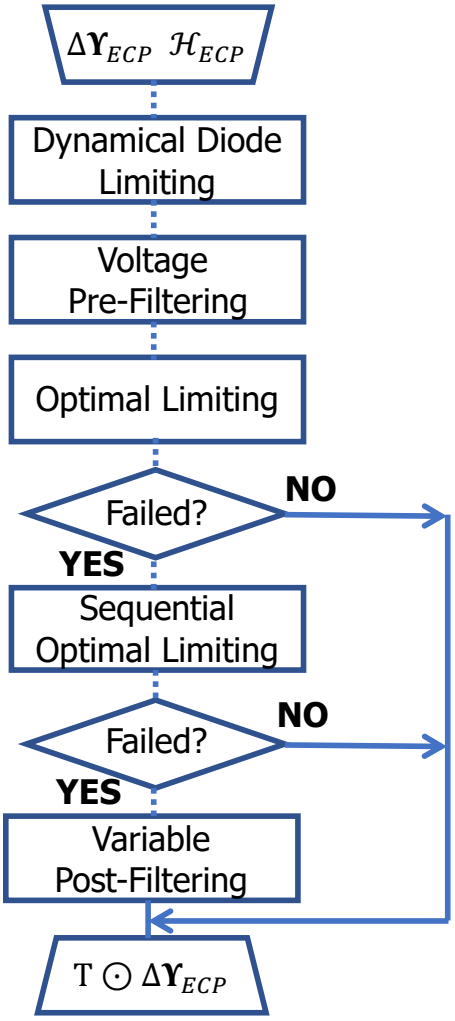

Figure 5.1. Flowchart of simulation techniques applied to limit the NR-step within the ECP solution process. Note the additional input that represents a set of heuristic parameters ($\mathcal{H}_{ECP}$) this time obtained from the physical characteristics of ECP problems.

Most importantly, if the Optimal Limiting fails to find the three step limiting factors that can decrease the ECP circuit residual, the algorithm further attempts to solve it within the two stages (5). In the first one, the exact line search is applied to minimize the residual of network equations only, and the obtained optimal step limiting factors are then used in attempt to further decrease the residual of the adjoint circuit. Lastly, in the worst case scenario, when the Sequential Optimal Limiting fails, we cannot count on optimally decreasing the circuit residual anymore, and the last technique applies the filtering of solution vector (6) purely based on the understanding of physical characteristics of the problem, as is currently done in SPICE.

Next, we provide a detailed discussion on each of the techniques briefly mentioned above.

5.1. Constant Diode Limiting

As it is well known and discussed in Chapter 2, the steep diode-like nonlinearities tend to cause the simulation overflow if not handled properly. Moreover, for a considered pair of complementary slackness conditions that enforce the limits on a particular network variable, it is important to ensure that during the NR iterations, the respective bounded primal and adjoint variables never exceed these implicitly modeled limits, and are always kept within the physically meaningful region of the solution search-space. Furthermore, in contrast to the traditional optimization IPMs that tend to find a single largest constant that ensures the feasibility of all variables, inspired by the circuit simulation approach we can further obtain the step limiting factor per each of the bounded variables. For instance, let $x_{s,i}$ be a network state with the respective adjoint variables related to its upper and lower bounds $\mu_{U,i}$ and $\mu_{L,i}$. The step limiting factors that strictly ensure their feasibility can be then computed as given by (5.2)-(5.4) for $\alpha_{DFS} = 1$.

$$\tau_{x_s,i} = \begin{cases} \min\left[1, \alpha_{DFS} \dfrac{X_{U,i} - x_{s,i}^k}{\Delta x_{s,i}}\right] & \text{if } \Delta x_{s,i} > 0 \\ \min\left[1, \alpha_{DFS} \dfrac{X_{L,i} - x_{s,i}^k}{\Delta x_{s,i}}\right] & \text{if } \Delta x_{s,i} < 0 \end{cases} \tag{5.2}$$

$$\tau_{\mu_U,i} = \begin{cases} \min\left[1, \alpha_{DFS} \dfrac{\mu_{min,i} - \mu_{U,i}^k}{\Delta \mu_{U,i}}\right] & \text{if } \Delta \mu_{U,i} < 0 \\ 1 & \text{else} \end{cases} \tag{5.3}$$

$$\tau_{\mu_L,i} = \begin{cases} \min\left[1, \alpha_{DFS} \dfrac{\mu_{min,i} - \mu_{L,i}^k}{\Delta \mu_{L,i}}\right] & \text{if } \Delta \mu_{L,i} < 0 \\ 1 & \text{else} \end{cases} \tag{5.4}$$

where $\mu_{min,i}$ is lowest possible value of the adjoint variable due to the CS approximation:

$$\mu_{min,i} = \frac{\varepsilon}{X_{U,i} - X_{L,i}} > 0 \tag{5.5}$$

However, if the bounded variable is set strictly at its limit, the problem will still overflow, and therefore, as in the case of fixed-step technique discussed in Chapter 2, the main idea behind this

diode limiting technique is to limit the rate on which the particular variable approaches its limit by reducing the damping factor α_{DFS}, as graphically presented in Figure 5.2.

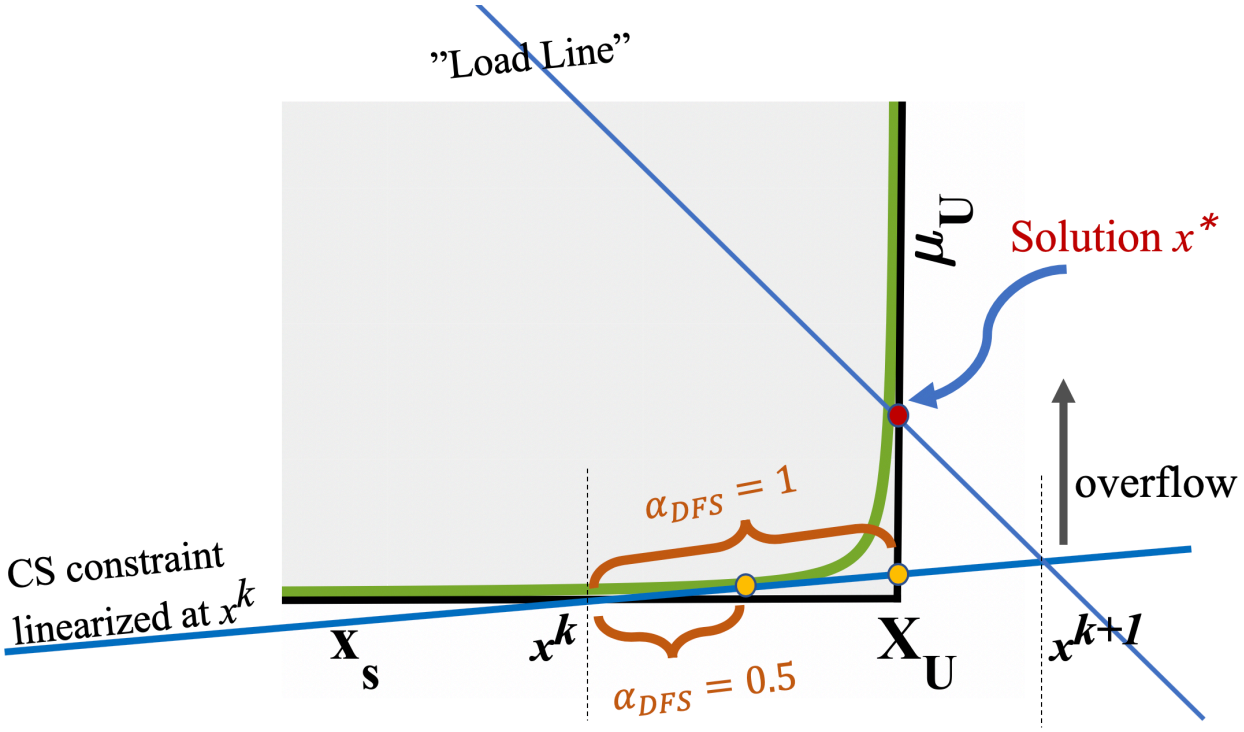

Figure 5.2. Graphical representation of a constant diode limiting technique.

For instance, as it can be seen from Figure 5.2, setting $\alpha_{DFS} = 0.5$ ensures that if a variable approaches its upper limit, the respective NR step is limited to the half way between the previous NR solution and the limit. Furthermore, after the rate of approaching the limit is damped, the step size limiting factor can be obtained from (5.2)-(5.4) for each of the variables separately and further used to update the solution vector as:

$$x_{s,i}^{k+1} = x_{s,i}^{k} + \tau_{x_s,i}\Delta x_{s,i} \tag{5.6}$$

$$\mu_{U,i}^{k+1} = \mu_{U,i}^{k} + \tau_{\mu_U,i}\Delta \mu_{U,i} \tag{5.7}$$

$$\mu_{L,i}^{k+1} = \mu_{L,i}^{k} + \tau_{\mu_L,i}\Delta \mu_{L,i} \tag{5.8}$$

As it is highlighted in Algorithm 5.1., this diode limiting technique is applied during the initialization process in order to ensure the primal feasibility of the bounded variables. Therefore, by using the midpoint between the upper and lower bounds as an $x_{s,i}^{k}$ value, and letting the initial

guess be $x_{s,i}^{k+1}$, we can further compute the required step limiting factor by (5.2), and use it to "correct" the initial guess if needed, as given by (5.6).

Lastly, it is important to emphasize that the general idea behind diode limiting techniques corresponds to applying the damping of respective NR steps to ensure that the CS conditions are completely satisfied only at the convergence of the entire circuit. Interestingly, a similar idea can be found behind the traditional IPMs that homotopically modify the complementary slackness violation parameter ε, and hence the CS function steepness, in order to reach the same goal; Namely, CS conditions are satisfied at the final problem convergence. Furthermore, with the constant diode limiting technique and a constant parameter α_{DFS} that is independent of circuit residual, the CS decrement cannot be always as efficiently controlled. Hence, the algorithm may require tuning of α_{DFS} in order to prevent the scenarios of a badly conditioned NR matrix way before the convergence of the remainder of the circuit, which can further result in significant slowing down of the convergence process due to the saturation of optimal limiting algorithms. Therefore, the ECP heuristics only uses constant diode limiting within the initialization process, in part to ensure strict feasibility before the actual damping of the rate at which CS is decreased within the residual dependent Dynamical Diode limiting.

5.2. Dynamical Diode Limiting

In order to ensure the stable control of the CS decrement that approaches the value of CS violation parameter ε concurrently with the convergence of the ECP circuit, we need to ensure that for some set of parameters, $\rho_{max,i}$ and $\rho_{min,i}$, the following two conditions hold:

$$\begin{aligned} \mu_{U,i}^{k+1}\left(X_{U,i} - x_{s,i}^{k+1}\right) &> \left[1 - \rho_{max,i}\right]\mu_{U,i}^{k}\left(X_{U,i} - x_{s,i}^{k}\right) \\ \mu_{L,i}^{k+1}\left(x_{s,i}^{k+1} - X_{L,i}\right) &> \left[1 - \rho_{min,i}\right]\mu_{L,i}^{k}\left(x_{s,i}^{k} - X_{L,i}\right) \end{aligned} \tag{5.9}$$

The CS violation at the $(k+1)^{th}$ NR iteration should decrease by no more than as set by parameters $\rho_{max,i}$ and $\rho_{min,i}$, and have the following characteristics:

- **Dependence on the initial CS violation**: the smaller initial CS violation is, the smaller values of $\rho_{max,i}$ and $\rho_{min,i}$. Primal and adjoint variables should be more damped in order to wait for the convergence of the rest of the ECP circuit.

- **Dependence on the ECP circuit L2 residual:** inversely proportional to the residual of the circuit – smaller $\rho_{max,i}$ and $\rho_{min,i}$, with increase in L2 residual– more damping in order to catch up with the rest of the circuit, and vice versa.
- **Dependence on the initial ECP circuit L2 residual:** should be a function of initial residual in order to make it generic for any size problem – normalized by the initial L2 residual of the circuit.

Hence, we propose a function presented in Figure 5.3 that satisfied the following characteristics:

$$\rho(\chi_i) = \rho_{max,i} = \rho_{min,i} = \begin{cases} \dfrac{\log \chi_i}{\sqrt{\chi_i}} & \text{if } \chi_i > e^2 \\ \dfrac{2}{e} & \text{else} \end{cases} \tag{5.10}$$

where χ_i is further defined in terms of the three predefined characteristics of CS decrement control:

$$\chi_i = \begin{cases} \dfrac{\|\mathrm{C}_{ECP}(x_s^k, \lambda^k, \mu^k)\|_2^2}{\min\left[e^{-\frac{93}{30}}, \mu_{U,i}^0\left(X_{U,i} - x_{s,i}^0\right)\right] \|\mathrm{C}_{ECP}(x_s^0, \lambda^0, \mu^0)\|_2^2} & \text{for upper bound} \\ \dfrac{\|\mathrm{C}_{ECP}(x_s^k, \lambda^k, \mu^k)\|_2^2}{\min\left[e^{-\frac{93}{30}}, \mu_{L,i}^0\left(x_{s,i}^0 - X_{L,i}\right)\right] \|\mathrm{C}_{ECP}(x_s^0, \lambda^0, \mu^0)\|_2^2} & \text{for lower bound} \end{cases} \tag{5.11}$$

Importantly, there are several things that should be emphasized from Figure 5.3 and (5.10)-(5.11):

1. For the first iteration, the ratio of residuals from (5.11) is equal to 1, which means that the initial starting point of $\rho_{max,i}$ and $\rho_{min,i}$ is chosen based on the initial CS violation, as predefined by the CS control characteristics.
2. Independently on the CS control conditions, the initial $\rho_{max,i}$ and $\rho_{min,i}$ cannot be larger than the ones defined by the maximum curvature point of function from (5.10), namely the function given for the value of $\chi_{crit} = e^{\frac{93}{30}}$, so they can exhibit the dynamical variations with the change in ECP circuit residual.
3. The definition of the function (5.10) is purely based on the intuition of how the CS decrement should behave and was further inspired by diode limiting techniques (some of which are discussed in Chapter 2).

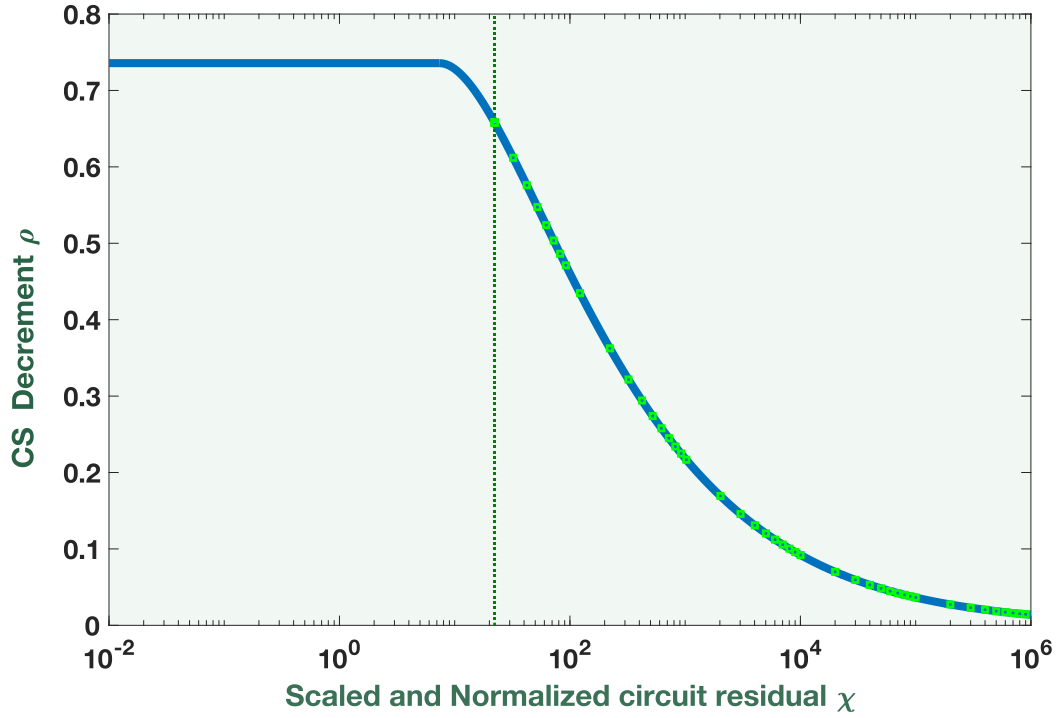

Figure 5.3. Dynamical Diode Limiting function that defines the amount of CS decrement for a given χ_i. Note that the vertical line indicates the point of maximum function curvature that also represents the highest initial CS decrement. The green dots further correspond to the possible initial starts that depend on the initial CS violation and are further varied as a function of normalized ECP L2 residual.

With the function that defines the desired behavior of $\rho_{max,i}$ and $\rho_{min,i}$ introduced, let $x_{s,i}$ again be a network state with the respective adjoint variables related to its upper and lower bounds $\mu_{U,i}$ and $\mu_{L,i}$. Hence, the step limiting factors ensure the controlled CS decrement as given by the conditions from (5.9) can be obtained by solving for variable-wise step limiting factors $\tau_{\mu_U,i}$, $\tau_{\mu_L,i}$ and $\tau_{x_s,i}$ from (5.12), while following the same logic as that used in Constant Diode limiting under the assumption of strict primal and dual feasibility that is ensured by the Constant Diode limiting.

$$\begin{aligned}\left(\mu_{U,i}^k + \tau_{\mu_U,i}\Delta\mu_{U,i}\right)\left(X_{U,i} - x_{s,i}^k - \tau_{x_s,i}\Delta x_{s,i}\right) &> \left[1 - \rho_{max,i}^k\right]\mu_{U,i}^k\left(X_{U,i} - x_{s,i}^k\right)\\ \left(\mu_{L,i}^k + \tau_{\mu_L,i}\Delta\mu_{L,i}\right)\left(x_{s,i}^k + \tau_{x_s,i}\Delta x_{s,i} - X_{L,i}\right) &> \left[1 - \rho_{min,i}^k\right]\mu_{L,i}^k\left(x_{s,i}^k - X_{L,i}\right)\end{aligned} \tag{5.12}$$

The exact solution recipe for determining the limiting factors $\tau_{\mu_U,i}$, $\tau_{\mu_L,i}$ and $\tau_{x_s,i}$ is further provided in Algorithm 5.2.

Algorithm 5.2. *Dynamical Diode Limiting for a pair of upper and lower CS conditions*

Given: $\rho_{max,i}^{k}$, $\rho_{min,i}^{k}$, $X_{U,i}$, $X_{L,i}$, $\mu_{U,i}^{k}$, $\mu_{L,i}^{k}$, $x_{s,i}^{k}$ and strictly feasible $\Delta x_{s,i}$, $\Delta\mu_{U,i}$, $\Delta\mu_{L,i}$

If $\Delta x_{s,i} > 0$

If $\Delta\mu_{U,i} > 0$

$$\tau_{\mu_U,i} = 1, \tau_{x_s,i} = \min\left[1, \frac{\left(X_{U,i} - x_{s,i}^{k}\right)\left(\rho_{max,i}^{k}\mu_{U,i}^{k} + \Delta\mu_{U,i}\right)}{\Delta x_{s,i}\left(\mu_{U,i}^{k} + \Delta\mu_{U,i}\right)}\right] \tag{5.13}$$

Elseif $\Delta\mu_{U,i} < 0$

$$\tau_{\mu_U,i} = \tau_{x_s,i} = \tau_U$$

$$\tau_U = \min\left[1, 0.5\left[\frac{X_{U,i} - x_{s,i}^{k}}{\Delta x_{s,i}} - \frac{\mu_{U,i}^{k}}{\Delta\mu_{U,i}} - \sqrt{\left(\frac{X_{U,i} - x_{s,i}^{k}}{\Delta x_{s,i}} - \frac{\mu_{U,i}^{k}}{\Delta\mu_{U,i}}\right)^2 + \frac{4\rho_{max,i}^{k}\mu_{U,i}^{k}\left(X_{U,i} - x_{s,i}^{k}\right)}{\Delta x_{s,i}\Delta\mu_{U,i}}}\right]\right] \tag{5.14}$$

End

$$\tau_{\mu_L,i} = \min\left[1, \frac{\mu_{L,i}^{k}\left(\rho_{min,i}^{k}\left(x_{s,i}^{k} - X_{L,i}\right) + \tau_{x_s,i}\Delta x_{s,i}\right)}{\Delta\mu_{L,i}\left(x_{s,i}^{k} + \tau_{x_s,i}\Delta x_{s,i} - X_{L,i}\right)}\right] \tag{5.15}$$

End

If $\Delta x_{s,i} < 0$

If $\Delta\mu_{L,i} > 0$

$$\tau_{\mu_L,i} = 1, \tau_{x_s,i} = \min\left[1, \frac{\left(X_{L,i} - x_{s,i}^{k}\right)\left(\rho_{min,i}^{k}\mu_{L,i}^{k} + \Delta\mu_{L,i}\right)}{\Delta x_{s,i}\left(\mu_{L,i}^{k} + \Delta\mu_{L,i}\right)}\right] \tag{5.16}$$

Elseif $\Delta\mu_{L,i} < 0$

$$\tau_{\mu_L,i} = \tau_{x_s,i} = \tau_L$$

$$\tau_L = \min\left[1, 0.5\left[\frac{X_{L,i} - x_{s,i}^{k}}{\Delta x_{s,i}} - \frac{\mu_{L,i}^{k}}{\Delta\mu_{L,i}} - \sqrt{\left(\frac{X_{L,i} - x_{s,i}^{k}}{\Delta x_{s,i}} - \frac{\mu_{L,i}^{k}}{\Delta\mu_{L,i}}\right)^2 + \frac{4\rho_{min,i}^{k}\mu_{L,i}^{k}\left(X_{L,i} - x_{s,i}^{k}\right)}{\Delta x_{s,i}\Delta\mu_{L,i}}}\right]\right] \tag{5.17}$$

End

$$\tau_{\mu_{max}} = \min\left[1, \frac{\mu_{U,i}^{k}\left(\rho_{max,i}^{k}\left(X_{U,i} - x_{s,i}^{k}\right) - \tau_{x_s,i}\Delta x_{s,i}\right)}{\Delta\mu_{U,i}\left(X_{U,i} - x_{s,i}^{k} - \tau_{x_s,i}\Delta x_{s,i}\right)}\right] \tag{5.18}$$

End

Output: $\tau_{\mu_U,i}$, $\tau_{\mu_L,i}$ and $\tau_{x_s,i}$

Finally, after the dynamically varied diode limiting is applied to each of the respective pairs of bounded primal and adjoint variables, the solution vector is updated as specified in (5.6)-(5.8), while the linearized circuit should have the significantly better conditioning, and the algorithm and our discussion further moves towards the other techniques, starting with Voltage Pre-Filtering.

5.3. Voltage Pre-Filtering Technique

Inspired by the idea of a widely used circuit simulation technique, fixed-step limiting, Voltage Pre-Filtering technique represents a simple technique that has been empirically proven to be effective for improving the simulation efficiency by decreasing the iteration count of the NR solution process. Namely, for the predefined "trusted NR step size", the network and adjoint circuit voltage steps are allowed to pass unaffected through the limiting heuristics at the current NR iteration. Moreover, as was the case in diode fixed-step limiting, where the allowed step-size was corresponding to $2V_T$, the "trusted step size" in an ECP circuit can be related to the physically meaningful quantity that is trusted not to do any harm on the iterative process and usually varies around ± 1, to $\pm 2.5\%$ NR step change difference. However, contrary to the traditional circuit simulation methods, the voltage quantities above the predefined threshold are not capped to a particular value but are rather passed further through the set of additional ECP heuristics, starting with the Optimal Limiting. Finally, the Voltage Pre-Filtering Technique, whose pseudo code is given in Algorithm 5.3, can be justified particularly in the line search based algorithms, as is the Optimal Limiting, due to the fact that a circuit usually doesn't converge equally at all locations, and hence, some of the "trusted" NR steps may be unnecessarily damped thereby causing slower convergence in general.

Algorithm 5.3. *Voltage Pre-Filtering Technique*

Given: vectors of real and imaginary network and adjoint circuit voltages, $\boldsymbol{V}^{k+1}$,$\boldsymbol{V}^{k}$, $\boldsymbol{\lambda}^{k+1}$and $\boldsymbol{\lambda}^{k}$ as well as predefined thresholds ν_V and ν_λ

$$\boldsymbol{V}^k = \begin{cases} V_i^{k+1} & \text{if } \left|V_i^{k+1} - V_i^k\right| < \nu_V \\ V_i^k & \text{if } \left|V_i^{k+1} - V_i^k\right| > \nu_V \end{cases} \tag{5.19}$$

$$\boldsymbol{\lambda}^k = \begin{cases} \lambda_i^{k+1} & \text{if } \left|\lambda_i^{k+1} - \lambda_i^k\right| < \nu_\lambda \\ \lambda_i^k & \text{if } \left|\lambda_i^{k+1} - \lambda_i^k\right| > \nu_\lambda \end{cases} \tag{5.20}$$

Output: $\boldsymbol{V}^{k+1}$,$\boldsymbol{V}^{k}$, $\boldsymbol{\lambda}^{k+1}$and $\boldsymbol{\lambda}^{k}$

5.4. Optimal Limiting

Contrary to the development of previous techniques that are all inspired by the circuit simulation methods, the Optimal Limiting represents an application of exact line search solved in mathematical optimization problems, as discussed in Chapter 2, but with two significant differences:

1. Instead of traditionally solving a one-dimensional problem, the exact line search in Optimal Limiting is defined in three dimensions, one per set of conductance and susceptance states with corresponding slack variables, and the third one for the rest of the ECP circuit response (voltages, etc.)
2. Not all of the terms that contribute to the ECP circuit residual are considered. Namely, the set of CS constraints, $\mathcal{D}_{ckt}(\boldsymbol{x_s}, \boldsymbol{\mu})$, is not included within the search problem due to the fact the CS decrement is already sufficiently ensured within the Dynamical Diode Limiting.

Therefore, considering a set of network and respective adjoint circuit governing equations defined in (5.1), we can now introduce the 3D exact search problem in terms of the three step limiting factors τ_V, τ_G, τ_B as:

$$\begin{aligned}\min_{\tau_V,\tau_G,\tau_B\in[0,1]} &\|\mathcal{C}_{ckt}(\boldsymbol{v}^k + \tau_V\Delta\boldsymbol{v}, \boldsymbol{g}^k + \tau_G\Delta\boldsymbol{g}, \boldsymbol{b}^k + \tau_B\Delta\boldsymbol{b})\|_2^2 \\ &+ \|\bar{\mathcal{A}}_{ckt}(\boldsymbol{v}^k + \tau_V\Delta\boldsymbol{v}, \boldsymbol{g}^k + \tau_G\Delta\boldsymbol{g}, \boldsymbol{b}^k + \tau_B\Delta\boldsymbol{b})\|_2^2\end{aligned} \tag{5.21}$$

where vectors $\boldsymbol{g}$ and $\boldsymbol{b}$ correspond to the set of admittance state variables ($\boldsymbol{G}$ and $\boldsymbol{B}$) that can also include the additionally added slack variables ($\boldsymbol{p_s}$ and $\boldsymbol{q_s}$), while vector $\boldsymbol{v}$ included all other network and adjoint circuit variables.

Importantly, based on the nature of network governing equations and physically meaningful constraints that can be enforced on a network response, it can be assumed that for the fixed circuit voltages, governing equations that model its steady-state response become linearly defined by the rest of the circuit states. That is, if we know every voltage within the network, we can trivially solve for all the other states. Hence, each component of the ECP set of governing equations can be further written in terms of a function that is linear in τ_G and τ_B, and whose

coefficients are further given as a function of τ_V. For instance, consider the set of real network currents $\boldsymbol{\mathcal{I}_R}$ from $\mathcal{C}_{ckt}(\boldsymbol{x_s}, \boldsymbol{\lambda})$ in (5.1) written as a function of three limiting factors:

$$\begin{aligned}\boldsymbol{\mathcal{I}_R} = [G_{RLC} + \mathrm{Tdiag}(\boldsymbol{G}^k + \tau_G \boldsymbol{\Delta G})]\big(\boldsymbol{V_R^k} + \tau_V \boldsymbol{\Delta V_R}\big) \\ - [B_{RLC} + \mathrm{Tdiag}(\boldsymbol{B}^k + \tau_B \boldsymbol{\Delta B})]\big(\boldsymbol{V_I^k} + \tau_V \boldsymbol{\Delta V_I}\big) + \boldsymbol{I_{SR}} + E_N\big(\boldsymbol{I_R^k} + \tau_V \boldsymbol{\Delta I_R}\big)\end{aligned} \tag{5.22}$$

By grouping all the terms related to τ_G and τ_B, (5.22) can be further rewritten as:

$$\begin{aligned}\boldsymbol{\mathcal{I}_R} = \boldsymbol{I_{SR}} + E_N\big(\boldsymbol{I_R^k} + \tau_V \boldsymbol{\Delta I_R}\big) + [G_{RLC} + \mathrm{Tdiag}(\boldsymbol{G}^k)]\big(\boldsymbol{V_R^k} + \tau_V \boldsymbol{\Delta V_R}\big) \\ - [B_{RLC} + \mathrm{Tdiag}(\boldsymbol{B}^k)]\big(\boldsymbol{V_I^k} + \tau_V \boldsymbol{\Delta V_I}\big) + \tau_G \mathrm{Tdiag}(\boldsymbol{\Delta G})\big(\boldsymbol{V_R^k} + \tau_V \boldsymbol{\Delta V_R}\big) \\ - \tau_B \mathrm{Tdiag}(\boldsymbol{\Delta B})\big(\boldsymbol{V_I^k} + \tau_V \boldsymbol{\Delta V_I}\big)\end{aligned} \tag{5.23}$$

Or in a more compact way:

$$\boldsymbol{\mathcal{I}_R} = \boldsymbol{\mathcal{I}_R^k} + \boldsymbol{\mathcal{I}_{RV}}(\tau_V) + \tau_G \boldsymbol{\mathcal{I}_{RG}}(\tau_V) + \tau_B \boldsymbol{\mathcal{I}_{RB}}(\tau_V) \tag{5.24}$$

where $\boldsymbol{\mathcal{I}_R^k}$ represents a vector contribution of the ECP circuit residual from previous NR iteration, while vectors $\boldsymbol{\mathcal{I}_{RV}}(\tau_V)$, $\boldsymbol{\mathcal{I}_{RG}}(\tau_V)$ and $\boldsymbol{\mathcal{I}_{RB}}(\tau_V)$ are function of τ_V given as:

$$\begin{aligned}\boldsymbol{\mathcal{I}_{RV}}(\tau_V) &= \tau_V E_N \boldsymbol{\Delta I_R} + \tau_V [G_{RLC} + \mathrm{Tdiag}(\boldsymbol{G}^k)]\boldsymbol{\Delta V_R} - \tau_V [B_{RLC} + \mathrm{Tdiag}(\boldsymbol{B}^k)]\boldsymbol{\Delta V_I} \\ \boldsymbol{\mathcal{I}_{RG}}(\tau_V) &= \mathrm{Tdiag}(\boldsymbol{\Delta G})\big(\boldsymbol{V_R^k} + \tau_V \boldsymbol{\Delta V_R}\big) \\ \boldsymbol{\mathcal{I}_{RB}}(\tau_V) &= -\mathrm{Tdiag}(\boldsymbol{\Delta B})\big(\boldsymbol{V_I^k} + \tau_V \boldsymbol{\Delta V_I}\big)\end{aligned} \tag{5.25}$$

Therefore, the 3D search problem from (5.21) can be now expressed in the following form:

$$\min_{\tau_V, \tau_G, \tau_B \in [0,1]} \mathrm{X_{ol}}(\tau_V, \tau_G, \tau_B) = \big\| \mathbf{C_{ECP}^k} + \boldsymbol{\Upsilon_{ol}}(\tau_V) + \tau_G \boldsymbol{\Gamma_{ol}}(\tau_V) + \tau_B \mathbf{B_{ol}}(\tau_V) \big\|_2^2 \tag{5.26}$$

Next, by differentiating (5.26) with respect to τ_G and τ_B, i.e.

$$\nabla_{\tau_G} \mathrm{X_{ol}} = \boldsymbol{\Gamma_{ol}^T}(\tau_V)\big[\mathbf{C_{ECP}^k} + \boldsymbol{\Upsilon_{ol}}(\tau_V) + \tau_G \boldsymbol{\Gamma_{ol}}(\tau_V) + \tau_B \mathbf{B_{ol}}(\tau_V)\big] = 0 \tag{5.27}$$

$$\nabla_{\tau_B} \mathrm{X_{ol}} = \mathbf{B_{ol}^T}(\tau_V)\big[\mathbf{C_{ECP}^k} + \boldsymbol{\Upsilon_{ol}}(\tau_V) + \tau_G \boldsymbol{\Gamma_{ol}}(\tau_V) + \tau_B \mathbf{B_{ol}}(\tau_V)\big] = 0 \tag{5.28}$$

the values of τ_G and τ_B can be analytically computed as functions of τ_V

$$\tau_G = \frac{\boldsymbol{\Gamma}_{\mathbf{ol}}^T(\tau_V)\left[\mathbf{C}_{\boldsymbol{ECP}}^{\boldsymbol{k}} + \boldsymbol{\Upsilon}_{\mathbf{ol}}(\tau_V)\right]\|\mathbf{B}_{\mathbf{ol}}(\tau_V)\|_2^2 - \mathbf{B}_{\mathbf{ol}}^T(\tau_V)\left[\mathbf{C}_{\boldsymbol{ECP}}^{\boldsymbol{k}} + \boldsymbol{\Upsilon}_{\mathbf{ol}}(\tau_V)\right]\boldsymbol{\Gamma}_{\mathbf{ol}}^T(\tau_V)\mathbf{B}_{\mathbf{ol}}(\tau_V)}{\left(\boldsymbol{\Gamma}_{\mathbf{ol}}^T(\tau_V)\mathbf{B}_{\mathbf{ol}}(\tau_V)\right)^2 - \|\boldsymbol{\Gamma}_{\mathbf{ol}}(\tau_V)\|_2^2\|\mathbf{B}_{\mathbf{ol}}(\tau_V)\|_2^2} \tag{5.29}$$

$$\tau_B = \frac{\mathbf{B}_{\mathbf{ol}}^T(\tau_V)\left[\mathbf{C}_{\boldsymbol{ECP}}^{\boldsymbol{k}} + \boldsymbol{\Upsilon}_{\mathbf{ol}}(\tau_V)\right]\|\boldsymbol{\Gamma}_{\mathbf{ol}}(\tau_V)\|_2^2 - \boldsymbol{\Gamma}_{\mathbf{ol}}^T(\tau_V)\left[\mathbf{C}_{\boldsymbol{ECP}}^{\boldsymbol{k}} + \boldsymbol{\Upsilon}_{\mathbf{ol}}(\tau_V)\right]\boldsymbol{\Gamma}_{\mathbf{ol}}^T(\tau_V)\mathbf{B}_{\mathbf{ol}}(\tau_V)}{\left(\boldsymbol{\Gamma}_{\mathbf{ol}}^T(\tau_V)\mathbf{B}_{\mathbf{ol}}(\tau_V)\right)^2 - \|\boldsymbol{\Gamma}_{\mathbf{ol}}(\tau_V)\|_2^2\|\mathbf{B}_{\mathbf{ol}}(\tau_V)\|_2^2} \tag{5.30}$$

By utilizing the property of a network problem that for a given set of voltages any other state can be trivially determined, as well as under the assumption that the τ_V dependent vectors from (5.26) can be expressed in terms of a n^{th} order polynomial of τ_V, we next discuss two important facts that will lead us to the introduction of Optimal Limiting algorithm.

- For a fixed τ_V^i sampled from a domain of (5.26), $\tau_V \in [0,1]$, the respective values of τ_G^i and τ_B^i can be computed from (5.29)-(5.30), projected back to the domain of (5.26), as demonstrated in Algorithm 5.4., and further used to compute the residual $\mathrm{X}_{\mathrm{ol}}^i\left(\tau_V^i, \tau_G^i, \tau_B^i\right)$.

Algorithm 5.4. *Projection of τ_G^i and τ_B^i to the domain of 3D search function*

Given: τ_V^i, τ_G^i and τ_B^i as well as the set of upper and lower bounds that define the domain of (5.26), $\tau_{G_U}, \tau_{G_L}, \tau_{B_U}$ and τ_{B_L}.

If $\left(\tau_G^i > \tau_{G_U} \vee \tau_G^i < \tau_{G_L}\right) \wedge \left(\tau_B^i > \tau_{B_U} \vee \tau_B^i < \tau_{B_L}\right)$

$$\tau_G^i = \begin{cases} \tau_{G_U} \text{ if } \tau_G^i > \tau_{G_U} \\ \tau_{G_L} \text{ if } \tau_G^i < \tau_{G_L} \end{cases} \qquad \tau_B^i = \begin{cases} \tau_{B_U} \text{ if } \tau_B^i > \tau_{B_U} \\ \tau_{B_L} \text{ if } \tau_B^i < \tau_{B_L} \end{cases}$$

Elseif $\left(\tau_G^i < \tau_{G_U} \wedge \tau_G^i > \tau_{G_L}\right) \wedge \left(\tau_B^i > \tau_{B_U} \vee \tau_B^i < \tau_{B_L}\right)$

$$\tau_B^i = \begin{cases} \tau_{B_U} \text{ if } \tau_B^i > \tau_{B_U} \\ \tau_{B_L} \text{ if } \tau_B^i < \tau_{B_L} \end{cases} \quad \tau_G^i = \frac{-\boldsymbol{\Gamma}_{\mathbf{ol}}^T(\tau_V^i)\left[\mathbf{C}_{\boldsymbol{ECP}}^{\boldsymbol{k}} + \boldsymbol{\Upsilon}_{\mathbf{ol}}(\tau_V^i)\right] - \boldsymbol{\Gamma}_{\mathbf{ol}}^T(\tau_V^i)\mathbf{B}_{\mathbf{ol}}(\tau_V^i)\tau_B^i}{\left\|\boldsymbol{\Gamma}_{\mathbf{ol}}(\tau_V^i)\right\|_2^2} \rightarrow \tau_G^i = \begin{cases} \tau_{G_U} \text{if } \tau_G^i > \tau_{G_U} \\ \tau_{G_L} \text{if } \tau_G^i < \tau_{G_L} \\ \tau_G^i \qquad \text{else} \end{cases}$$

Elseif $\left(\tau_G^i > \tau_{G_U} \vee \tau_G^i < \tau_{G_L}\right) \wedge \left(\tau_B^i < \tau_{B_U} \wedge \tau_B^i > \tau_{B_L}\right)$

$$\tau_G^i = \begin{cases} \tau_{G_U} \text{ if } \tau_G^i > \tau_{G_U} \\ \tau_{G_L} \text{ if } \tau_G^i < \tau_{G_L} \end{cases} \quad \tau_B^i = \frac{-\mathbf{B}_{\mathbf{ol}}^T(\tau_V^i)\left[\mathbf{C}_{\boldsymbol{ECP}}^{\boldsymbol{k}} + \boldsymbol{\Upsilon}_{\mathbf{ol}}(\tau_V^i)\right] - \mathbf{B}_{\mathbf{ol}}^T(\tau_V^i)\boldsymbol{\Gamma}_{\mathbf{ol}}(\tau_V^i)\tau_G^i}{\left\|\mathbf{B}_{\mathbf{ol}}(\tau_V^i)\right\|_2^2} \rightarrow \tau_B^i = \begin{cases} \tau_{B_U} \text{ if } \tau_B^i > \tau_{B_U} \\ \tau_{B_L} \text{ if } \tau_B^i < \tau_{B_L} \\ \tau_B^i \qquad \text{else} \end{cases}$$

Output: bounded τ_G^i and τ_B^i

- Under the assumption that the vectors $\boldsymbol{\Upsilon}_{\mathbf{ol}}(\tau_V)$, $\boldsymbol{\Gamma}_{\mathbf{ol}}(\tau_V)$ and $\mathbf{B}_{\mathbf{ol}}(\tau_V)$ can be expressed in terms of n polynomial components of τ_V, which represents a good assumption for network optimization problems, the respective components need to be computed only once per NR iteration, which doesn't represent an additional computational burden on the solution process. The approach is, however, generic for any function with the caveat of increased simulation complexity, since the terms from vector components that are not polynomial in nature need to be recomputed for every τ_V sample.

Finally, by considering the two previously discussed facts, we introduce the Optimal Limiting algorithm. The pseudocode is presented in Algorithm 5.5. that represents a process of generating N_{OL} uniform samples of τ_V, solving for the respective bounded τ_G and τ_B factors as given by Algorithm 5.4, and from evaluating the 3D search function and picking up the combinations of 3 optimal limiting factors that minimize function the most.

Algorithm 5.5. *Optimal Limiting*

Given: number of samples N_{OL}

Initialize: $\tau_V^* = \tau_G^* = \tau_B^* = 0$ and $\mathrm{X}_{\mathrm{ol}}^* = \infty$

For $i = 0 : N_{OL}$

$\tau_V^i = \frac{i}{N_{OL}}$

Compute τ_G^i and τ_B^i as given by Algorithm 5.4.

Evaluate 3D search function for $\mathrm{X}_{\mathrm{ol}}^i(\tau_V^i, \tau_G^i, \tau_B^i)$

If $\mathrm{X}_{\mathrm{ol}}^i(\tau_V^i, \tau_G^i, \tau_B^i) < \mathrm{X}_{\mathrm{ol}}^* \rightarrow \{\mathrm{X}_{\mathrm{ol}}^* = \mathrm{X}_{\mathrm{ol}}^i(\tau_V^i, \tau_G^i, \tau_B^i), \tau_V^* = \tau_V^i, \tau_G^* = \tau_G^i, \tau_B^* = \tau_B^i\}$

End

Output: τ_V^*, τ_G^* and τ_B^*, $\mathrm{X}_{\mathrm{ol}}^*$

It is important to emphasize that as can be seen from Algorithm 5.5., the Optimal Limiting represents a sampled evaluation of 3D search function, and as such, it does not introduce significant additional overhead in computational complexity, as will be shown in chapters that follow. Lastly, if we recall that admittance state variables introduced the nonconvexities within the modeling of linear AC network response, it intuitively makes sense to assign a separate limiting factor for each of the two sets of variables and remove some burden from τ_V factor. Namely, by

expanding the exact line search problem to the 3D solution space, we introduce the larger degree of freedom for the residual minimization, as well as allow some of the three limiting factors to saturate during a NR iteration, which is not possible with a single limiting factor.

5.5. Sequential Optimal Limiting

Along with the application of the Voltage Pre-Filtering technique, as well as the additional degrees of freedom introduced by the 3D search problem, the Optimal Limiting can still enforce the small step sizes in order to further decrease the residual, particularly with $\|\boldsymbol{\Upsilon}_{\mathbf{ol}}(\tau_V^*)\|_2^2 \gg \boldsymbol{\Upsilon}_{\mathbf{ol}}^T(\tau_V^*)\mathbf{C}_{\boldsymbol{ECP}}^{\boldsymbol{k}}$. Hence, in order to ensure the efficiency of the NR solution process, and considering that the τ_V corresponds to the "main" optimal step size, we further define a threshold, e.g. $\tau_V^* < 0.1$, below which the algorithm doesn't continue with the NR iterations. For such occurrences, the algorithm rather moves further with the application of limiting techniques, as described in Figure 5.1. Therefore, if τ_V^* is below the tolerance, the algorithm tries to obtain the new voltage step-size that will further minimize the ECP circuit residual by removing the contribution of adjoint circuit equations within the 3D search problem, and instead trying to determine a new set of limiting factors by applying the two stage Optimal Limiting, such as Sequential Optimal Limiting.

The idea of Sequential Optimal Limiting is inspired by the algorithm discussed in [54], where the authors attempt to apply the backtracking line search on the primal problem only, if the backtracking on the residual of complete set of KKT conditions fails. After the residual of a primal problem is decreased, the NR step sizes of dual variables are simply set to zero [54] and the iteration process is continued. The authors provided the proof of global convergence of such algorithm under the certain assumptions [54]. However, beside the idea of solving the line-search on the primal problem only, the Sequential Optimal Limiting widely differs in everything else in reference to the algorithm presented in [54]. First, the primal or our network problem is solved by using the 3D search incorporated within the Voltage Limiting algorithm as described in the section above. Second, simply setting all the adjoint NR steps to zero can be really dangerous, particularly because it significantly increases the chances of convergence to some of the nonoptimal saddle points in the solution space. Therefore, after the application of Optimal Limiting to the original network, the linear 3D search is solved to further determine the set of three adjoint step limiting

parameters that minimize the adjoint circuit residual with already limited primal network variables. The discussion on both stages of Sequential Optimal Limiting algorithm follows.

As already outlined above, the first stage of Sequential Optimal Limiting algorithm solves a version of a 3D search problem from (5.21) with removed contributions of the adjoint circuit equations:

$$\min_{\tau_V,\tau_G,\tau_B\in[0,1]} \|\mathcal{C}_{ckt}(\boldsymbol{v}^k + \tau_V\Delta\boldsymbol{v}, \boldsymbol{g}^k + \tau_G\Delta\boldsymbol{g}, \boldsymbol{b}^k + \tau_B\Delta\boldsymbol{b})\|_2^2 \tag{5.31}$$

If the coupling between the network and its adjoint is considered to ensure the problem feasibility, the coupling sources are assigned to the optimal limiting factors by respecting the nature of the quantity they represent. Namely, adjoint admittances are assigned to τ_G and τ_B respectively, while the other couplings represent the feasibility current and voltage sources and are, therefore, assigned to τ_V factor. It is also important to emphasize that the respective vectors that define the problem from (5.31) were already generated within the Optimal Limiting algorithm, (5.26) and hence the terms related to the network equations can be reused here and do not have to be rebuilt again.

Next, the Voltage Limiting algorithm described by Algorithm 5.4 and Algorithm 5.5 is applied to obtain the optimal factors of (5.31):

$$[\tau_V^*, \tau_G^*, \tau_B^*] = \underset{\tau_V,\tau_G,\tau_B\in[0,1]}{\operatorname{argmin}} \|\mathcal{C}_{ckt}(\boldsymbol{v}^k + \tau_V\Delta\boldsymbol{v}, \boldsymbol{g}^k + \tau_G\Delta\boldsymbol{g}, \boldsymbol{b}^k + \tau_B\Delta\boldsymbol{b})\|_2^2 \tag{5.32}$$

However, if the coupling between the network and its adjoint was considered, before going to the second stage and trying to further minimize the adjoint circuit residual, we need to first make sure that a set of three new adjoint limiting factors, $\tau_\lambda, \tau_{\lambda_G}, \tau_{\lambda_B}$, does not increase the already minimized residual of the network equations from the first stage. Therefore, to ensure that the adjoint circuit residual is minimized while preserving (or even improving) the residual minimization of the original network, the bounds on $\tau_\lambda, \tau_{\lambda_G}, \tau_{\lambda_B}$ can be computed from the condition:

$$\|\mathcal{J}(\tau_V^*, \tau_G^*, \tau_B^*) + \tau_A\Delta\boldsymbol{\lambda}\|_2^2 < \|\mathcal{J}(\tau_V^*, \tau_G^*, \tau_B^*) + \tau^*\Delta\boldsymbol{\lambda}\|_2^2 \tag{5.33}$$

Where $\mathcal{J}(\tau_V^*, \tau_G^*, \tau_B^*)$ represents a set of network equations that are coupled with respective adjoint variables $\Delta\boldsymbol{\lambda}$, while τ_A stands for one of the three new adjoint limiting factors $(\tau_\lambda, \tau_{\lambda_G}, \tau_{\lambda_B})$, and τ^*

corresponds to an optimal limiting factor obtained in the stage 1 for which was the adjoint coupling source assigned. From (5.33), the upper and lower bounds on τ_A correspond to:

$$\tau_{A_U} = \min\left[1, \max\left[\tau^*, -\tau^* - \frac{\mathcal{J}(\tau_V^*, \tau_G^*, \tau_B^*)^T \Delta\boldsymbol{\lambda}}{\|\Delta\boldsymbol{\lambda}\|_2^2}\right]\right] \tag{5.34}$$

$$\tau_{A_L} = \max\left[0, \min\left[\tau^*, -\tau^* - \frac{\mathcal{J}(\tau_V^*, \tau_G^*, \tau_B^*)^T \Delta\boldsymbol{\lambda}}{\|\Delta\boldsymbol{\lambda}\|_2^2}\right]\right] \tag{5.35}$$

With proper bounds on adjoint limiting factors computed, we can next define the second stage linear 3D search problem whose solution can be trivially obtained. This solution provides the set of three adjoint limiting factors that reduce the adjoint circuit residual, while preserving the minimized residual of the network equations:

$$\min_{\tau_\lambda . \tau_{\lambda_G}, \tau_{\lambda_B} \in \mathcal{P}} \left\| \bar{\mathcal{A}}_{ckt}\left(\boldsymbol{x_s} + \tau^* \Delta\boldsymbol{x_s}, \boldsymbol{\lambda_v^k} + \tau_\lambda \Delta\boldsymbol{\lambda_v}, \boldsymbol{\lambda_G^k} + \tau_{\lambda_G} \Delta\boldsymbol{\lambda_G}, \boldsymbol{\lambda_B^k} + \tau_{\lambda_B} \Delta\boldsymbol{\lambda_B}\right)\right\|_2^2 \tag{5.36}$$

Where $\boldsymbol{\lambda_v}$ represents a set of all adjoint variables other than the adjoint admittances and set $\mathcal{P}$ defines the bounds on $\tau_\lambda . \tau_{\lambda_G}, \tau_{\lambda_B}$ obtained from (5.34)-(5.35).

5.6. Variable Post-Filtering Technique

Thus far we have introduced new sets of techniques and algorithms inspired by and conceived from the notion of embedding the "domain specific knowledge" techniques developed around the state-of-art circuit simulator SPICE within the continuous optimization algorithms. Furthermore, as discussed in Chapter 2, the circuit simulation algorithms usually do not guarantee the residual decrement at each NR iteration, but are really efficient and robust in general. This can sometimes, particularly if the current NR iterate gets stuck within some really bad region, provide an advantage over the algorithms based on decreasing the circuit residual that would start saturating, and thereby slowing down the iteration process. Therefore, if after the Sequential Optimal Limiting is solved, τ_V or τ_λ are still less than predefined threshold, all the respective NR steps that correspond to the saturated limiting factors are passed through the Post-Filtering technique, as presented in Algorithm 5.6. The saturation of optimal limiting factors indicates that the residual cannot be minimized at the current NR iteration, and the pure circuit simulation

heuristics based on the "trusted" step limiting factors have to be applied before continuing the iteration process.

Algorithm 5.6. *Variable Post-Filtering Technique*

Given: vectors of variables that correspond to the saturated optimal limiting factors, $\boldsymbol{x}^{k+1}$,$\boldsymbol{x}^{k}$, as well as predefined thresholds, ν_{th}, defined based on the physical characteristics of the problem

$$\boldsymbol{x}^{k} = \begin{cases} x_i^{k+1} & \text{if } \left|x_i^{k+1} - x_i^{k}\right| < \nu_{th} \\ x_i^{k} & \text{if } \left|x_i^{k+1} - x_i^{k}\right| > \nu_{th} \end{cases} \tag{5.37}$$

Output: $\boldsymbol{x}^{k+1}$,$\boldsymbol{x}^{k}$

In conclusion, this chapter provided the final piece of the puzzle related to solving an ECP problem based on developing techniques and algorithms inspired by of the combination of mathematical optimization techniques and circuit simulation methods. Most importantly, with the introduction of developed ECP heuristics, the theoretic as well as algorithmic part of the thesis and the ECP framework in general is concluded, and the following chapters focus solely on application of these algorithms to power system simulation and optimization problems.

Chapter 6 Power System Modeling and Analysis within the Equivalent Circuit Programming Framework

Pioneered by Nikola Tesla and George Westinghouse, an electrical AC power system corresponds to an electro-mechanical circuit consisting of interconnected generation plants and load demands, and is considered one of the most important inventions of 20th century. Electrical power systems represent critical infrastructure of every country in the world. Notably, from the early days of power grid expansion, the reliable, safe and efficient operation of a power system represented one of the key factors in political and public debates [55]. Hence, accurate and realistic power grid analyses became, and still remains, one of primary research topics.

Presently, the decisions on the electrical power dispatch and system operation are determined within an Energy Management System (EMS) comprised of a set of computer aided tools used to monitor, control and optimize the performance of a power grid. Namely, these tools correspond to solvers for several different power system simulation and optimization problems that are required to be ran by the operators, sometimes executed several times per hour, in order to ensure the reliable grid operation. Moreover, an electrical power grid continuously evolves, particularly with the integration of renewable energy sources and other emerging grid technologies, and hence the need for their accurate and more expansive modeling within the existing simulation and optimization framework. However, the inherent nonlinearities of the existing standard power-mismatch formulations [56]-[57] used to model and solve the problems within most of the EMS tools already struggle with robustness for large-scale simulations [58]-[59]. Therefore, the additional incorporation of new, more complex models, as well as the other realistic constraints consequently creates additional challenges with robustness and efficiency.

The second equally important challenge for the accuracy and efficiency of EMS tools is the significant discrepancy between the research performed within the largest portion of the power system simulation and optimization academic community, and the industry desired solutions to the realistic scale power grid problems. There are dozens of papers published every month on various convexification algorithms and techniques applied to "large-scale" cases of 14 to 500 bus systems, which were considered as large-scale by the founders of power-mismatch formulation half a century ago. However, the incorporation of a complete set of realistic industry constraints can result in nonlinear problems of over several million of variables. This forces the industry to use less accurate but convex models and rely on the generalized convex optimization toolboxes that can suffer from efficiency problems at scales of millions of variables. Finally, to circumvent the problem of less accurate solutions, the grid operators mastered the "art of tuning" the nonlinear algorithms based on their experience and physical characteristics of the grid in order to produce the meaningful results that can be used to determine the decisions on power system operation. Most importantly, due to the fact that most of the real-life problems are nonconvex in nature, a local optimal solution that considers all realistic, in this case power grid constraints, is better than a global one that does not. Therefore, the tendency of both academia and industry for convexifying and relaxing the power grid problems can be explained by the lack of robust, efficient and scalable nonlinear optimization toolboxes capable of providing an optimal solution that satisfies all of the desired constraints.

To address the lack of nonlinear solvers for robust and scalable power grid simulation and optimization problems, the rest of the thesis applies the proposed ECP framework to power system analyses. It is demonstrated that a power grid steady-state response can be, without loss of accuracy, modeled by the generalized formulation for representing a network response introduced in Chapter 3, and as such included within the ECP framework. Most importantly, beside the capability of robustly and efficiently solving the traditionally postulated power grid problems, the ECP framework is demonstrated to further facilitate the incorporation of a full set of real-life constraints and device characteristics within the power grid analysis. Therefore, the rest of this chapter focuses on a Power Flow problem as one of the main components of every EMS. First, a revisited history on the origin of power flow is provided together with a comparison between its solutions obtained using the ECP compatible formulation with respective algorithms, and the other existing formulations from the literature. Furthermore, we discuss power flow feasibility as well

as operational limits and device characteristics that are required to obtain a realistic power flow solution. From this, we can theorize that a real-life power flow problem indeed corresponds to a generalized nonlinear optimization, rather than a "simple" simulation problem, which can be now robustly and efficiently solved within the ECP framework.

6.1. Evolution of analyzing the power system steady-state response

Characterizing and analyzing a power grid steady-state response in terms of power-mismatch formulation and phasor voltage state variables has been widely accepted as a standard, particularly in transmission level grid analyses. Importantly, as any other electrical circuit, an electrical power system is governed by physical conservation laws that are naturally defined in terms of current and voltage state variables related by KVL and KCL. Thus, the same circuit formalism developed within the circuit simulation community has to be directly compatible with the power grid analysis, without loss of generality. It is, however, not often discussed why, when and how the power system and circuit simulation analyses took the disparate paths in defining the respective network response problems. Therefore, before showing that a power grid response can be naturally incorporated within the generalized network modeling framework developed in Chapter 3, it is important to revisit the history of origins of analyzing the grid steady-state response.

As found from the first papers written on the topic of power system steady-state analysis in 1940s and 50s [60]-[61], the original formulations for analyzing the grid response utilized current and voltage state variables. Moreover, such KCL and KVL based formulations remained used at the early beginning of the new era that started with the introduction of first digital computers, and hence also represent the first formulation implemented on a digital computer by Ward and Hale in 1956 [61]-[62]. However, beside the natural and probably more intuitive way of modeling a power grid response at that time, the original current and voltage formulations suffered from the two serious drawbacks:

1. Macro-modeling the steady-state response of induction and synchronous machines as well as bulk demand loads by constraining their supplied/absorbed AC power introduces nonlinearities within the governing power system KCL and KVL equations, hence requiring iterative schemes to be applied in order to obtain the desired steady-state set point of the grid.

2. The sparsity of the network problems was not utilized. Moreover, the solution to a sparse matrix problem was yet to be found.

As it can be noticed, the common denominator of both drawbacks represents a significant computational burden for early digital computers. Namely, the first applied iterative schemes can be characterized as the 'derivative-free" fixed point iteration methods, and Newton Raphson was still infeasible to implement due to high computational complexity, particularly when combined with full matrix representation of network problems that are significantly sparse in nature.

To address the problem of memory requirements for power flow simulation as well as slow convergence of the power system steady-state simulators from that era, leading Bonneville Power Administration engineer William Tinney [56],[63]-[64] introduced a Newton method for solving a power flow problem in terms of power mismatch equations. The structure of a power flow network admittance matrix further served as an inspiration for developing a sparse NR solver, which was soon demonstrated to represent one of the first generalized solutions to a sparse matrix problem, capable of solving large-scale cases of that era, with systems ranging from 500-1000 buses on a 32K core memory. Soon after, the efficiency of sparse NR power flow formulation led Hermann Dommel [57] to attempt implementing the originally used formulations based on KCL [60], which did not seem like a promising path to pursue, particularly due to the problems in modeling the voltage controlling machines [31]. It was later proven [65] that the Jacobian matrix of a power flow problem defined within the power mismatch formulation remains positive definite, while the modeling of voltage-controlled nodes in all other formulations introduces the negative eigenvalues, and hence it is more prone to cause convergence instabilities if not handled properly.

Beside the significant increase of additional inherent nonlinearities in using the power conservation law to characterize the power system steady-state response (particularly linear RLC transmission network) and diverging from the unified models that can be used for both time domain and steady-state analyses, the power mismatch formulation was shown to efficiently handle the initially examined large scale simulations and was appealing for the memory requirements of the existing digital computers. Thereafter, the steady-state analysis of the power grid took a disparate direction from the other circuit analysis in terms of characterizing the electrical circuit steady-state response.

However, *the solution to the sparse matrix problem is completely independent from a NR convergence process, and the positive definiteness of a Jacobian matrix does not guarantee convergence*. Therefore, as the computing power of early computers increased, it was realized that as in the case with any other generic NR algorithm, the convergence of power mismatch-based power flow is dependent on the initial starting point, particularly with the increase in size of the test cases [58]-[59]. In the meantime, significant research in the electronic circuit simulation space led to the development of SPICE [11]-[17]. It was demonstrated that the NR method, once combined with physical characteristics of the equivalent circuit models derived from first principles, allows for robust and efficient circuit simulation that today scales to circuits with over a billion nodes. Moreover, the equivalent circuit models used in SPICE often feature significantly steeper and more severe nonlinearities compared to those introduced by power system macro-models. The inherent nonlinearities of power mismatch formulation for characterizing the steady-state response of a power system, however, made the application of a similar circuit formalism impractical for the simulation of power flow.

The last recently introduced step in the evolution of power flow steady-state analysis that is graphically shown in Figure 6.1, represents the equivalent split-circuit formulation and representation of the power flow problem in terms of current and voltage state variables as initially explored by Dommel [57]. Notably, even though this now called Current Injection formulation [31] mathematically corresponds to the previously examined current-voltage formulations, the equivalent circuit perspective to the problem was demonstrated [11]-[17] to allow the extension of SPICE equivalent circuit formalism to power system simulation problems. The application of developed circuit simulation techniques and homotopy methods was shown to overcome the challenges introduced in modeling the voltage-controlled PV nodes, and therefore allow the robust simulations of industry size power flow problems. However, due to the nonlinear current injection bus models [31] that define the AC power constraints, various homotopy methods [31]-[33] were required to improve convergence robustness while sometimes significantly increasing the iteration count, thereby decreasing the efficiency of the solution process. Most importantly, even though the current-injection based split-circuit formulation represented a first step towards model unification while allowing the large-scale simulations, the current injection nonlinearities are not practically compatible with the optimal limiting algorithms from the perspective of the ECP framework due to the inversely proportional voltage terms. In the following section we conclude

the evolutionary process of power flow modeling by incorporating it within the generalized network framework introduced in Chapter 3. We further utilize the conductance and susceptance state variables to constrain the respective bus power injections of traditionally defined power flow models.

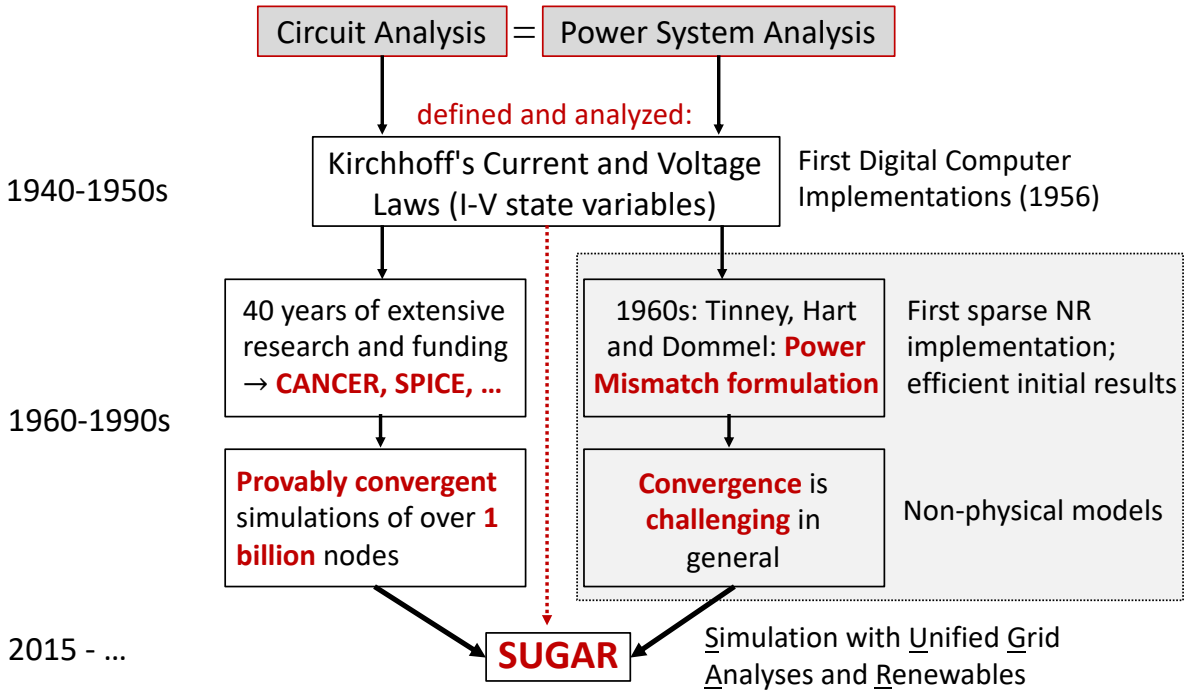

Figure 6.1. Evolution of the power grid steady-state analysis.

6.2. Generalized network formulation for modeling a power flow problem

Consider a power system whose steady-state response is characterized in terms of phasor voltages and currents ($\tilde{V}_{ik} = V_{R,ik} + jV_{I,ik}$ and $\tilde{I}_{ik} = I_{R,ik} + jI_{I,ik}$) at a fundamental frequency, and further governs the relationships between a set of generators $\mathcal{G}_B$ and load demands $\mathcal{D}_B$, interconnected by a set of transmission network elements, $\mathcal{T}_X$. It is important to emphasize that from the perspective of currents and voltages in the network, and under the assumptions set by the traditionally postulated power flow problem [56],[62], the nonlinearities in modeling the power system response are introduced to constrain the powers injected to the network as well as certain bus voltage magnitudes, hence are locally related to each bus. Furthermore, all of the transmission

network elements are linear and correspond to RLC circuit models, and hence the basic modeling components that define a power flow problem can be classified into two categories as:

1. Linear Elements
    - Transmission lines
    - Fixed shunt devices
    - Slack generator (Reference) bus
    - Transformers
2. Nonlinear Elements
    - PQ loads
    - Voltage Regulation (VR) devices
    - PV generators

The first category defines linear power flow equivalent circuit models presented in Figure 6.2 that can be mapped to the equivalent split-circuit domain, as discussed in Chapter 3. More details can be also found in [18]-[33]. Moreover, in terms of the input parameters to the traditionally postulated power flow problem, the linear power flow elements are represented within a bus admittance matrix, and therefore, the respective adjoint split-circuit component can be defined by its transpose, or elementwise, as given in Chapter 2.

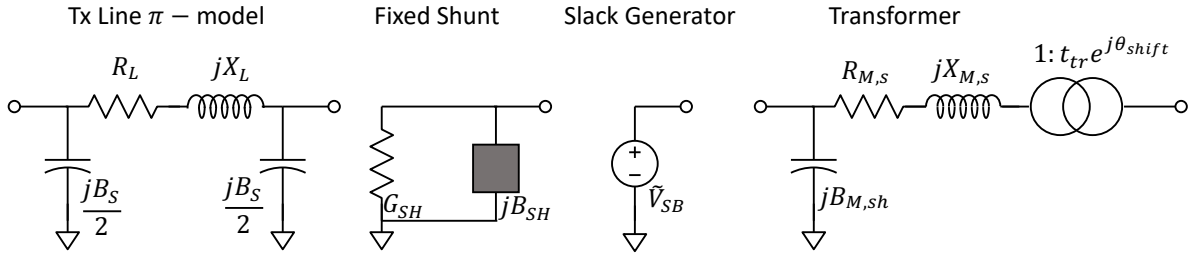

Figure 6.2. Complex equivalent circuit models for linear power flow elements.

Notably, the linear power flow split-circuits directly correspond to the models defined within the Current Injection formulation, and hence are only included here for completeness. The fundamental difference from Current Injection formulation, however, is the modeling of nonlinear elements for which we focus our further discussion.

In order to relate the nonlinear power flow elements to the generalized network formulation introduced in Chapter 3, it is important to emphasize and fully understand their behavior within

the power flow problem. As can be seen from Figure 6.3, a PQ load model represents a network device that supplies the pre-specified real and reactive powers (P_L and Q_L) that is further independent of any other voltage or current within the power grid. On the other side, the PV generator, as well as any other VR device (a subset of PV generator models with generated real power, P_G set to zero), in addition to the fixed real power, adjust the reactive power in order to maintain the voltage magnitude of its own or another bus within the system to a particular prespecified value.

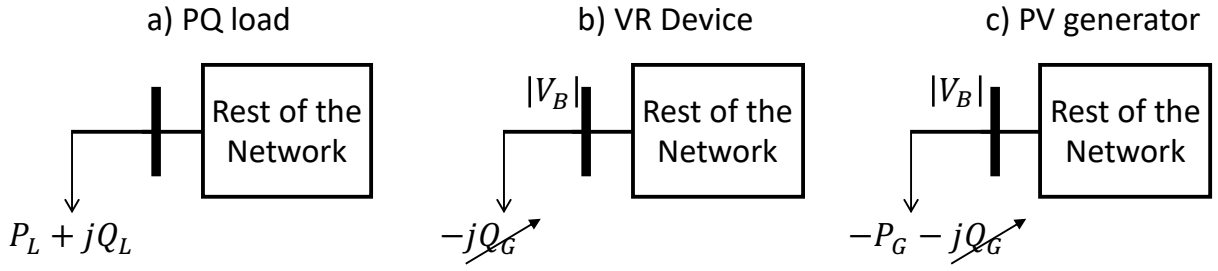

Figure 6.3. Schematic representation of nonlinear element characteristics within a power flow problem.

As can be seen from Figure 6.3, the nonlinear power flow devices exhibit the exact network response characteristics that require the introduction of conductance and susceptance state variables from Chapter 3. Therefore, if we recall the generalized governing network response equations from (3.3) with the T matrix set to be an identity matrix due to the locally related nonlinear elements within a power flow problem,

$$\begin{aligned}
[G_{RLC} + \mathrm{diag}(\boldsymbol{G})]\boldsymbol{V_R} - [B_{RLC} + \mathrm{diag}(\boldsymbol{B})]\boldsymbol{V_I} + E_N\boldsymbol{I_{SB,R}} &= \mathbf{0} \\
[G_{RLC} + \mathrm{diag}(\boldsymbol{G})]\boldsymbol{V_I} + [B_{RLC} + \mathrm{diag}(\boldsymbol{B})]\boldsymbol{V_R} + E_N\boldsymbol{I_{SB,I}} &= \mathbf{0} \\
E_N\boldsymbol{V_R} - \boldsymbol{V_{SB,R}} &= \mathbf{0} \\
E_N\boldsymbol{V_I} - \boldsymbol{V_{SB,I}} &= \mathbf{0} \\
f_G(\boldsymbol{V_R}, \boldsymbol{V_I}, \boldsymbol{G}, \boldsymbol{B}) &= \mathbf{0} \\
f_B(\boldsymbol{V_R}, \boldsymbol{V_I}, \boldsymbol{G}, \boldsymbol{B}) &= \mathbf{0}
\end{aligned} \tag{6.1}$$

Where the additional set of equations $f_G(\boldsymbol{V_R}, \boldsymbol{V_I}, \boldsymbol{G}, \boldsymbol{B})$ and $f_B(\boldsymbol{V_R}, \boldsymbol{V_I}, \boldsymbol{G}, \boldsymbol{B})$ correspond to the constraints required to enforce the desired behavior on powers and voltage magnitudes within the system. Namely, for the given bus admittance matrices that define the linear network elements, G_{RLC} and B_{RLC}, as well as prespecified slack bus voltages $\boldsymbol{V_{SB,R}}$ and $\boldsymbol{V_{SB,I}}$, a set of shunt connected

conductance and susceptance states is added to model a net power network injection at each bus in the system.

As shown in Figure 6.4, modeling the nonlinear power flow elements can be further seen in terms of a generalized GB bus model that is added to the system model, consisting of linear circuit elements from Figure 6.2. that enforce the desired grid device behaviors. Then, for a given bus i and a pair of conductance and susceptance state variables (G_i and B_i), a set of constraints is added to enforce that the real and reactive power absorbed by the admittance states correspond to the net power difference between the N_G generators and N_L loads connected at the respective bus:

$$\begin{aligned} f_{G,i}(V_{R,i}, V_{I,i}, G_i, B_i): &\qquad G_i\left(V_{R,i}^2 + V_{I,i}^2\right) - \sum_{k=1}^{N_L} P_{L,k} + \sum_{m=1}^{N_G} P_{G,m} = 0 \\ f_{B,i}(V_{R,i}, V_{I,i}, G_i, B_i): &\qquad B_i\left(V_{R,i}^2 + V_{I,i}^2\right) + \sum_{k=1}^{N_L} Q_{L,k} - Q_{G,i} = 0 \\ &\qquad V_{R,j}^2 + V_{I,j}^2 - |V_s|^2 = 0 \end{aligned} \tag{6.2}$$

Where $Q_{G,i}$ corresponds to the total generated reactive power needed to maintain the predefined voltage magnitude of bus j, and therefore, represents an additional slack variable added to enforce the respective voltage magnitude constraint. Notably, the first two additional constraints can be now seen as the locally defined power mismatch equations given for every bus, which further highlights the generality of the GB bus model to include all forms of laws of conservation of energy within a power system.

Finally, with the GB bus introduced, the new generalized power flow formulation is fully compatible with the ECP framework, and hence can be utilized to model the network constraints within the power grid optimization problems. However, instead of now solving the optimization problems, we first demonstrate the applicability of developed the ECP framework, namely the Voltage and Post filtering as well as Optimal limiting techniques, for improving the efficiency and robustness of simulation problems. For the chosen sample of 20 power flow test cases ranging from 1354 to 70k buses [66]-[68] that include the grid representations of Polish, French and European grids, as well as synthetic cases of US grid including the Eastern Interconnection whose

specifications are shown in Table 6.1, we analyze simulation results obtained by solving the power flow problem defined in terms of the following formulations and solution methodologies:

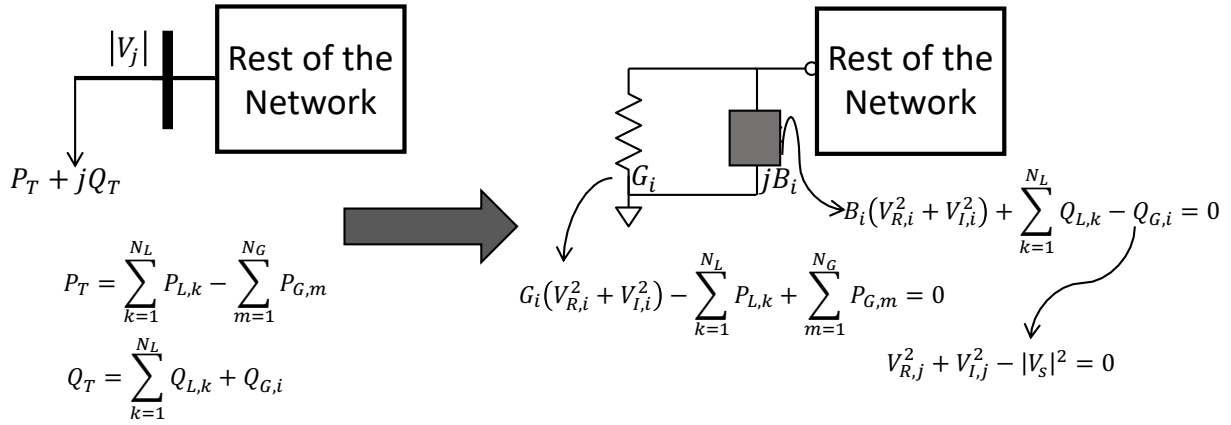

Figure 6.4. Mapping the nonlinear power flow elements to a generalized GB bus model.

1. Power mismatch formulation in polar coordinates (Polar PQV) [56]
2. Power mismatch formulation in rectangular coordinates (Rectangular PQV) [69]
3. Current Injection formulation in polar coordinates (Polar I-V) [68]
4. Current Injection formulation in rectangular coordinates (Rectangular I-V) [70]
5. Rectangular Current Injection formulation solved within SUGAR [31]
6. Generalized GB power flow formulation solved with ECP heuristics within SUGAR

The power flow solutions for the first four formulations are obtained within the MATPOWER open source grid simulation and optimization toolbox [68], while the Current Injection formulation with circuit simulation heuristics is solved within the Python prototype version of SUGAR [31]. Lastly, the solution to the ECP compatible GB formulation is obtained within the implemented ECP prototype solver in MATLAB that will be also used to obtain all the other optimization results throughout the remainder of the thesis, unless specified otherwise. The iteration count comparisons between all six formulations, initialized both by a flat voltage start and the initial guess, are provided from the input files and presented in Table 6.2. All the simulations were run on a MacBook Pro 2.9 GHz Intel Core i7 for the same convergence criterion of $\epsilon = 10^{-6}$ on an absolute variable step difference.

Table 6.1. Device specification of examined power flow test cases.

Device # case	Gen.	TxLine	Xfmr	Fixed Shunt	Load	Description
1354pegase	259	1751	240	1082	673	Part of European high-voltage system
1888rte	280	2122	409	45	1000	French very-high voltage trans. network
1951rte	357	2106	490	24	1015	French very-high voltage trans. network
2383wp	326	2726	170	0	1826	Polish system during winter 1999-00 peak
2736sp	238	3102	167	1	2048	Polish system during summer 2004 peak
2746wp	369	3110	169	0	2024	Polish system during winter 2003-04 peak
2848rte	418	3212	564	48	1511	French very-high voltage trans. network
2868rte	464	3196	612	33	1551	French very-high voltage trans. network
2869pegase	509	4077	505	2197	1491	Part of European high-voltage system
3012wp	297	3371	201	9	2271	Polish system during winter 2007-08 peak
3120sp	247	3487	206	9	2314	Polish system during summer 2008 peak
3375wp	391	3778	383	9	2434	Polish system during winter 2007-08 peak
6468rte	342	7667	1333	97	3661	French high voltage trans. network
6470rte	633	7659	1346	73	3670	French high voltage trans. network
6515rte	562	7657	1380	102	3673	French high voltage trans. network
9241pegase	1444	14715	1334	7327	4895	European high-voltage system
ACTIVSg10k	1454	11731	975	281	4170	Synthetic footprint of US West Interconnect
13659pegase	4091	14738	5729	8754	5544	European system
ACTIVSg25k	2752	29131	3098	741	8096	Synthetic footprint of US North East. grid
ACTIVSg70k	5894	83126	5081	3477	32460	Synthetic footprint of US East. Interconnect

As can be seen from Table 6.2, the convergence profiles for all of the six examined formulations behave as expected and described at the end of Section 6.1:

1. Utilizing the physical characteristics of the problem and further embedding the domain knowledge within the set of algorithms used to control the NR step, as done in SPICE, resulted in a significant improvement over the traditionally implemented formulations solved within MATPOWER simulator. This is particularly evident when the good initial start is not provided.
2. Furthermore, the additional combining of the optimization and circuit simulation approaches within the ECP framework results in the most robust and efficient simulations in terms of iteration count.
3. In referring to the formulations solved within MATPOWER *only*, the initial starting point played a significant role in the convergence process. As can be seen, most of the cases converged when initialized with the good starting point that also usually represents a start

really close to the actual solution. Moreover, the lack of robustness when the good initial guess is not provided is particularly emphasized as the size of the cases increase.

4. By further comparing the first four formulations solved without utilizing any of the domain specific knowledge, the overall performance of Polar PQV formulation with provably [65] positive definite Jacobian matrix is slightly better in reference to the other three formulations. The positive definite Jacobian, however, doesn't guarantee the convergence, and therefore, it can be seen that there are some cases that converge with other formulations while not converging with a Polar PQV.

Table 6.2. Power Flow Simulation Iteration Count Comparison. It was validated that all of the formulations (if converge) converged to the identical power flow solutions. Importantly, the comparison is based on the best- and worst-case scenarios of initial starting points, in order to emphasize the robustness that can be achieved within SUGAR.

Formulation	Polar PQV		Rectangular PQV		Polar I-V		Rectangular I-V		SUGAR Rect. I-V		**SUGAR ECP GB**	
case	Flat	Input	Flat	Input	Flat	Input	Flat	Input	Flat	Input	Flat	Input
1354pegase	5	4	6	4	∞	4	∞	4	5	1	**4**	**1**
1888rte	∞	2	∞	2	∞	2	∞	2	10	2	**5**	**1**
1951rte	∞	3	∞	3	∞	3	∞	3	14	2	**5**	**1**
2383wp	5	6	5	∞	6	5	6	5	6	2	**3**	**2**
2736sp	6	4	∞	4	∞	4	∞	4	5	2	**3**	**2**
2746wp	6	5	∞	5	∞	4	∞	4	5	1	**3**	**1**
2848rte	10	3	∞	3	∞	3	∞	3	5	2	**2**	**1**
2868rte	∞	5	∞	5	16	4	21	4	10	2	**5**	**1**
2869pegase	5	7	8	6	∞	4	∞	4	6	1	**4**	**1**
3012wp	∞	3	∞	3	∞	3	∞	3	7	1	**3**	**1**
3120sp	6	6	∞	∞	8	8	∞	∞	6	2	**3**	**2**
3375wp	∞	2	∞	2	∞	2	14	2	7	2	**4**	**1**
6468rte	∞	3	∞	3	∞	3	∞	3	5	2	**3**	**1**
6470rte	∞	3	∞	3	∞	3	∞	3	7	2	**4**	**1**
6515rte	∞	3	∞	3	∞	3	∞	3	8	2	**5**	**1**
9241pegase	7	6	∞	6	∞	4	∞	4	8	1	**4**	**1**
ACTIVSg10k	∞	5	∞	5	∞	5	∞	5	14	2	**5**	**2**
13659pegase	∞	6	∞	6	∞	5	∞	5	9	2	**5**	**2**
ACTIVSg25k	6	5	∞	5	∞	4	∞	4	17	2	**5**	**1**
ACTIVSg70k	∞	6	∞	8	∞	5	∞	5	72	2	**7**	**2**

∞-indicates the divergence of the simulation

It is also important to emphasize that the solutions for these test cases were all obtained by solving the most basic form of power flow analysis, which did not include any of the network operational limits, such as limits on generator reactive powers. Incorporating operational limits in existing industry standard simulators is not done implicitly and requires the addition of the outer simulation

loops around the NR solver [24], [31]. These outer loops heuristically adjust the controlled power flow variables while rerunning the NR solver until all of the desired states are bounded, or if the maximum outer loop iteration count is reached. However, due to the primitiveness of these approaches that can cause the significant increase in total iteration counts and are prone to divergence and oscillations [31],[71], they are only mentioned here for completeness. We next explore the optimization nature of the power flow problem by showing that the operational, as well as any other grid performance limits, can be naturally included within the ECP optimization problems discussed in the rest of the chapter.

Lastly, even when the real and reactive powers supplied by the slack bus are unbounded, and the operational and performance limits are not incorporated, it is still possible that no feasible power flow solution exists [30],[72]. Therefore, as already emphasized in Chapters 3 and 4, simply constraining the powers injected to a network can cause the infeasibility of the simulation problem, and by itself calls for solving an optimization problem to identify the power flow infeasibilities.

6.3. Evaluating Power Flow feasibility through ECP

Incorporating the domain specific knowledge within the power flow simulations drastically improves the problem convergence profile, thus making it less volatile to the choice of initial starting point. However, the "simplistic" macro-modeling of nonlinear elements in terms of constant power constraints, as well as their independency on the power system operational frequency (that is sometimes modeled), creates the possibility of no feasible power flow solution that satisfies the conservation of energy within the system. Moreover, since divergence cannot be avoided when the power flow problem is infeasible, it is difficult to distinguish systems that have diverged due to "lack of simulation robustness" from those that are "truly infeasible." For instance, consider the simulation profile of the ill-conditioned 11-bus test case [73] shown in Figure 6.5, which was demonstrated to fail by both circuit simulation techniques and the ECP algorithms. Importantly, even though our intuition suggests the problem infeasibility due to the characteristics of divergence and saturation of OL algorithms, we cannot still claim it with full certainty.

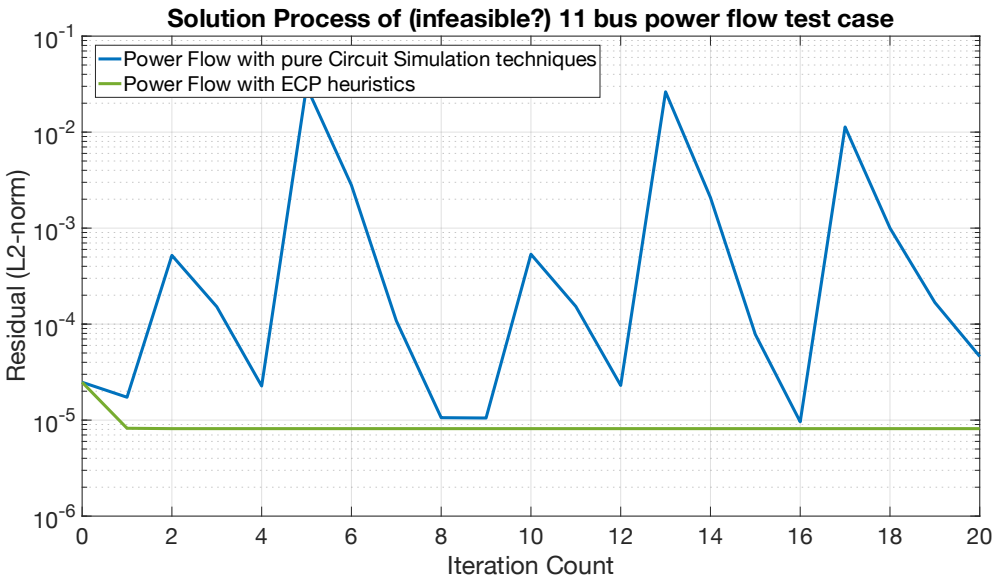

Figure 6.5. Power flow convergence profile for the ill-conditioned 11 bus test case.

To tackle the problem of simulation infeasibility, it is important to recall that for a power flow network defined by (6.1), there exists a uniquely defined adjoint circuit that, as shown in Chapter 4, can be used to indicate, quantify and localize the simulation problem infeasibility. Furthermore, by introducing the coupling between the network and its adjoint, the power flow infeasibilities are "redirected" to excite the adjoint circuit that will now ensure the optimally minimized energy exchange between them. Importantly, we can further define the types of coupling between the network and its adjoint that can be solely or interchangeably used to preserve the energy conservation within the system as follows:

a) Coupling the set of KCL equations by the respective adjoint voltages.
b) Coupling the set of local power mismatch and voltage magnitude equations by the respective adjoint admittances.

By referring to the definition of the ECP feasibility problem from Chapter 4, the power flow feasibility problem can be also defined in the standard optimization form as given by (6.3), and as such, used for validation and comparisons between the ECP approach for obtaining its solution and the traditional state-of-art optimization algorithms.

Standard Optimization Form of a Power Flow Feasibility ECP:

$$\min_{\dots} \frac{1}{2}\|\boldsymbol{w_R} \odot \boldsymbol{I_{\Delta R}}\|_2^2 + \frac{1}{2}\|\boldsymbol{w_I} \odot \boldsymbol{I_{\Delta I}}\|_2^2 + \frac{1}{2}\|\boldsymbol{w_p} \odot \boldsymbol{\Delta p}\|_2^2 + \frac{1}{2}\|\boldsymbol{w_q} \odot \boldsymbol{\Delta q}\|_2^2 \tag{6.3}$$

such that

$$[G_{RLC} + \text{diag}(\boldsymbol{G})]\boldsymbol{V_R} - [B_{RLC} + \text{diag}(\boldsymbol{B})]\boldsymbol{V_I} + E_N\boldsymbol{I_{SB,R}} = \boldsymbol{I_{\Delta R}}$$

$$[G_{RLC} + \text{diag}(\boldsymbol{G})]\boldsymbol{V_I} + [B_{RLC} + \text{diag}(\boldsymbol{B})]\boldsymbol{V_R} + E_N\boldsymbol{I_{SB,I}} = \boldsymbol{I_{\Delta I}}$$

$$E_N\boldsymbol{V_R} - \boldsymbol{V_{SB,R}} = \boldsymbol{0}$$

$$E_N\boldsymbol{V_I} - \boldsymbol{V_{SB,I}} = \boldsymbol{0}$$

$$f_G(\boldsymbol{V_R}, \boldsymbol{V_I}, \boldsymbol{G}, \boldsymbol{B}) = \boldsymbol{\Delta p}$$

$$f_B(\boldsymbol{V_R}, \boldsymbol{V_I}, \boldsymbol{G}, \boldsymbol{B}, \boldsymbol{Q_G}) = \boldsymbol{\Delta q}$$

Solving an ECP. All of the following experiments that correspond to solving a problem from (6.3) are performed within the developed ECP MATLAB prototype, executed on a MacBook Pro 2.9 GHz Intel Core i7, and following the methodology discussed in Chapters 4 and 5. The default convergence criterion was set to $\epsilon = 10^{-6}$ for the absolute variable step difference and the problem residual, while the objective function weights are all set to 1.

6.3.1. Simulation and analysis of the infeasible 11 bus network

As demonstrated in [73], the 11-bus distribution test case is genuinely ill-conditioned beyond a maximum loading factor of 99.82%. Hence, numerical error or the choice of convergence criterion can cause the difference between infeasibility (divergence of the numerical algorithm) or convergence to the operating solution as demonstrated by Figure 6.5. In this study, the power flow feasibility problem is solved for slight loading factor increments to locate and examine the appearance and evolution of infeasible regions within the test case. The simulation results representing the network topology for four different loading factors (three of which are provably infeasible) are presented in Figure 6.6 (left). Referring to Figure 6.6, after the known point of collapse is reached, the system first becomes infeasible (indicated by the heatmap around the infeasible bus) furthest from the slack generator (bus 11). As the loading factor keeps increasing, the infeasibility, which represents the amount of additional current needed to prevent the violation of KCL at each bus, evolves throughout the system.

Finally, since the bus 11 initially causes the problem infeasibility, the LASSO-like algorithm from Chapter 4 can be further applied to localize the infeasibility to that bus only. The sparse infeasibility information can be now used to determine the value of a capacitor that can be "installed" at bus 11 in order to prevent power flow infeasibility for all of the four examined loading factors as shown in Figure 6.6 (right).

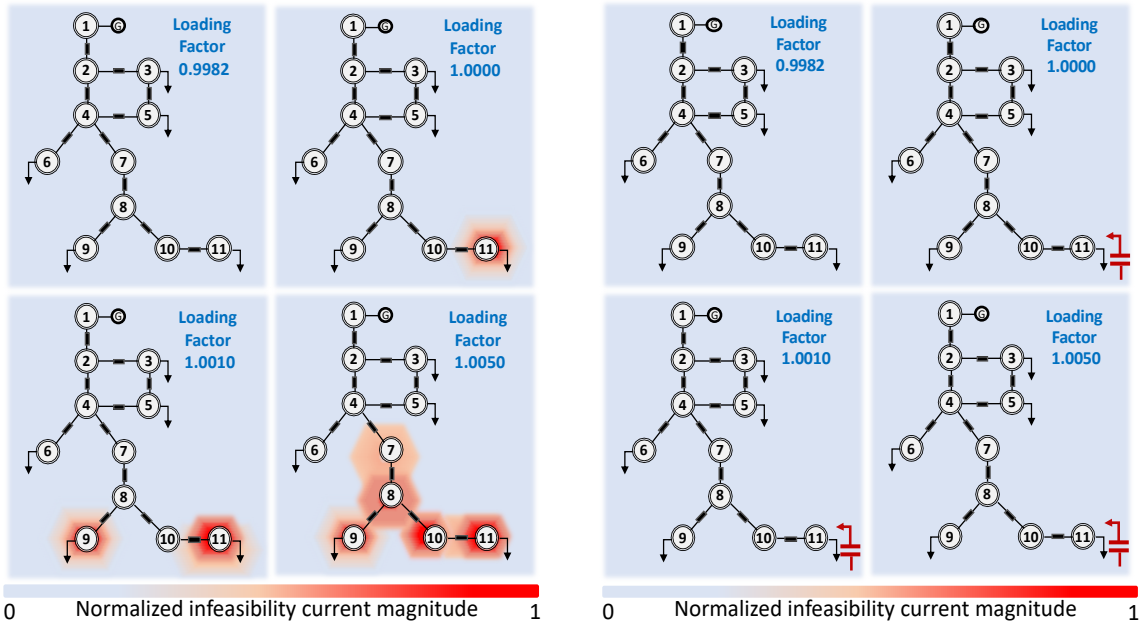

Figure 6.6. Evaluating the feasibility of ill-conditioned 11 bus test case. The magnitude of infeasibility current is normalized with respect to the highest one encountered throughout the simulation of all four cases.

6.3.2. N-1 contingency analysis on a Synthetic representation of the power grid of entire USA

The scalability of the ECP framework is further tested by analyzing the feasibility of a synthetic test case representing the entire US grid [67] for an N-1 contingency. The N-1 contingency we applied represented disconnecting the branch between buses 23510 (SENECA 71) and 23515 (SENECA76) within the Oconee Nuclear station, near Seneca, SC. The ECP simulation converged in 10 iterations and the results indicate that this contingency represents an infeasible system, with the local area of infeasibility shown in Figure 6.7 (left). Furthermore, after analyzing the affected infeasible area and replacing the fixed shunt capacitor connected at the most infeasible bus (SENECA 7.1) with a variable shunt device as presented in Figure 6.7(right), the system becomes feasible again.

As shown by the simulation results so far, the coupling between the power flow network and its adjoint can inform various corrective actions or planning decisions in addition to simply locating the power flow infeasibilities. For instance, the 11-bus test case presents an application toward optimal capacitor placement, while, placing the coupling sources at nodes of critical infrastructure within the grid model can allow optimal planning for a new corrective device that would ensure N-1 contingency criteria required by NERC are met [74].

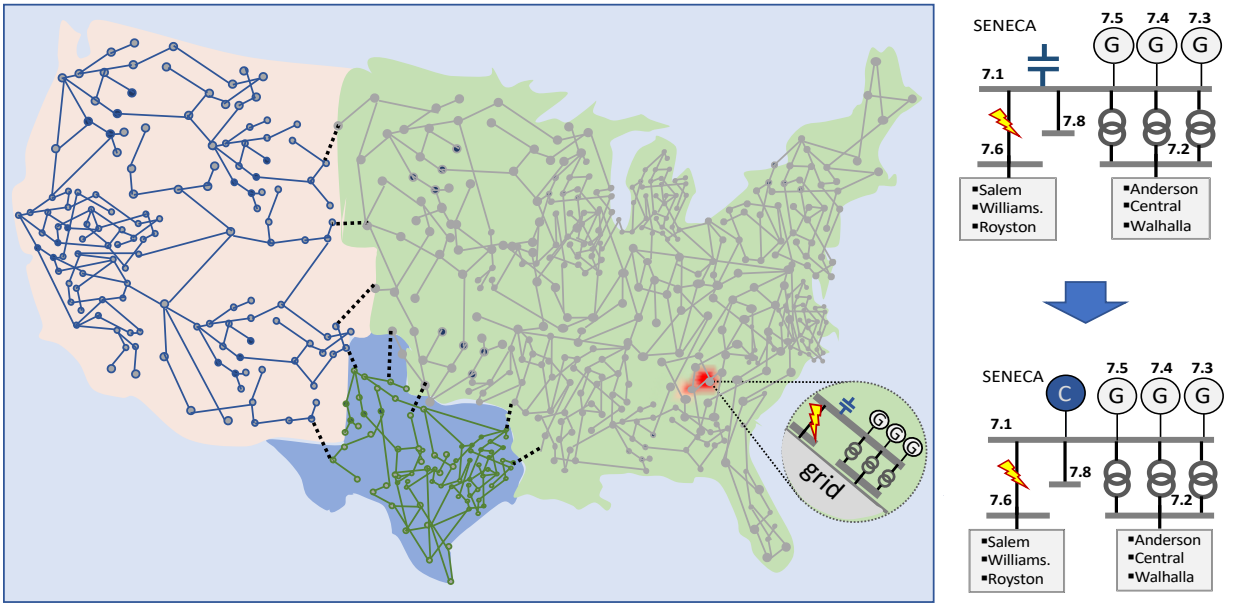

Figure 6.7. Detecting infeasibility due to the contingency in synthetic test case representation of USA grid. Note that replacing the fixed shunt capacitor at bus 23515 with a variable capacitor restores the feasibility of the power flow.

6.3.3. Comparisons with the existing optimization algorithms

So far, we have presented results obtained from the ECP framework that indicate the significant improvements in power flow simulation robustness in comparison with the existing solution methodologies. More importantly, with the capability of solving the infeasible power flow cases, the initial doubt of understanding the source of simulation divergence is dispelled. Now, divergence of coupled simulation of power flow and its respective adjoint circuit indicates problems with the algorithms used to control the NR step, and further helps to fine-tune those algorithms.

The first step in demonstrating the efficiency of ECP framework is to compare it with the existing state-of-art optimization algorithms, starting from the equality constrained optimization problems, as is the power flow feasibility problem from (6.3). Therefore, in order to have a fair comparison between the two, and considering the efficiency of circuit simulation approach for building the Hessian and Jacobian matrices, we have developed the prototype circuit simulator in MATLAB, where the Gradient and Hessian information are built on the same way as in the ECP circuit simulator, and the *only difference represents the respective set of existing optimization algorithms applied to control the NR step size*. Moreover, the algorithm used for comparisons through the rest of the thesis is implemented within the FMINCON MATLAB toolbox, and can

be generally described as a Primal-Dual Interior Point Method combined with a trust region approach [39]-[42] as implemented in most of the large-scale state-of-art optimization toolboxes. Thus, the purpose of the following experiment based on the power flow feasibility problem is to provide a comparison between the two solution methodologies. Namely, the one behind the traditional mathematical optimization algorithms based on the one-dimensional line search problem, and the set of solution methodologies implemented within the ECP framework based on Variable Filtering and Optimal Limiting algorithms.

Consider the following five realistic-size power flow cases whose description and detailed specifications are provided in Table 6.1.

1. Case3375wp
2. Case9241pegase
3. CaseACTIVSg10k
4. CaseACTIVSg25k
5. CaseACTIVSg70k

In order to test the robustness and efficiency of the ECP framework, the power flow feasibility problem from (6.3) is solved with the current feasibility sources coupled to the set of KCL system equations (corresponding to minimizing the L2 norm of KCL infeasibilities) for the 3 operating conditions. Namely, for the nominal loading condition as provided within the input file, as well as conditions simulating the additional OFF and ON peak scenarios by respectively decreasing and increasing the system generation and demand by 25%. Furthermore, each of the three conditions is run within ECP as well as the traditional framework implemented within FMINCON when initialized from both a flat voltage start, and the information provided within the test case input file. Lastly, as in all of the previous experiments, the simulations were performed on a MacBook Pro 2.9 GHz Intel Core i7, while the obtained results depicting the simulation runtime comparisons are presented in Figure 6.8-Figure 6.10.

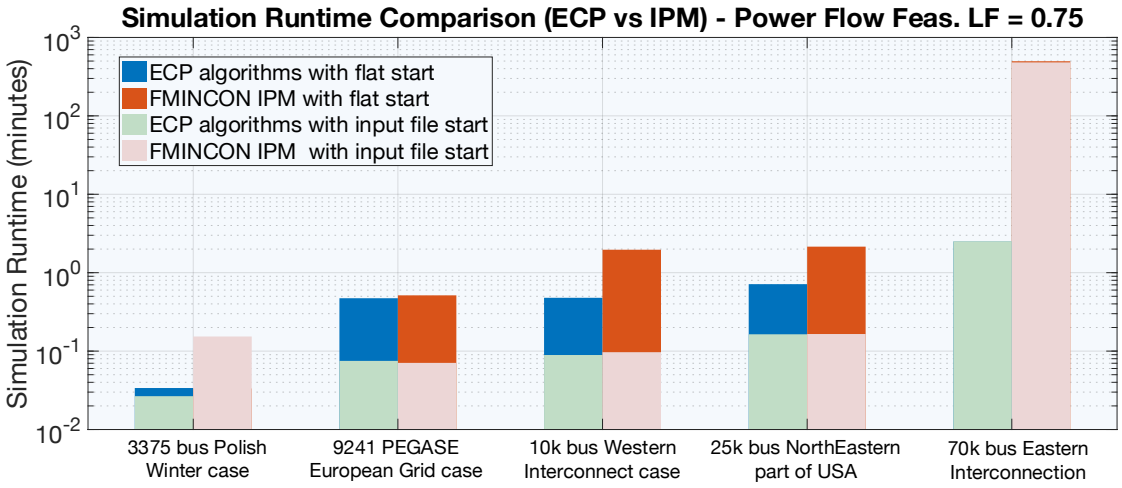

Figure 6.8. Power flow feasibility problem simulation runtime comparisons between ECP and traditional optimization algorithms, OFF-peak loading scenario (-25% load and generation decrement).

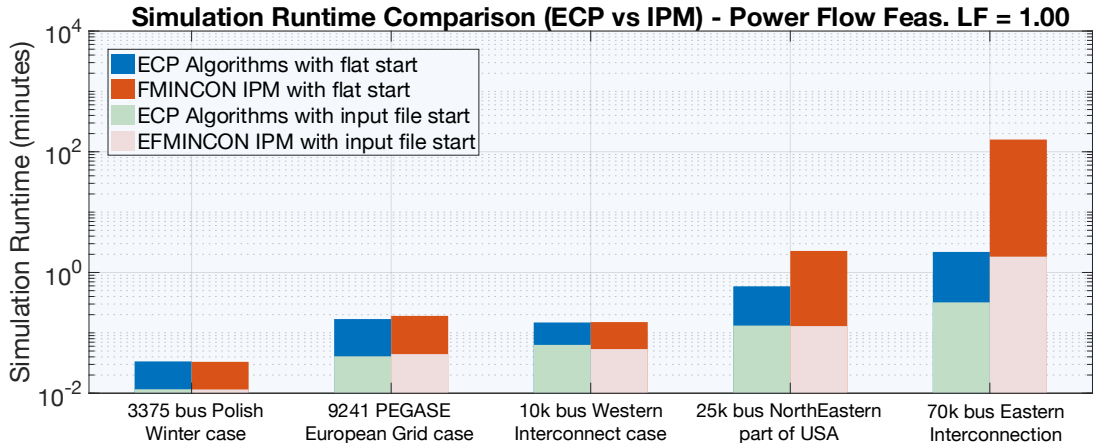

Figure 6.9. Power flow feasibility problem simulation runtime comparison between ECP and traditional optimization algorithms, nominal loading scenario.

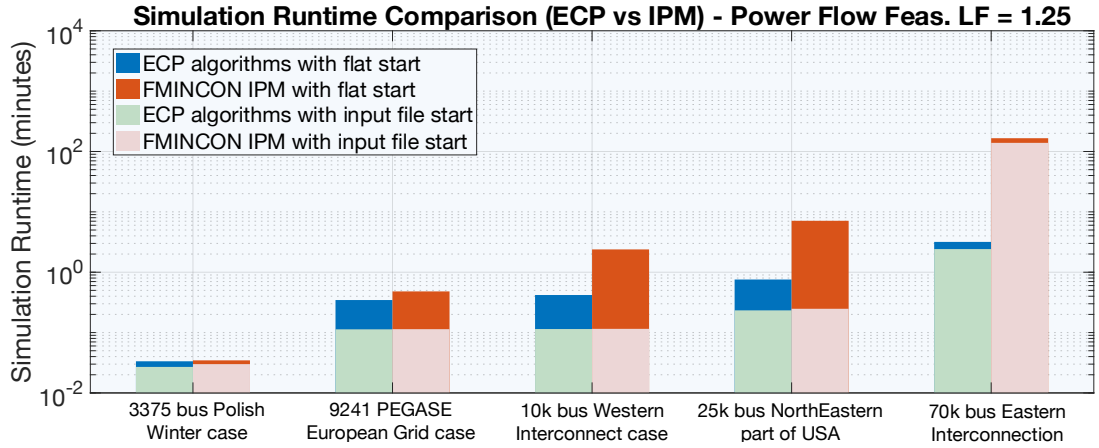

Figure 6.10. Power flow feasibility problem simulation runtime comparisons between ECP and traditional optimization algorithms, ON-peak loading scenario (+25% load and generation decrement).

As presented in Figure 6.8-Figure 6.10, the simulation runtime profiles behave according to our intuition and discussion provided in Chapter 2:

i. It can be said that the two smaller-size test cases performed equally well with both ECP and traditional heuristics for all scenarios and initializations. This can be further explained by the initial starting points of the examined equality constrained optimization problems being in the vicinity of the respective optimal solutions.
ii. As the size of problem increases and the initial starting points move away from the optimization solutions (increased loading, flat start, etc.), the traditionally based heuristics start slowing down the convergence process due to the single step line-search methodology that limits all of the NR steps with a single constant factor.
iii. In contrast to the traditional optimization heuristics, however, the heuristics based on physical characteristics of the problem incorporated within the ECP solver significantly overperforms the traditional optimization heuristics.
iv. Finally, the experiments performed also indicate the importance of robust and efficient simulation and optimization framework during the analyses for which the good initialization is not known, such as for contingency and other planning analyses. The preliminary results indicate the significant correlation between the "goodness" of the initialization and the traditional simulator efficiency, which is particularly highlighted as the size of cases increases.

It is important to note that even though the power flow feasibility problem defined in (6.3) can indicate and quantify the original power flow infeasibilities, the obtained results can be still far from the realistic solutions, since none of the operational and performance limits are considered. To analyze the impact of not enforcing these limits to the examined test cases, we first consider the set of three operational limits:

1. The reactive power Q_G supplied by each of the PV generators, as well as other VR devices, has to be between the device operational limits.
2. The bus voltages within the power grid need to be bounded to ensure the proper voltage levels within the grid.
3. In most realistic cases, there is more than one generator that picks up the slack power within the system in order to ensure the stable operation, and the whole process is

significantly more complicated [31],[75]. Moreover, it can be seen as a distribution of slack power among more generators in the grid, which is in stark contrast to a single generator scenario in traditional power flow problems. Therefore, we examine the percent capacity of real power on which the slack bus generator operates.

The simple power grid device violations for the 5 examined test cases are presented in Table 6.3.

Table 6.3 Documenting the number of operational constraint violations of the examined set of 5 power flow test cases solved within the ECP framework. Note that the generator bounds are also scaled with the loading factor.

Load. Factor	**Nominal -25%**			**Nominal**			**Nominal +25%**		
case	# Q_G violations	# V_M violations	Slack Gen (%) Capacity	# Q_G violations	# V_M violations	Slack Gen (%) Capacity	# Q_G violations	# V_M violations	Slack Gen (%) Capacity
3375wp	164	80	74	184	35	100	207	26	129
9241pegase	295	64	14.3	151	0	60	451	165	115.5
ACTIVSg10k	897	9	72.5	776	0	107	807	3	149.5
ACTIVSg25k	1627	8	-98.7	1396	0	99.9	1787	0	330.2
ACTIVSg70k	3418	1243	-234.4	2952	2	92	3522	699	107.5

As it can be seen from Table 6.3:

- There are generators (including VR devices) in every case and operating condition that violate the respective operational limits.
- In comparing the bus voltage violations, it can be seen that 3 out of 5 cases have the voltage levels within the predefined operational bounds for the nominal operation, while there exist buses with violated voltage limits in all other cases and scenarios.
- Slack bus generators operate within the predefined capacity limits for most of the cases operating during the nominal loading conditions, while the capacity limits are significantly exceeded, in On and Off-peak scenarios. Moreover, the negative percent capacity indicates that the generator needs to act as a load in order to ensure the preservation of energy within the grid, which is not realistic in actual, and further highlights the non-physical nature of a slack bus.

In conclusion, even though a “simple” solution to the feasibility problem can be robustly and efficiently obtained within the ECP framework, it is not enough, and we have to dig deeper into the domain of constrained optimizations to incorporate the more realistic power grid constraints.

This will also further provide the answer about the "true nature" of a power flow problem and show that a realistic power flow analysis is an optimization rather than a simulation problem.

6.4. True nature of real-world power flow problems

To incorporate the operational limits within the power flow feasibility problem from (6.3), it is important to fully understand the power system device characteristics and behavior at the steady-state grid condition under which the operational limits hold. Therefore, we start with a brief discussion of control characteristics for the Automatic Voltage Regulation (AVR) and Automatic Generator Control (AGC) that have to be considered while embedding the operational limits within the respective power flow models.

6.4.1. Automatic Generator Regulation (AVR) and Automatic Generator Control (AGC) Characteristics

Referring to the model of VR devices and PV generators, note that the reactive power represents a variable that is adjusted (solved for) in order to control the desired bus voltage magnitude as given by (6.2). However, as can be seen from the previously examined power flow results, the reactive power is not bounded, and hence can often exceed the predefined operational limits. Most importantly, since the reactive power controls the voltage magnitude, once the operational limit is approached, the device can no longer control the desired voltage which results in disjunctive characteristics, as shown in Figure 6.11 (left). Mathematically, this disjunctive behavior can be defined for j^{th} VR device as:

$$\begin{Bmatrix} Q_{MIN,j} < Q_{G,j} < Q_{MAX,j} \ \wedge \ V_R^2 + V_I^2 = |V_S|^2 \\ Q_{G,j} = Q_{MAX,j} \ \wedge \ V_R^2 + V_I^2 < |V_S|^2 \\ Q_{G,j} = Q_{MIN,j} \ \wedge \ V_R^2 + V_I^2 > |V_S|^2 \end{Bmatrix} \tag{6.4}$$

Conversely, when represented within the power flow analysis, the AGC corresponds to nothing more but the distribution of the real slack power among the generators in the system. Moreover, system slack real power Δ_S is not assigned to a single generator, as in the case of traditional power flow analysis, but is rather distributed by a specified participation factor π_i,

among the generators that now "participate" in AGC. This causes their real power to become an additional variable defined as:

$$P_{G\Delta,\mathrm{i}} = P_{G,i} + \pi_i \Delta_S \tag{6.5}$$

However, since the real generated power is not a constant anymore, the respective operational limits has to be taken into the consideration too. If the operational real power limit is approached, the generator can no longer participate in AGC, which again results in a disjunctive characteristics, as shown in Figure 6.11 (right), or in terms of this mathematical representation for the i^{th} generator:

$$\left\{\begin{array}{c} P_{MIN,i} < P_{G\Delta,\mathrm{i}} < P_{MAX,i} \ \wedge \ P_{G\Delta,\mathrm{i}} = P_{G,i} + \pi_i \Delta_S \\ P_{G\Delta,\mathrm{i}} = P_{MAX,i} \ \wedge \ P_{G\Delta,\mathrm{i}} < P_{G,i} + \pi_i \Delta_S \\ P_{G\Delta,\mathrm{i}} = P_{MIN,i} \ \wedge \ P_{G\Delta,\mathrm{i}} > P_{G,i} + \pi_i \Delta_S \end{array}\right\} \tag{6.6}$$

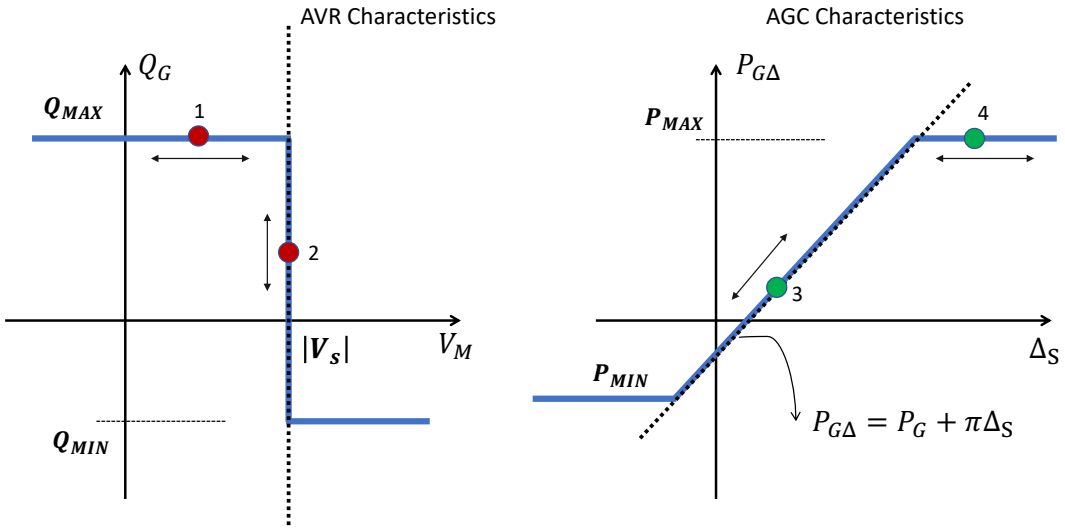

Figure 6.11. Automatic Voltage Regulation (AVR) and Automatic Generator Control (AGC) characteristics.

Considering that the respective disjunctive behavior is often modeled in terms of integer variables, it becomes very clear why the traditional formulations attempt in modeling the device control within the outer loops around power flow NR simulation. Notably, the traditional solvers already suffer from the robustness issues with quadratic like nonlinearities, and the addition of steep and discontinuous nonlinearities would further strain the robustness of those nonlinear solvers.

6.4.2. Understanding the AVR and AGC from the perspective of ECP feasibility problem

To understand the disjunctive AVR and AGC characteristics from the perspective of conservation of energy within the power system, refer to Figure 6.11 and the four points shown on the respective nonlinear functions. It is important to note that the real and reactive power values corresponding to the points 2 and 3 are determined by the network response itself, and not the nonlinear functions from (6.4) and (6.6). Similarly, if the real and/or reactive powers are approaching the respective operational limits, as in the case of points 1 and 4, the voltage magnitude as well as the real slack power Δ_S are driven by the network response and not the adjunctive functions themselves. These respective values now correspond to the operating point for which the energy conservation laws hold within the power grid.

Therefore, if we simply enforce all of the operational constraints within the power flow feasibility problem from (6.3) that also include bounds on the voltage magnitudes given for the j^{th} bus as $V_{MIN,j}^2$ and $V_{MAX,j}^2$:

$$\begin{aligned} Q_{MIN,i} < Q_{G,i} < Q_{MAX,i} \\ V_{R,j}^2 + V_{I,j}^2 - v_{s,j} = 0 \\ v_{s,j} - |V_s|^2 = 0 \\ V_{MIN,j}^2 < v_{s,j} < V_{MAX,\mathrm{j}}^2 \end{aligned} \tag{6.7}$$

$$\begin{aligned} P_{MIN,i} < P_{G\Delta,i} < P_{MAX,i} \\ P_{G\Delta,i} - P_{G,i} - \pi_i \Delta_S = 0 \end{aligned} \tag{6.8}$$

There are two possible scenarios that can happen:

a) If there exists an operating point that satisfies all of the constraints, great! The optimization problem will converge, and the operating point will now take into the consideration all of the considered operational limits.
b) If, however, the network drives the operating point that satisfies the conservation of energy under the enforced operational limits within the system, but further violates some of the additional constraints, set voltage, distributed power, etc., then there doesn't exist a point

that satisfies all of the constraints and the optimization problem will be infeasible. Furthermore, the problem infeasibility can be also quantified by the existence of variables Δv and Δp_S that now correspond to the difference between the network operating point and the additionally enforced constraints. Moreover, the optimization problem feasibility can be recovered if for some given Δv and Δp_S constraints in (6.9) hold.

$$\begin{aligned} v_{s,j} - |V_s|^2 &= \Delta v_j \\ P_{G\Delta,i} - P_{G,i} - \pi_i \Delta_S &= \Delta p_{S_i} \end{aligned} \tag{6.9}$$

The additional constraints from (6.9) can be also seen in terms of an ECP feasibility problem, where the Δv and Δp_S correspond to the couplings between the network and its adjoint circuit introduced to ensure the problem feasibility. Namely, if the problem is infeasible due to its contradicting constraints, the infeasibilities will be redirected as an excitation to the adjoint circuit that now ensures that the network operating points maintains the energy conservation laws satisfied. Most importantly, as in any other ECP problem, an optimal solution is driven by the conservation of energy within the system, and therefore, the nonzero values of the coupling feasibility sources correspond to the differences between the network operating point and the additional constraints enforced by the problem.

In terms of a standard mathematical optimization form, the power flow feasibility problem enhanced with the additional operational limits from (6.14) is obtained by appending the set of constraints from (6.7)-(6.8) to the ECP problem in (6.3). However, contrary to (6.3), the couplings (infeasibility variables that are to be minimized) must be *chosen more carefully* in order to prevent contradicting objectives. Namely,

i) A bus with only load demand connected to it can have either feasibility power or current variables that are to be minimized, as was the case in (6.3):

$$\begin{aligned} \{[G_{RLC} + \mathrm{diag}(\boldsymbol{G})]\boldsymbol{V_R} - [B_{RLC} + \mathrm{diag}(\boldsymbol{B})]\boldsymbol{V_I}\}_l &= I_{\Delta R,l} \\ \{[G_{RLC} + \mathrm{diag}(\boldsymbol{G})]\boldsymbol{V_I} + [B_{RLC} + \mathrm{diag}(\boldsymbol{B})]\boldsymbol{V_R}\}_l &= I_{\Delta \mathrm{I},l} \end{aligned} \tag{6.10}$$

Or

$$G_l\left(V_{R,l}^2 + V_{I,l}^2\right) - \sum_{k=1}^{N_L} P_{L,k} = \Delta p_l$$
$$B_l\left(V_{R,l}^2 + V_{I,l}^2\right) + \sum_{k=1}^{N_L} Q_{L,k} = \Delta q_l \tag{6.11}$$

ii) A bus $g_A$with a connected generator that participates in AGC requires the presence of only infeasibility variables related to modeling the AGC and AVR response (Δv_j and Δp_{S_i}). This can be intuitively explained due to the fact that the reactive power is bounded, and hence adding the extra current or reactive power infeasibilities can introduce the conflicts in the objectives.

$$\{[G_{RLC} + \text{diag}(\boldsymbol{G})]\boldsymbol{V_R} - [B_{RLC} + \text{diag}(\boldsymbol{B})]\boldsymbol{V_I}\}_{g_A} = 0$$
$$\{[G_{RLC} + \text{diag}(\boldsymbol{G})]\boldsymbol{V_I} + [B_{RLC} + \text{diag}(\boldsymbol{B})]\boldsymbol{V_R}\}_{g_A} = 0$$
$$G_{g_A}\left(V_{R,g_A}^2 + V_{I,g_A}^2\right) - \sum_{k=1}^{N_L} P_{L,k} + \sum_{m=1}^{N_G} P_{G\Delta,m} = 0$$
$$B_{g_A}\left(V_{R,g_A}^2 + V_{I,g_A}^2\right) + \sum_{k=1}^{N_L} Q_{L,k} - Q_{G,g_A} = 0 \tag{6.12}$$
$$v_{s,j} - |V_s|^2 = \Delta v_j$$
$$P_{G\Delta,m} - P_{G,g_m} - \pi_m \Delta_S = \Delta p_{S,m} \quad \forall m \in g_A$$

iii) A bus g_N with a generator that doesn't participate in AGC, can have the feasibility real power only, in addition to the feasibility variable related to AVR, Δv_j, since everything else will be conflicting with bounded reactive power at a bus:

$$\{[G_{RLC} + \text{diag}(\boldsymbol{G})]\boldsymbol{V_R} - [B_{RLC} + \text{diag}(\boldsymbol{B})]\boldsymbol{V_I}\}_{g_N} = 0$$
$$\{[G_{RLC} + \text{diag}(\boldsymbol{G})]\boldsymbol{V_I} + [B_{RLC} + \text{diag}(\boldsymbol{B})]\boldsymbol{V_R}\}_{g_N} = 0 \tag{6.13}$$

$$G_{g_N}\left(V_{R,g_N}^2 + V_{I,g_N}^2\right) - \sum_{k=1}^{N_L} P_{L,k} + \sum_{m=1}^{N_G} P_{G,m} = \Delta p_{l,g_N}$$

$$B_{g_N}\left(V_{R,g_N}^2 + V_{I,g_N}^2\right) + \sum_{k=1}^{N_L} Q_{L,k} - Q_{G,g_N} = 0$$

$$v_{s,j} - |V_s|^2 = \Delta v_j$$

Standard Optimization Form of a Power Flow Feasibility ECP with Operational Limits:

$$\min_{\dots} \frac{1}{2}\|\boldsymbol{w_R} \odot \boldsymbol{I_{\Delta R}}\|_2^2 + \frac{1}{2}\|\boldsymbol{w_I} \odot \boldsymbol{I_{\Delta I}}\|_2^2 + \frac{1}{2}\left\|\boldsymbol{w_p} \odot \boldsymbol{\Delta p}\right\|_2^2 + \frac{1}{2}\left\|\boldsymbol{w_q} \odot \boldsymbol{\Delta q}\right\|_2^2$$

such that

$$\begin{gathered}
[G_{RLC} + \mathrm{diag}(\boldsymbol{G})]\boldsymbol{V_R} - [B_{RLC} + \mathrm{diag}(\boldsymbol{B})]\boldsymbol{V_I} + E_N \boldsymbol{I_{SB,R}} = \boldsymbol{I_{\Delta R}} \\
[G_{RLC} + \mathrm{diag}(\boldsymbol{G})]\boldsymbol{V_I} + [B_{RLC} + \mathrm{diag}(\boldsymbol{B})]\boldsymbol{V_R} + E_N \boldsymbol{I_{SB,I}} = \boldsymbol{I_{\Delta I}} \\
E_N \boldsymbol{V_R} - \boldsymbol{V_{SB,R}} = \boldsymbol{0} \\
E_N \boldsymbol{V_I} - \boldsymbol{V_{SB,I}} = \boldsymbol{0} \\
\overline{f}_G(\boldsymbol{V_R}, \boldsymbol{V_I}, \boldsymbol{G}, \boldsymbol{B}, \boldsymbol{P_{G\Delta}}, \boldsymbol{Q_G}, \boldsymbol{v_s}) = \boldsymbol{\Delta p} \\
\overline{f}_B(\boldsymbol{V_R}, \boldsymbol{V_I}, \boldsymbol{G}, \boldsymbol{B}, \boldsymbol{P_{G\Delta}}, \boldsymbol{Q_G}, \boldsymbol{v_s}) = \boldsymbol{\Delta q} \\
\boldsymbol{Q_{MIN}} < \boldsymbol{Q_G} < \boldsymbol{Q_{MAX}} \\
\boldsymbol{P_{MIN}} < \boldsymbol{P_{G\Delta}} < \boldsymbol{P_{MAX}} \\
\boldsymbol{V_{MIN}^2} < \boldsymbol{v_s} < \boldsymbol{V_{MAX}^2}
\end{gathered} \tag{6.14}$$

where $\overline{f}_G(\cdot)$ and $\overline{f}_B(\cdot)$ now also include the additional equality constraints from (6.7)-(6.8), while the respective infeasibility sources are chosen as defined by (6.10)-(6.13).

With the operational limits and the respective device characteristics modeled and incorporated within the power flow feasibility problem from (6.14), we can finally perform the experiments and fully compare the solution methodologies that support the ECP framework against the traditional optimization algorithms incorporated within FMINCON MATLAB optimization toolbox. Consider again the five test cases examined in Section 6.3.3, operating at the nominal loading conditions and now incorporating operational limits and respective device

AGC and AVR characteristics. Each of the five test cases is run within both ECP and the circuit simulator that runs FMNCON algorithms for both flat voltage and input file starting point and the results are presented in Figure 6.12 and Figure 6.13. Moreover, since the data on AGC participation factors was not provided, we applied the following recipe for calculating the participation for each of the generators in the system:

- If the set generator real power already exceeds, or is at the upper operational limit, its power is kept constant and it doesn't participate in AGC
- The participation factors for all of the other generators are chosen according to their real power capacity with the formula for i^{th} generator given as:

$$\pi_i = \frac{P_{MAX,i} - P_{MIN,i}}{\|\boldsymbol{P_{MAX}} - \boldsymbol{P_{MIN}}\|_1} \tag{6.15}$$

Next, as it was the case in solving (6.3), the weights for the basic set of feasibility variables are set to 1 for simplicity, while the newly introduced weights associated with modeling the AGC and AVR response are chosen as 100 in order to prioritize the minimized variables. Lastly, the maximum complementary slackness (CS) violation parameter for diode models within ECP is set to $\varepsilon = 10^{-11}$, which also represents the convergence tolerance that is applied to the ECP circuit (KKT optimality conditions) residual. All the problems were solved on MacBook Pro 2.9 GHz Intel Core i7.

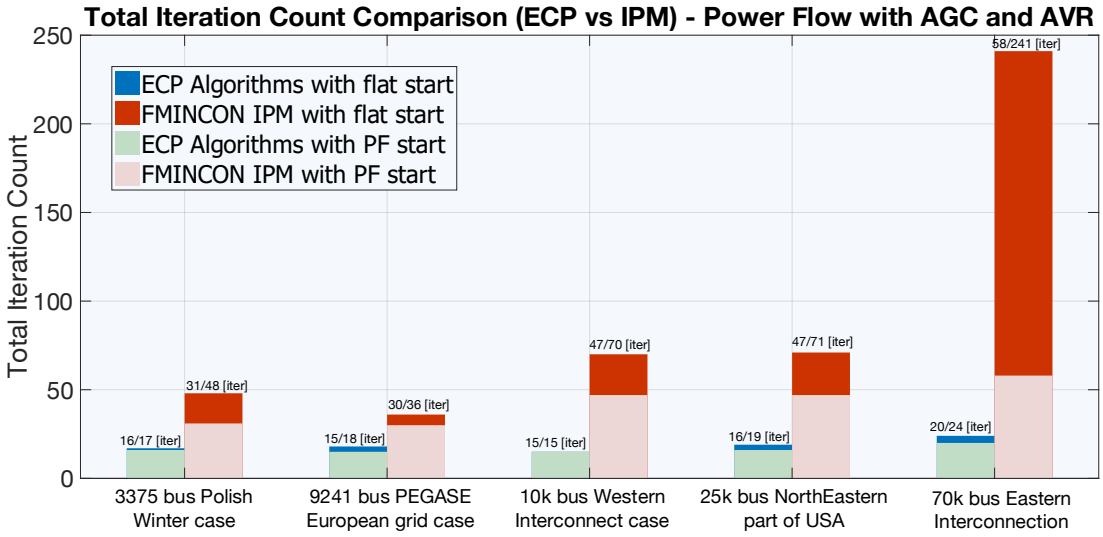

Figure 6.12. Power flow feasibility problem within incorporated operational constraints total iteration comparison between ECP and traditional optimization algorithms.

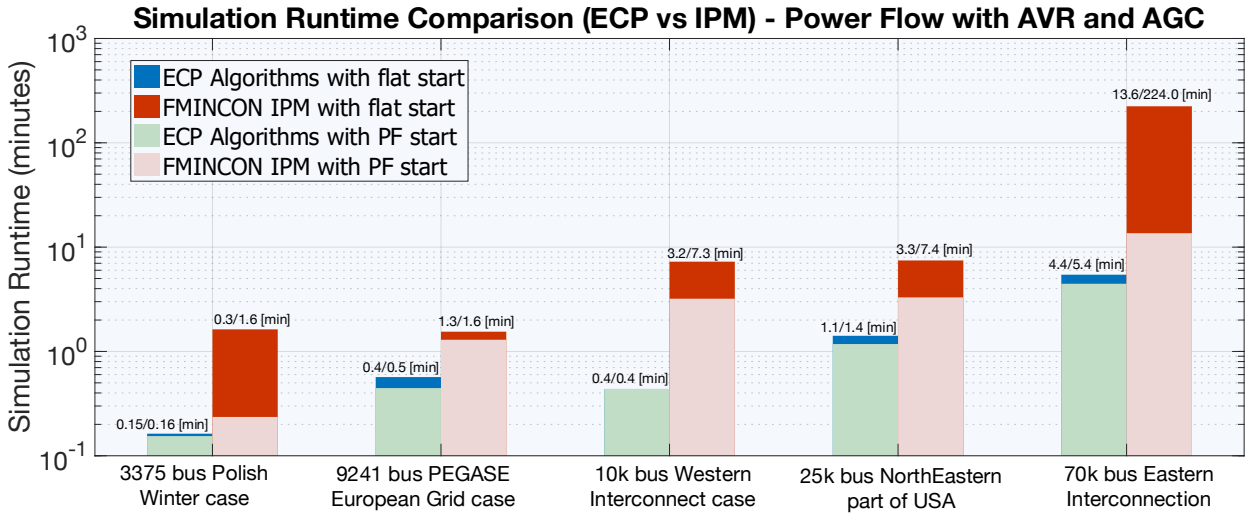

Figure 6.13. Power flow feasibility problem within incorporated operational constraints simulation runtime comparison between ECP and traditional optimization algorithms.

Before discussing the accuracy of modeling the disjunctive device characteristics by using the set of feasibility variables, we first refer to the comparison given in Figure 6.12 and Figure 6.13. As can be seen, the presented comparisons follow the same trend as demonstrated in Section 6.3.3, with one significant difference. Notably, with the incorporated set of inequality constraints within the optimization problem, even the smaller cases performed worse under the traditional algorithms. This is the behavior that is expected and elaborated in Chapter 2 and can be attributed to the conservative limiting techniques applied to ensure feasibility of variables within the IPMs. The conservativeness of limiting the NR-step is additionally highlighted in the cases of initialization from a flat voltage start, which now required significantly more iterations and thereby affected the runtime and efficiency of the solution process. In contrast, the diode limiting techniques incorporated within the ECP framework treats each of the step sizes separately and further adjusts the amount of damping based on the convergence of the ECP circuit. This was demonstrated to provide a significant boost in efficiency of the solution methodology. Most importantly, the correlation between the initial start and the simulation efficiency is significantly reduced.

Finally, in order to test whether the devices that take part in AVR and AGC modeled with the use of ECP feasibility approach behave as desired, we first need to recall that a power system, just as any other network, represents an interconnected system, and hence some of the infeasibilities that capture the constraint violations within the AGC and AVR responses can also affect the respective buses in the area around them. Namely, we counted on the “redirection” of

infeasibilities to excite the adjoint circuit, however, due to the network topology this excitation can further backfire and provide some additional input to the places in power flow network model where it should not, which can be also seen as a "relaxation error." For instance, there may be a generator that approached its reactive power limit, and as such, affects the other buses in the local area around it. Hence, the application of regularization algorithm introduced in Chapter 4 may be required after an optimal solution to (6.14) is obtained, in order to reduce the impact of these relaxation errors. However, we first focus on the optimization results obtained from solving the ECP in (6.14) for the five examined test cases. Table 6.4 presents the following:

i. Number of AVR participating devices that are at the operational limit, and hence cannot maintain the control of the desired voltage magnitudes in the system, but properly follow the AVR characteristics as given by the disjunctive function from (6.4).
ii. Number of AGC participating devices that are at the operational limit, and further properly follow the AGC characteristics as given by the disjunctive function from (6.5).
iii. Number of AVR devices that violate the desired characteristics defined by (6.4). Namely, even though the respective reactive power bounds are not approached, the voltage magnitude changed due to the relaxation error.
iv. Number of AGC devices that violate the desired characteristics defined by (6.5). The relationship between the generated real power and the distributed system slack defined by the respective participation factors is not maintained, as a result of relaxation error.
v. Real Slack Power Δ_S distributed among the generators participating in AGC.
vi. L2-norm of system infeasibility sources that do not include the respective AGC and AVR ones and hence serve as a further indicator of the problem infeasibility.

Table 6.4. Quantifying the exactness of AGC and AVR behavioral models. It is important to note that due to the enforced tolerances, every variable that is in $\sqrt{\varepsilon}$ vicinity to the bound is called as bounded. Lastly, the same criterion was used to determine the violations of AVR and AGC characteristics.

case	# Q_G@ a limit	# $P_{G\Delta}$@ a limit	AVR violation	AGC violation	Δ_S	$\|F\|_2$.
3375wp	90	116	3	0	6.66E-05	3.22E-10
9241pegase	178	1	50	1	-5.1863	0.3527
ACTIVSg10k	644	0	0	0	-0.0217	5.19E-10
ACTIVSg25k	1144	0	0	0	2.8950	9.09E-09
ACTIVSg70k	2039	1	0	0	-0.0935	1.32E-08

As seen from Table 6.4, the feasibility based modeling of AVR and AGC characteristics, performs extremely well considering the nonlinearity of disjunctive functions models that are now replaced with a quadratic objective function that are obtained from understanding the physical conservation laws within the network and its adjoint. Moreover, the solutions to the three largest cases do not even require further regularization and now correspond to the realistic network power flows that take into the consideration the operational limits with incorporated AGC and AVR characteristics. Interestingly, these solutions that often traditionally [76]-[78] required the use of integer variables, or outer loops around NR solver in modeling the nonlinear device characteristics, are obtained for the same cost as solving a continuous optimization problem that can be now efficiently done within the ECP framework. Lastly, the regularization algorithm from Chapter 4 is further applied in order to reduce the impact of the relaxation errors to the two smaller test cases. The results that include the number of additional NR iterations taken by the regularization algorithm as well as successfully "corrected" number of AVR and AGC violations are presented in Table 6.5.

Table 6.5. Correcting the AGC and AVR relaxation errors by means of LASSO-like regularization algorithm. Note that the correction of respective relaxation errors results in all five feasible cases whose power flows satisfy the desired operational limits while ensuring the proper device characteristics.

case	**# Q_G@ a limit**	**# $P_{G\Delta}$@ a limit**	**AVR violation**	**AGC violation**	**Δ_S**	**$\|F\|_2$.**	**Extra NR iterations**
3375wp	89	116	0	0	4.08E-05	5.16E-10	**4**
9241pegase	161	2	0	0	-5.3295	1.66E-05	**13**
ACTIVSg10k	644	0	0	0	-0.0217	5.19E-10	0
ACTIVSg25k	1144	0	0	0	2.8950	9.09E-09	0
ACTIVSg70k	2039	1	0	0	-0.0935	2.37E-10	0

Lastly, it is important to emphasize the conditions used to initialize the corrections within the LASSO-like regularization algorithm. Notably, the system infeasibilities are considered to be a relaxation errors if one of the following three conditions is satisfied:

1. Basic nonzero network infeasibilities are considered for correction if one of the respective bounds on a bus voltage magnitude is approached.
2. Nonzero AVR voltage infeasibility is considered for correction if the reactive power of an AVR participating device is not in vicinity to the respective operational limit.
3. Nonzero AGC infeasibility is considered for correction if the real power of an AGC participating generator is not in vicinity to the respective operational limit.

In conclusion, the power flow problem for characterizing and analyzing a power system steady-state response has taken a long journey from its introduction and sparse implementation that also represented one of the first general solutions to a sparse matrix problem. Now with its incorporation within a circuit simulation framework in SUGAR, a more realistic power flow solution can take into consideration the operational limits and respective device characteristics that define a problem as an optimization rather than a simulation problem.

As demonstrated in this chapter, the larger size power flow problems that include the realistic operational limits and device characteristics incorporated within the traditional optimization algorithms become intractable to solve during the operationally required timeframe, particularly when the good initialization cannot be provided. By referring to the discussion from Chapter 2, this can be attributed to the conservativeness of the traditional NR-step limiting algorithms that are applied without taking the physical characteristics of the problem into the consideration. Furthermore, it also most likely stands for one of the key reasons why the more realistic power flow analyses are still not widely applied for large-scale systems.

Finally, the preliminary power flow results obtained within the ECP framework demonstrate the significant improvements in runtime efficiency, while preserving the robustness previously achieved by the application of circuit simulation methods. Most importantly, the large-scale power flow “simulation” within SUGAR can now efficiently incorporate the realistic operational constraints as well as highly nonlinear grid device characteristics, while further providing the feasible power flow solution. Lastly, it is worth noting that if for an incorporated set of realistic operational limits, a power flow problem indicates infeasibility, the reliable grid operation may be affected. Therefore, one possible future remedy is solving a new optimization problem to determine the generation redispatch that changes the grid operational point, which is the focus of the next chapter.

Chapter 7 Optimizing Electrical Power Dispatch within the Equivalent Circuit Programming Framework

The capability of efficiently incorporating the realistic operational limits and respective power grid device characteristics within the power flow problem provides a more detailed picture of the grid response, as well as the reliability of its operation. However, what should the grid operator do if such picture clearly indicates the infeasibility of power flows within the grid? The answer to this question is not as simple as one would initially think. Notably, the power flow operating point is governed by the set of dispatched base generation and load demands, and therefore, the infeasibility of problem whose modeling approaches the realistic grid behavior can be worrisome. Moreover, it indicates that the power grid set point modeled within a power flow problem may not be secure for the analyzed scenario or operating condition. In addition, it is also important to note that traditional power flow does not incorporate the frequency information and uses primitive macro-modeling abstractions for representing the generation and load demand. Therefore, the answer to the above asked question is “maybe, it depends!” If the simulated scenario represents the present or upcoming operating grid condition, it may be already too late to worry, and blackout could occur. At a minimum, the chances for this scenario to happen is significantly increased. If, however, the analyzed scenario represents a contingency simulation for some of the grid planning cases, there is definitely more time to make the necessary changes and decisions.

In considering the bigger picture, the solution that represents a good remedy for the problem described above, which also eliminates the significant work stress of our grid operator, is to determine the grid operating point that reduces the scenarios of power flow infeasibility to a bare minimum. This can be done by incorporating them as the additional set of constraints within

the power dispatch optimization problems. It, however, turns out that this is way easier said than done, and obtaining such operating point from the solution of an optimization problem has been traditionally shown as quite challenging due to the highly nonlinear problem constraints as well as scalability of existing solution methodologies. Most notably, the financial market is defined by nonlinear pricing, and the electrical power flow problem exhibits the nonlinear characteristics in modeling the generators and loads. Both combined with additional security constraints create a daunting large-scale optimization problem, and therefore, in practice, the utility industry has relied upon approximations and good engineering judgment to obtain the best possible, rather than most optimal, power flow solutions. Notably, FERC has reported [79] that today's "approximate-solution techniques may unnecessarily cost tens of billions of dollars per year" and "result in environmental harm from unnecessary emissions and wasted energy."

Meanwhile, the larger portion of academic research in power flow optimization is still devoted towards finding a global optimal solution [80]-[82] to the basic optimal power flow dispatch that does not model any of the additional contingencies and operational scenarios. The solution would most likely not be used by grid operators since it doesn't guarantee the grid security in terms of robustness during the contingency scenarios. In fact, it can be said that contrary to the global optimal power flow solution for the basic problem, finding any optimal point that will ensure the grid security during the set of examined contingencies would be a more desirable solution.

This chapter focuses on electrical power dispatch optimization problems. If we recall the preliminary findings presented in the previous chapter, the efficiency of solution process can be significantly decreased with the less conservative ECP NR-step limiting algorithms that now also consider the physical problem characteristics in addition to traditionally based optimization techniques. This physical modeling framework further preserves the simulation robustness, as is the case with circuit simulation problems, and thereby makes the ECP framework more suitable for possible extremely large-scale optimizations, such as the realistic optimal power dispatch problem.

The reminder of this chapter first demonstrates that even obtaining an optimal solution to the full realistic base AC-OPF problem can be quite challenging, particularly with the increase in problem size. Next, the further consideration of different operating scenarios, and more periods in

future, results in a more realistic optimal dispatch solution, but can drastically increase the size of the optimization problem, and adds overhead to the solution process of the already challenging problem. To that effect, we provide the extensive comparison on base AC-OPF solutions obtained within the ECP framework as well as the traditional used formulations and optimization solvers. The sample of various existing large-scale test cases is considered in addition to the recently introduced OPF cases used in currently ongoing grid optimization competition sponsored by ARPA-E [76]. Furthermore, by running the realistic power flow simulations discussed in Chapter 6, we provide the analysis on number of cases that remain truly infeasible if only the solution to the base AC-OPF problem is considered. Lastly, it is demonstrated that the additional consideration of those problematic scenarios within the AC-OPF problem reduces their infeasibilities and further provides a promising problem that can be now solved within the ECP circuit framework, as done in existing circuit simulators that operate on problems of extreme scale.

7.1. Base AC Optimal Power Flow (AC-OPF) problem

Consider a power system such as those introduced in Chapter 6, whose steady-state response is characterized in terms of phasor voltages and currents ($\tilde{V}_{ik} = V_{R,ik} + jV_{I,ik}$ and $\tilde{I}_{ik} = I_{R,ik} + jI_{I,ik}$) at a fundamental frequency, and further governs the relationships between a set of generators $\mathcal{G}_B$ and load demands $\mathcal{D}_B$, interconnected by a set of transmission network elements, $\mathcal{T}_X$. A traditionally defined AC-OPF problem is based on finding an optimal solution to a cost of generated real power dispatch, often modeled in terms of a quadratic objective function $\mathcal{F}(\boldsymbol{P_G})$ that is subjected to the power flow network model, as well as other operational constraints. Moreover, in terms of the generalized network formulation for modeling a power grid steady-state response introduced in Chapters 3 and 6, an AC-OPF problem can be further stated in standard optimization form as:

$$\min_{\boldsymbol{P_G},\dots} \mathcal{F}(\boldsymbol{P_G}) = a_G + \sum_{i=1}^{N_G} b_{G_i} P_{G,i} + c_{G,i} P_{G,i}^2 \tag{7.1}$$

such that

$$[G_{RLC} + \text{diag}(\boldsymbol{G})]\boldsymbol{V_R} - [B_{RLC} + \text{diag}(\boldsymbol{B}) + E_{sh}\boldsymbol{B_{sh}}]\boldsymbol{V_I} = \boldsymbol{0}$$

$$[G_{RLC} + \text{diag}(\boldsymbol{G})]\boldsymbol{V_I} + [B_{RLC} + \text{diag}(\boldsymbol{B}) + E_{sh}\boldsymbol{B_{sh}}]\boldsymbol{V_R} = \boldsymbol{0}$$

$$F_G(\boldsymbol{V_R}, \boldsymbol{V_I}, \boldsymbol{G}, \boldsymbol{B}, \boldsymbol{P_G}, \boldsymbol{Q_G}, \boldsymbol{v_s}, \boldsymbol{i_{tx}}, \boldsymbol{s_{xfmr}}) = \boldsymbol{0}$$

$$F_B(\boldsymbol{V_R}, \boldsymbol{V_I}, \boldsymbol{G}, \boldsymbol{B}, \boldsymbol{P_G}, \boldsymbol{Q_G}, \boldsymbol{v_s}, \boldsymbol{i_{tx}}, \boldsymbol{s_{xfmr}}) = \boldsymbol{0}$$

$$\boldsymbol{P_{MIN}} < \boldsymbol{P_G} < \boldsymbol{P_{MAX}}$$

$$\boldsymbol{Q_{MIN}} < \boldsymbol{Q_G} < \boldsymbol{Q_{MAX}}$$

$$\boldsymbol{V_{MIN}^2} < \boldsymbol{v_s} < \boldsymbol{V_{MAX}^2}$$

$$\boldsymbol{B_{MIN}} < \boldsymbol{B_{sh}} < \boldsymbol{B_{MAX}}$$

$$\boldsymbol{i_{tx}} < \boldsymbol{I_{MAX}^2}$$

$$\boldsymbol{s_{xf}} < \boldsymbol{S_{MAX}^2}$$

Where b_{G_i} and c_{G_i} are the cost coefficients corresponding to an i^{th} generator, a_G represents a fixed generation cost, while the operational limits stand for the bounds on generated real and reactive powers ($\boldsymbol{P_G}$ and $\boldsymbol{Q_G}$), as well as bus voltage magnitudes and variable shunt device limits ($\boldsymbol{v_s}$ and $\boldsymbol{B_{sh}}$). The last two performance limits, that are additional to the set of constraints defined in Chapter 6, correspond to congestion limits depicting the maximum current flows in transmission lines and the transformer apparent power limits. It is important to note that the AC-OPF problem is solved in order to obtain the grid operating point for a given optimal generation dispatch, and hence, there is no need to incorporate the AGC and AVR characteristics yet. These characteristics will have to be, however, considered in modeling the contingency scenarios. Finally, the set of additional constraints on power system steady-state response $F_G(\cdot)$ and $F_B(\cdot)$, that are also bounded by the operational and performance limits, include:

a) Locally modeled power mismatch equations in terms of conductance and susceptance states, as well as the constraints on voltage magnitude of, now, every bus in the network, which for i^{th}bus are given as:

$$G_i\left(V_{R,i}^2 + V_{I,i}^2\right) - \sum_{k=1}^{N_L} P_{L,k} + \sum_{m=1}^{N_G} P_{G,m} = 0 \qquad (7.2)$$

$$B_i\left(V_{R,i}^2 + V_{I,i}^2\right) + \sum_{k=1}^{N_L} Q_{L,k} - Q_{G,i} = 0$$

$$V_{R,i}^2 + V_{I,i}^2 - v_{s,i} = 0$$

b) Transmission line 'from' and 'to'- side, current magnitude constraints that relate the system voltages to the congestion limits and can be written for n^{th} transmission line π-model in terms of 'from' and 'to'-side real and imaginary voltages (V_{RF}, V_{RT}, V_{IF} and V_{IT}) as:

$$\begin{aligned} I_{RF,n}^2\left(V_{RF,n}, V_{IF,n}, V_{RT,n}, V_{IT,n}\right) + I_{IF,n}^2\left(V_{RF,n}, V_{IF,n}, V_{RT,n}, V_{IT,n}\right) - i_{txF,n} = 0 \\ I_{RT,n}^2\left(V_{RF,n}, V_{IF,n}, V_{RT,n}, V_{IT,n}\right) + I_{IT,n}^2\left(V_{RF,n}, V_{IF,n}, V_{RT,n}, V_{IT,n}\right) - i_{txT,n} = 0 \end{aligned} \tag{7.3}$$

c) Transformer 'from' and 'to'-side, apparent power constraints that relate the system voltages to the congestion limits and can be written for m^{th} transformer branch model [31],[68],[76] in terms of 'from' and 'to'-side real and imaginary voltages (V_{RF}, V_{RT}, V_{IF} and V_{IT}) as:

$$\begin{aligned} \left(V_{RF,m}^2 + V_{IF,m}^2\right)\left[I_{RF,m}^2(\cdot) + I_{IF,m}^2(\cdot)\right] - s_{xfF,m} = 0 \\ \left(V_{RT,m}^2 + V_{IT,m}^2\right)\left[I_{RT,m}^2(\cdot) + I_{IT,m}^2(\cdot)\right] - s_{xfT,m} = 0 \end{aligned} \tag{7.4}$$

Lastly, the additional coupling between the network and its adjoint can be added in order to ensure the feasibility of the problem; however, this time with greater caution, due to the fact that we need to first ensure the solution doesn't find the operating point where it is cheaper to "generate" power from infeasibility sources than the optimized generator dispatch. Hence, a good pick for the weight can be a million times the largest linear cost coefficient from the generator cost objective function.

With the base AC-OPF problem introduced in (7.1), it is important to emphasize that even though it was first formulated over half of a century ago [83]-[84], today's powerful nonlinear solvers cannot robustly obtain the optimum for the problem as it has been traditionally formulated, nor do they solve the problem fast enough for control of the grid. Therefore, our first experiment considers a sample of ten (10) power flow test cases previously examined in Chapter 6. First, the AC-OPF problem is solved within the open source grid simulation and optimization solver

MATPOWER 7.0. while considering the 4 existing formulations for modeling the power flow response:

1. Power mismatch formulation in polar coordinates (Polar PQV) [84]
2. Power mismatch formulation in rectangular coordinates (Rectangular PQV) [68],[79]
3. Current Injection formulation in polar coordinates (Polar I-V) [68],[79]
4. Current Injection formulation in rectangular coordinates (Rectangular I-V) [68],[79]

Next, each of the considered test cases presented in Table 7.1 is initialized for a different pair of flat voltage starting conditions with generator real and reactive power set by:

- A trivial flat start (equal to zero),
- Values provided within the input file,

The problem is run within three of the available optimization toolboxes, namely, internal MATPOWER – MIPS solver, FMINCON as well as commercial optimization toolbox - KNITRO. Finally, the results are compared with the AC-OPF problem defined in terms of generalized network formulation for modeling the power grid response that is solved within ECP framework.

In terms of optimization parameters used, the maximum complementary slackness (CS) violation parameter for diode models within ECP is set to $\varepsilon = 10^{-11}$, which also represents the convergence tolerance that is applied to the ECP circuit (KKT optimality conditions) residual. As in the previous experiments performed, all the problems were solved on MacBook Pro 2.9 GHz Intel Core i7. Lastly, it is important to emphasize and recall that the gradient of the objective function represents an excitation to the adjoint circuit. Moreover, since a quadratic AC-OPF objective function can have any values set for its cost coefficients, we further introduced the adjoint per unit normalization of the adjoint excitation sources within ECP formulation in order to improve the conditioning of the adjoint circuit. Importantly, scaling of the cost function by a positive constant doesn't affect its minima and the accuracy of the problem is preserved, hence we can obtain the base-factor that normalizes the objective function as:

$$b_{apu} = \max[\max(\boldsymbol{b_G}, 2\boldsymbol{c_G})] \tag{7.5}$$

The comparison demonstrating the best-case simulation results obtained for two different initialization scenarios within the MATPOWER solver, in reference to the AC-OPF solution

obtained within the ECP framework, is presented in Table 7.1. It is important to emphasize that the commercial KNITRO optimization toolbox provided the best performance in terms of iteration count, as well as that all of the presented results converged to the same optimal solutions that are further reported in Table 7.1.

Table 7.1. Iteration count comparison between the best-case results obtained within MATPOWER by solving the AC-OPF problem defined in terms of traditional formulations and GB formulation implemented within ECP solver. Notably, the criterion for choosing the best-case results was first the objective function value followed by the iteration count performance. Moreover, the reported iteration counts for KNITRO only indicate the full NR iterations, and the additional Conjugate Gradient iteration count performed within each of the NR iterations are not reported.

case	**MATPOWER: Flat PQ start**		**MATPOWER: Input PQ start**		**ECP solver and GB formulation**		**Cost [$/hr.]**
	Iteration #	**Formulation**	**Iteration #**	**Formulation**	**Iteration # - Flat**	**Iteration # - Input**	
1354pegase	28	Polar IV	24	Polar IV	**15**	**13**	74064.2
2383wp	32	Polar PQV	31	Polar PQV	**22**	**16**	1863597.5
2736sp	23	Polar PQV	22	Polar PQV	**19**	**18**	1307998.3
2869pegase	27	Polar PQV	26	Polar PQV	**19**	**17**	133993.5
3012wp	31	Polar IV	31	Polar IV	**24**	**19**	2584033.9
6468rte	35	Polar IV	37	Polar IV	**22**	**18**	87139.7
9241pegase	56	Polar IV	56	Polar IV	**26**	**20**	315902.5
ACTIVSg10k	80	Polar IV	65	Polar IV	**25**	**20**	2488650.0
ACTIVSg25k	48	Polar PQV	45	Polar PQV	**24**	**25**	6019821.2
ACTIVSg70k	138	Polar PQV	132	Polar PQV	**34**	**39**	16538287.9

As can be seen from Table 7.1, the polar PQV and IV formulations generally performed better among the traditional formulations considered within the MATPOWER solver. Most importantly, a trend that indicates a dependency of the problem size to the total iteration count is continued as in the preliminary results from the previous chapter. Namely*, the larger a problem gets*, the more inequality constraints, and *therefore, the larger impact of conservativeness introduced by the traditionally used NR step limiting techniques*. In contrast, the dependency between the problem size and the performance of the solution process is not as strongly indicated for the results obtained within the ECP framework, which again demonstrates the advantages of treating each of the NR step sizes more independently and based on their physical characteristics. Lastly, it is important to highlight that even though the best-case results provide a decent comparison to the generalized network (GB) formulation solved within the ECP framework, we can further confirm the large variance of the obtained AC-OPF results, both in terms of iteration counts as well as the objective

function values, that varied depending on the formulation as well as the optimization toolbox used within MATPOWER.

The second data set that is examined consists of a sample of 10 different network cases ranging from 500 to 10k buses that was recently introduced for the Grid Optimization (GO) competition sponsored by ARPA-E [76] and used for the initial testing of the competing solution methodologies. The more detailed description of the examined GO competition test cases follows:

Table 7.2. Device specification of examined GO- competition test cases.

Network Model	Bus #	Gen. #	Load #	Branch #	Transformer #	Fixed Shunts #	Switched Shunts #
1	500	90	200	468	131	0	17
3	793	210	568	769	143	49	50
6	2000	384	1010	2743	896	32	141
7	2312	617	1529	2156	857	121	201
8	3013	865	1793	2836	1290	129	405
81	3288	379	4236	3421	1455	0	23
84	4601	408	3501	5135	2180	0	17
9	4918	1340	3070	4412	2315	246	486
12	9591	365	6659	10927	4988	0	122
13	10000	2089	3982	10819	2374	99	434

For each of the ten provided networks, we have examined three different scenarios that are publicly available [85] and correspond to the different network configurations, which thus make a total number of examined test cases equal to 30.

Furthermore, the basic AC-OPF problem, as defined in (7.1), is solved within the ECP framework for each of the 30 test cases modeled by the generalized network (GB) formulation and while considering the two different initial conditions:

- **Real-Time initial condition** that corresponds to the initial guess resembling a power flow solution provided within the input file
- **Offline initial condition** that corresponds to the flat voltage start with trivially initialized real and reactive generation powers and variable shunt values (equal to zero)

All of the simulations were performed on a MacBook Pro 2.9 GHz Intel Core i7 for the same default parameters that were discussed in the previous experiment. The results demonstrating

the iteration count comparisons among the three different network scenarios and the types of initializations are presented in Figure 7.1 and Figure 7.2 respectively, while the corresponding minimized generation cost values are reported in Table 7.3.

Table 7.3. Minimized generator dispatch cost values.

Network Model	Scenario 1 [$/hr.]		Scenario 2 [$/hr.]		Scenario 3 [$/hr.]	
	Real Time	Offline	Real Time	Offline	Real Time	Offline
1	24,519.0	24,519.0	6,246.0	6,246.0	116,446.0	116,446.0
3	901.7	901.7	1,028.9	1,028.9	1,302.9	1,302.9
6	507,556.5	507,556.5	620,066.0	620,066.0	945,947.0	945,947.0
7	3,610.0	3,610.0	4,206.0	4,206.0	5,658.6	5,658.6
8	4,944.5	4,944.5	5,093.1	5,093.1	6,061.3	6,061.3
81	535,622.5	535,622.5	587,984.8	587,984.8	2,573,922.0	2,573,922.0
84	777,814.0	777,814.0	777,814.0	777,814.0	1,026,483.0	1,026,483.0
9	5,060.9	5,060.9	5,206.0	5,206.0	6,236.0	6,236.0
12	1,009,044.3	1,009,044.3	1,036,114.4	1,036,114.4	1,207,061.0	1,207,061.0
13	1,193,330.9	1,193,330.9	1,460,350.0	1,460,350.0	2,076,476.0	2,076,476.0

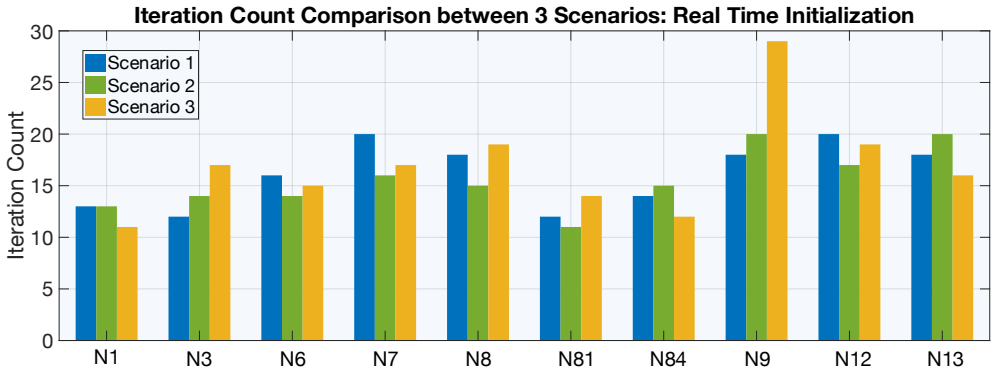

Figure 7.1. AC-OPF iteration count comparisons among the three scenarios of 10 examined GO-competition networks obtained within ECP SUGAR for the real time initialization.

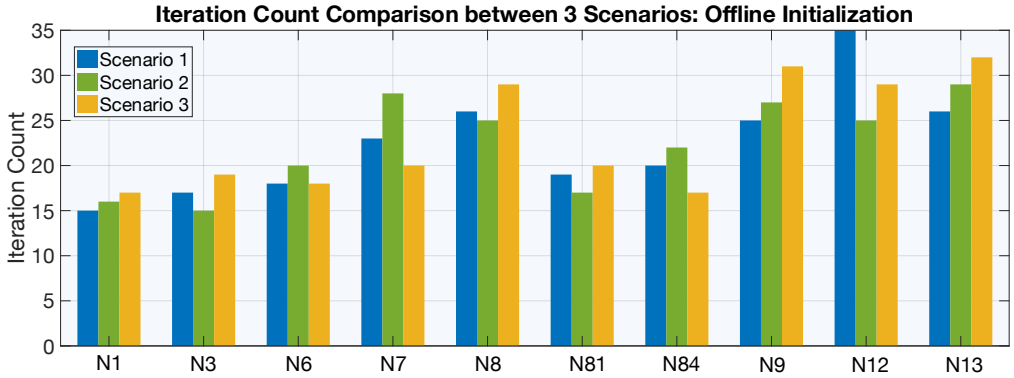

Figure 7.2. AC-OPF iteration count comparisons among the three scenarios of 10 examined GO-competition networks obtained within ECP SUGAR for the offline initialization.

Referring to the AC-OPF results, note that independent of a starting point used to initialize the solver, all of the examined problems converged to the same respective optimal solutions. Moreover, as expected, the better initial starts consequently result in more efficient solution processes in terms of iteration counts. Most importantly, however, the problem efficiency is not as dependent on its size as it is the "conditioning" of the optimized networks. For instance, it can be verified that most of the cases that were considered "more difficult to converge" contain unreasonably small series line impedances that almost approach the models of "superconductive" transmission lines, which is not a physical reality. In terms of a matrix problem, the small line impedances result in the huge conductance values that are stamped into the admittance matrix. This can be also explained from the perspective of Ohm's Law, which indicates the sensitivity of current flowing through the large conductance branch to a small voltage change, particularly if that current is limited, as in the case of optimal power flow problems.

The insertion of a small series impedance is well known in power flow modeling for use in "measuring" the branch current, but this is primarily due to the lack of an ideal ammeter model, namely, a zero valued voltage source, which is applied for circuit simulation problems in SPICE and in general. Consequently, a small line impedance can prolong the convergence process, as well as cause the oscillations in corner cases, where the two controlled devices connected by a "superconductive" transmission line may start oscillating throughout the NR iterations. This further highlights the advantage of a physical model for the optimization problem that can be now utilized to allow for more efficient handling of such non-physical corner cases.

Finally, with the decreased dependency between a solution process and the problem size that is achieved by embedding the problem physical characteristics within the respective solution methodologies, we next devote our focus towards analyzing the impact of the base AC-OPF solutions to the robustness of grid operation during contingencies scenarios. We further propose a framework for ensuring the grid feasibility by means of solving the Security Constrained AC Optimal Power flow problem.

7.2. Towards a Fully Secured Optimal Power Dispatch – Security Constrained Optimal Power Flow problem (SC AC- OPF)

With preliminary results indicating the robustness and efficiency of the proposed ECP framework in solving for the basic optimal power dispatch, as well as the realistic power flows, the question of analyzing the robustness of grid operating point remains. Namely, can we use the feasibility analysis postulated and solved in Chapter 6 to examine how many cases are "truly" infeasible given the basic optimal power dispatch.

Toward this goal, for our next experiment, we consider the sample of 30 GO-competition test cases for which basic power dispatch was determined as described in the previous section. We run the realistic power flow analysis from (6.14) with addition of congestion constraints on a set of contingency scenarios that were provided to analyze the robustness of the obtained generation dispatches. All of the simulations were performed for the same default parameters that were used in the previous experiments with one important difference. Considering the large amount of simulations that are fully parallelizable, as well as the increasing scale of these optimization problems, the results are obtained using a commercial version of SUGAR-ECP cloud-based platform, courtesy of Pearl Street Technologies. The results are presented in Table 7.4.

Table 7.4. Quantifying the number of "truly" infeasible contingency scenarios at the base AC-OPF power dispatch in reference to the total number of contingencies considered for each of the examined GO–cases given.

Network Model	Scenario 1	Scenario 2	Scenario 3
	# of Infeasible Contingencies	# of Infeasible Contingencies	# of Infeasible Contingencies
1	**22**/386	**25**/407	**65**/416
3	**9**/86	**19**/90	**16**/97
6	**4**/2594	**31**/2608	**37**/2618
7	**34**/953	**35**/973	**34**/953
8	**3**/1959	**9**/1957	**42**/1968
81	**73**/4650	**87**/4649	**76**/4649
84	**48**/7075	**48**/7075	**25**/7084
9	**17**/5065	**17**/5066	**54**/5085
12	**62**/4377	**62**/4377	**66**/4377
13	**70**/9519	**370**/9519	**421**/9622

As can be seen from Table 7.4, and in contrast to the previously performed realistic power flow simulations in Chapter 6, almost all of the considered networks exhibited the cases of

infeasibility within a number (~4% in average) of the examined contingency scenarios. Importantly, it can be verified that most of the infeasible cases correspond to the loss of a generator. This intuitively makes sense considering that a case of a generator outage occurs in an area with low percent of generation units available. Moreover, due to the strictly enforced line congestions in the analysis performed, the demand in the affected area may not be satisfied, thus causing the infeasibilities to appear.

Finally, enforcing the full set of realistic power grid operational and performance limits significantly decreases the solution space in terms of the problem feasibility, and hence results in non-robust operating points when determined by simply considering the basic AC-OPF problem. To further improve to the robustness, however, requires consideration of *all* of the respective contingency scenarios within the optimization problem.

In terms of the equivalent circuit framework, one way of determining a more robust optimal dispatch set point is by coupling the ECP representation of a base AC-OPF problem with the corresponding circuits that model the realistic power flow scenarios during the considered contingencies, as presented in Figure 7.3. Mathematically, this equates to appending of the additional constraints defined in (6.14) for each of the contingency scenarios to the base AC-OPF problem in (7.1). Moreover, these constraints now define the network responses during contingencies and are further coupled with the base case set of governing equations through the generator real power and voltage variables. Notably, the solution to such SC AC-OPF problem now provides the operating set point that takes the contingency cases into consideration.

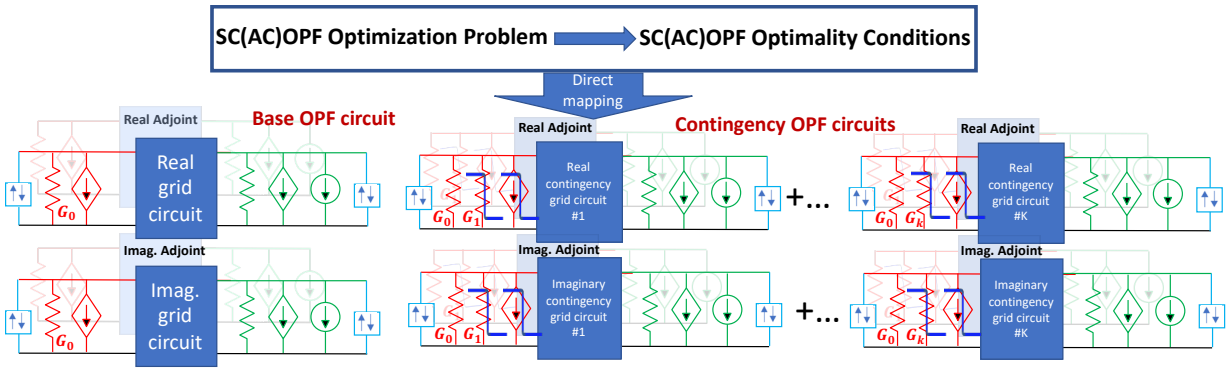

Figure 7.3. Circuit representation of the proposed way for solving the SC AC-OPF problem.

The first fact that can be immediately noticed is the significant increase of problem size with increase of considered contingency scenarios. For instance, the ECP problem representation

of a 10k bus network model 13 from the GO-competition dataset contains approximately 171k variables. The total number of variables corresponding to a particular SC AC-OPF problem, as discussed above, will then correspond to the size of the base case with addition to its size multiplied by the number of contingencies. Therefore, if we only consider the contingency cases that are infeasible for a given basic AC-OPF dispatch in Scenario 1, the number of variables rises to ~72 million. However, such an obtained operating point does not ensure that some of the other contingency case will not become infeasible for the new optimal set point, particularly considering that the total set of contingency cases result in an incredibly large ~1.6 billion variable problem.

Most importantly, the circuit simulation problems approaching this, and the corresponding matrix sizes that exhibit the Bordered Block Diagonal (BBD) form shown in Figure 7.4, are performed today [17] with distributed sparse LU solver implementations. A schematic diagram of our proposed system is presented in Figure 7.5.

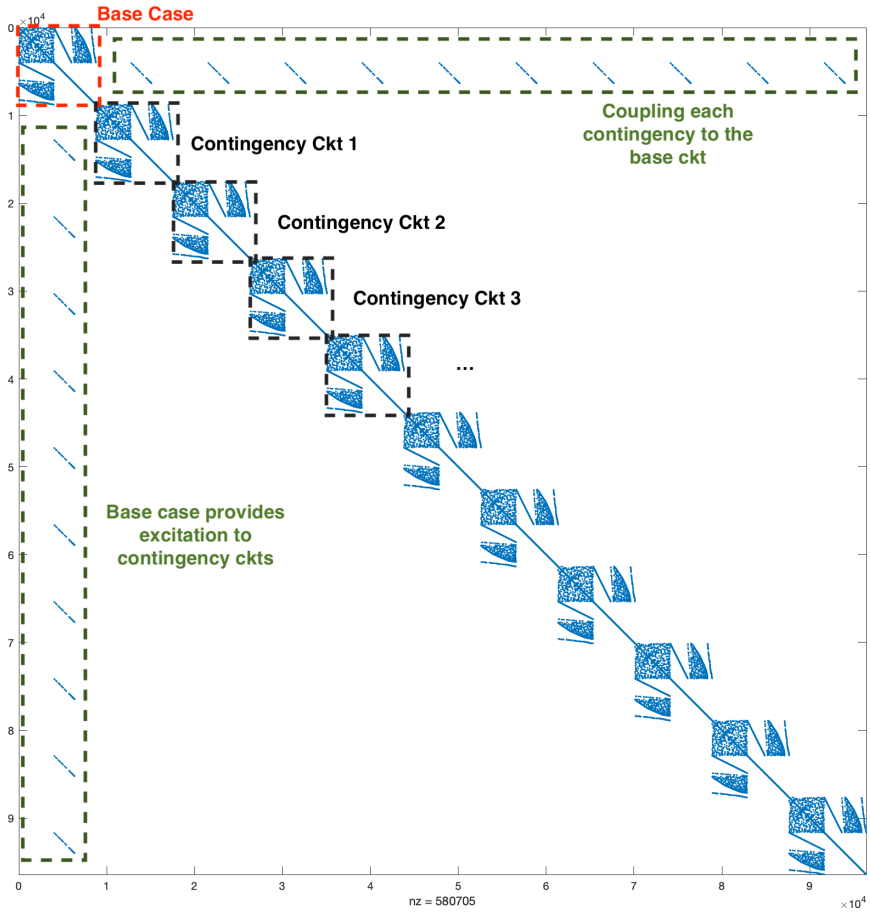

Figure 7.4. The Bordered Block Diagonal (BBD) sparsity pattern of Network 1 model with the addition of 10 contingency circuits.

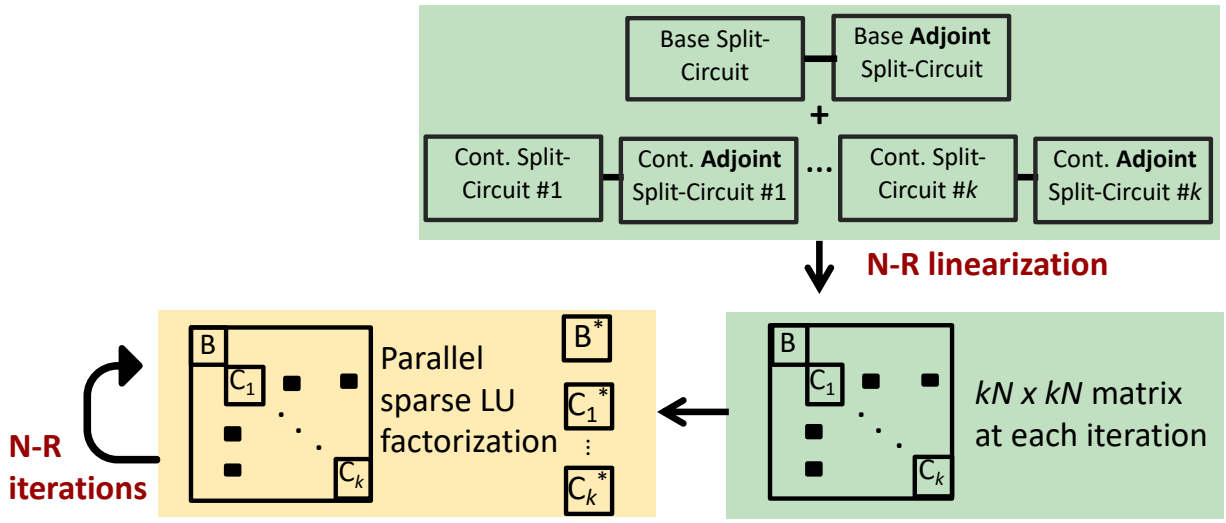

Figure 7.5. The idea behind the SUGAR-ECP approach developed by Pearl Street Technologies.

The distributed matrix computation, however, is not considered to fall under the scope of this thesis, and herein we only seek to analyze the dependency between the increase of problem size within the SC AC-OPF formulation and the developed set of ECP algorithms. Hence, a set of previously examined GO competition test cases is considered again, this time with addition of the first 10 contingency cases. The SC AC-OPF problem is formulated as an ECP, initialized in the same way as was done for the base AC OPF case, and further solved on a MacBook Pro 2.9 GHz Intel Core i7 for the same default parameters from the previous experiments. The simulation results depicting the required NR iteration counts are presented in Figure 7.6 and Figure 7.7.

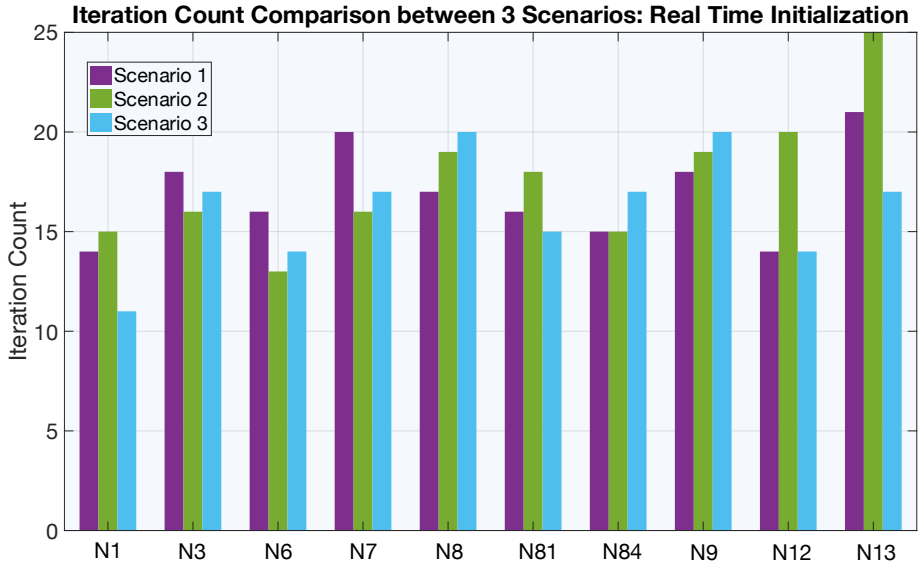

Figure 7.6. SC AC-OPF (first 10 contingency cases) iteration count comparisons among the three scenarios of 10 examined GO-competition networks obtained within ECP for the Real-time initialization.

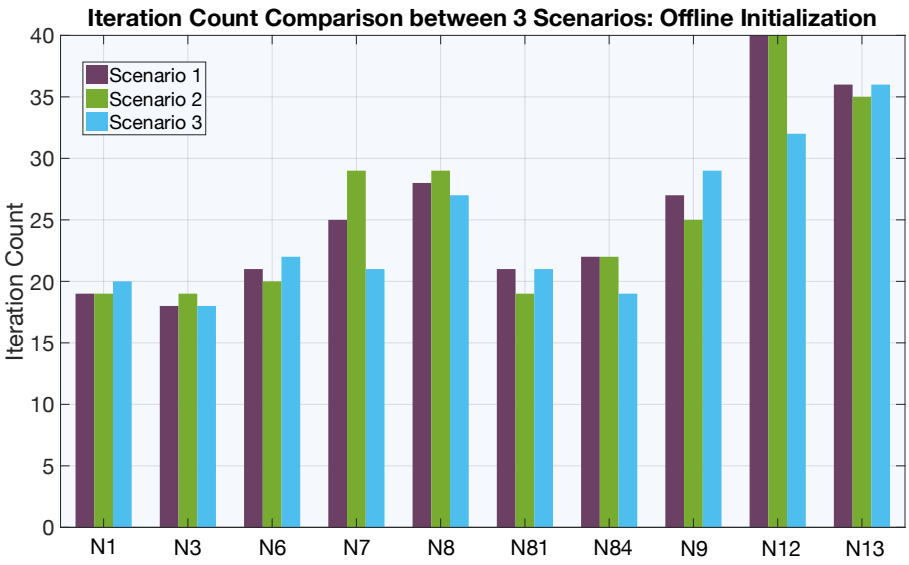

Figure 7.7. SC AC-OPF (first 10 contingency cases) iteration count comparisons among the three scenarios of 10 examined GO-competition networks obtained within ECP for the Offline initialization.

In referring to the presented preliminary results in Figure 7.6 and Figure 7.7, the iteration counts closely match the ones obtained while running the basic AC-OPF problems, and further follow the same trends as discussed in the previous section. The better initial start results in a more efficient solution process, while the flat start initialization does not represent significant additional burden on the efficiency in terms of iteration count. These preliminary results further highlight the aforementioned advantages regarding an ECP set of algorithms; namely that the efficiency of the solution process is more dependent on the network conditioning than the problem size. In the case of SC AC-OPF in particular, the additional constraints correspond to the same network under different scenarios, and therefore, the total iteration count should not significantly vary from the ones obtained by solving the base case only.

In conclusion, this chapter provides the additional insight into the realistic power flow analyses and the optimal generation dispatch problems in particular. As indicated by the preliminary results, utilizing the problem characteristics from the perspective of equivalent circuits and the laws of physics provides one with a complete picture on the optimization problem and its solution process. Furthermore, with ECP set of algorithms introduced, the relationship between the solution process and the problem size is not as strongly dependent, which with the efficient implementation of large distributed matrix solvers, can facilitate scalability to problems of over 1 billion variables, such as those presently accommodated in the circuit simulation field.

Chapter 8 Conclusions and Future Work

The field of mathematical optimization reached a steady-state in terms of progress two decades ago, but is presently being explored possibly more than ever. Similarly, circuit simulation research plateaued after the development of SPICE [11]-[12] and its numerous derivatives and advancements [13]-[16], but has seen a recent resurgence as well for solving problems on the scale of billions of nodes. Circuit simulation has been such a longstanding success because of how it utilized the physical properties of the problem to produce powerful solution methodologies that scale to extremely large-size nonlinear systems. In this thesis, inspired by the solution methodologies developed within the circuit simulation community, as well as the indications provided by NFL theorems [9], we have introduced a generic Equivalent Circuit Programming (ECP) framework for continuous network optimization problems.

The chapters of this thesis were structured within the two main parts as follows. The first part established the required theory and algorithms that are generally applicable to any continuous network optimization problem. To that effect, Chapter 3 generalized the modeling of a network steady-state response by introducing an additional set of network states, namely admittance state variables, that are added to the system model to constrain the particular components of network response required. The chapter concluded with the extension of generalized network steady-state modeling to the Adjoint circuit theory, a linear version of which is presently utilized within SPICE for noise analyses [34]-[36].

With the generalization of steady-state response modeling and its respective representation within the Adjoin circuit domain, Chapter 4 connected the dots between the network theory and the fundamentals of mathematical optimizations. It demonstrated that the Adjoint circuits represent a fundamental connection between circuit simulation and the optimality conditions of a network optimization problem. Notably, a new physical perspective that can be further utilized to obtain the complete understanding of physical characteristics behind the problem optimality conditions

was established. Hence, the solution process of a network optimization can be now seen as simulating the response of a circuit consisting of a joint equivalent circuit model and its excited adjoint. Further introduction of coupling between them ensures the simulation feasibility and provides the sparse locations of infeasibilities within the network. Moreover, if the adjoint circuit remains passive for all small perturbations around the obtained operating point, it was shown that the point also represents an optimal solution to the simulated ECP problem.

Followed by the establishment of fundamental connections, as well as mapping of a network optimization to the circuit simulation problem, Chapter 5 introduced a new set of simulation techniques for solving ECP optimization problems. These techniques were inspired by the circuit simulation methods developed within SPICE, and were further merged with aspects of the optimization solution methodologies that are utilized within the existing state-of-art algorithms. Therefore, newly introduced techniques such as Dynamical Diode Limiting, or Optimal Limiting algorithms can be now used to eliminate the existing homotopy based Interior Point Methods while ensuring the more robust, scalable and efficient solution processes.

The second part of this thesis makes the developed theory behind ECP and respective sets of simulation algorithms useful and focuses on the applications found within the power system simulation and optimization problems. Chapter 6 demonstrated that a power grid steady-state response modeled by a power flow problem can be, without loss of generality or accuracy, represented in terms of generalized network theory introduced in Chapter 3. Hence it is fully applicable and can be efficiently solved within the ECP framework. This was demonstrated by the preliminary results that indicated the superior convergence properties from an arbitrary initial point, as well as the scalability and efficiency in comparison to the existing formulations. Most importantly, building on the circuit representation of a power flow problem and its incorporation within a circuit simulation ECP framework within SUGAR, Chapter 6 concluded by demonstrating that a more realistic power flow solution can now take into consideration the operational limits and respective device characteristics that make a power flow problem more of an optimization than a simulation. The preliminary power flow results obtained within the ECP framework demonstrated the significant improvements in runtime efficiency in reference to the existing optimization state-of-art algorithms while preserving the robustness. We further postulated that the large-scale power flow “simulation” within SUGAR can now efficiently incorporate the

realistic operational constraints, as well as the highly nonlinear grid device characteristics, while producing a feasible power flow solution.

Finally, the thesis concluded with consideration of the electrical power dispatch problems solved within the AC-OPF and Security Constrained AC-OPF analyses. It was demonstrated that in addition to overperforming the existing state-of-art formulations and optimization toolboxes, particularly as the scale of a problem increases, the introduced physical characteristics embedded within a set of ECP techniques significantly reduces the dependency between an optimization problem size and the efficiency in terms of iteration count. More notably, preliminary results indicated that the prolonged iteration processes are shown to be more likely caused by the conditioning of optimized networks than its size in term of variable count.

In terms of the guidelines for the future work and further extensions of the proposed ECP framework to the other power system optimization problems, as well as to other fields of engineering where the ECP framework can be applied, it is important to highlight the following. The results and problems considered in the second part of the thesis represent a small number of possible applications, even just within the domain of power system optimization problems. First, there is a huge potential for advancement of static, as well as dynamic, state estimation (SE) problems. Furthermore, as was recently demonstrated in [86]-[88], power system measurement data can be naturally included within the circuit-based framework, which thereby makes the SE problems corresponding to a fully observable grid trivial to solve; with inclusion of both Phasor Measurement units (PMU) and Remote Terminal Units (RTU) components. SE exploration is also a path toward solving the problems of bad data detection and networks that are only partially observable, where the additional knowledge of the complete physical characteristics provided by an ECP framework can be of great benefit.

Another potential direction for research is toward incorporation of more detailed models within the power flow simulation and optimization problems. Notably, the ECP framework can efficiently incorporate nonlinear device characteristics such as the ones used for modeling AGC and AVR grid responses. To that end, the feasibility-based modeling methodology introduced in Chapter 6 can be further extended to include the more realistic generation plant models and remote voltage control devices that presently introduce the most challenges within the power flow analysis. A third direction for further research is to address problems of size and complexity that

previously been considered unimaginable. This includes Multi-Periodic analyses such as SC AC-OPF, as well as the introduction (if needed) of integer variables within the ECP framework.

In terms of other fields of engineering, the ECP framework can accommodate any network optimization problem, and a natural direction for exploration would be electronic circuit design problems. Since any design problem is essentially an optimization problem, "simulating" the circuits to obtain the optimal design values and parameters is a seemingly promising direction. Lastly, exploring the embedding of physical properties of a problem within the mathematical optimizations in general, if applicable, could advance optimization methods research dramatically.

References:

[1] A. Das and B. K. Chakrabarti, "Quantum Annealing and Related Optimization Methods*,"* Lecture Note in Physics, Vol. 679, Springer, Heidelberg (2005)

[2] C. A. Desoer and E. S. Kuh, "*Basic Circuit Theory*," McGraw-Hill, New York, 1969.

[3] S. Boyd, L. Vandenberghe, "*Convex Optimization*," Cambridge University Press, New York, NY, USA, 2004.

[4] E. Alpaydin, "*Introduction to Machine Learning*," 2nd Edition, MIT Press, 2010.

[5] S. Russell, P. Norvig, "*Artificial Intelligence – A Modern Approach*," Prentice Hall Press Upper Saddle River, NJ, USA, 2009.

[6] W. Press, S. Teukolsky, W. Vetterling, B. Flannery, "*Numerical Recipes in C – The Art of Scientific Computing*," Second Edition, Cambridge University Press, 1992.

[7] Dimitri P. Bertsekas, "*Nonlinear Programming,"* Athena Scientific, 2nd Edition, 1995.

[8] S. Das and P. N. Suganthan, "Differential Evolution: A Survey of the State-of-the-art", *IEEE Trans. on Evolutionary Computation*, Vol.15, No.1, pp.4-31, Feb.2011.

[9] D. H. Wolpert and W. G. Macready, "No free lunch theorems for optimization," in *IEEE Transactions on Evolutionary Computation*, vol. 1, no. 1, pp. 67-82, April 1997. doi: 10.1109/4235.585893.

[10] B.D.H, Tellegen, "A general network theorem with applications," *Philips Research Reports*. 7: 259–269, 1952.

[11] L. Nagel, R. Rohrer, "Computer Analysis of Nonlinear Circuits, Excluding Radiation (CANCER)", IEEE Journal on Solid-State Circuits, Vol. Sc-6, No.4, August 1971.

[12] Nagel, L. W, and Pederson, D. O., *SPICE (Simulation Program with Integrated Circuit Emphasis)*, Memorandum No. ERL-M382, University of California, Berkeley, Apr. 1973.

[13] L. W. Nagel, "SPICE2: A Computer Program to Simulate Semiconductor Circuits," Memorandum No. ERL-M520, University of California, Berkeley, May 1975.

[14] W. J. McCalla, "*Fundamentals of Computer-Aided Circuit Simulation*", Kluwer Academic Publishers, Boston, 1988.

[15] L. Pileggi, R. Rohrer, C. Visweswariah, "*Electronic Circuit & System Simulation Methods*", McGraw-Hill, Inc., NY, NY, USA, 1995.

[16] M. Celik, L. Pileggi. A. Odabasioglu, "IC Interconnect Analysis," Kluwer Academic Publishers, Springer, Boston, MA, 2002.

[17] Private communication with Hui Zheng from Pearl Street Technologies and Altan Odabasioglu from ANSYS.

[18] D. Bromberg, M. Jereminov, L. Xin, G. Hug, L. Pileggi, “An Equivalent Circuit Formulation of the Power Flow Problem with Current and Voltage State Variables”, *PowerTech Eindhoven, June 2015.*

[19] M. Jereminov, D. M. Bromberg, L. Xin, G. Hug, L. Pileggi, “Improving Robustness and Modeling Generality for Power Flow Analysis,” *T&D Conference and Exposition, 2016 IEEE PES.*

[20] M. Jereminov, D. M. Bromberg, A. Pandey, X. Li, G. Hug, L. Pileggi, “An Equivalent Circuit Formulation for Three-Phase Power Flow Analysis of Distribution Systems,” *IEEE T&D Dallas*, May 2016.

[21] A. Pandey, M. Jereminov, X. Li, G. Hug, L. Pileggi, “Unified Power System Analyses and Models using Equivalent Circuit Formulation,” *IEEE PES ISGT*, Minneapolis, USA, 2016.

[22] M. Jereminov, A. Pandey, D. M. Bromberg, X. Li, G. Hug, L. Pileggi, “Steady-State Analysis of Power System Harmonics Using Equivalent Split-Circuit Models”, ISGT Europe, Ljubljana, October 2016.

[23] M. Jereminov, A. Pandey, H.A. Song, B. Hooi, C. Faloutsos, L. Pileggi, “Linear Load Model for Robust Power System Analysis”, IEEE PES Integrative Smart Grid Technologies Europe, September 2017.

[24] A. Pandey, M. Jereminov, M. Wagner, D. M. Bromberg, G. Hug, L. Pileggi, “Robust Power Flow and Three Phase Power Flow Analyses*”, IEEE Trans. on Power Systems*. DOI: 10.1109/TPWRS.2018.2863042.

[25] M. R. Wagner, A. Pandey, M. Jereminov, and L. Pileggi. Robust Probabilistic Analysis of Transmission Power Systems based on Equivalent Circuit Formulation, Proceedings of the International Conference on Probabilistic Methods Applied to Power Systems, June 2018.

[26] A. Agarwal, A. Pandey, M. Jereminov, L. Pileggi, “Implicitly Modeling Frequency Control with Power Flow,” IEEE PES Innovative Smart Grid Technologies Europe Conference, 2019.

[27] A. Pandey, A. Agarwal, M. Jereminov, M.R. Wagner, D.M. Bromberg, L. Pileggi, “Robust Sequential Steady-State Analysis of Cascading Outages,” IEEE PES Innovative Smart Grid Technologies Europe Conference, 2019.

[28] A. Pandey, M. Jereminov, G. Hug, L. Pileggi, “Improving power flow robustness via circuit simulation methods,” IEEE PES General Meeting, Chicago, 2017.

[29] M. Jereminov, A. Pandey and L. Pileggi, "Equivalent circuit formulation for solving AC optimal power flow," *IEEE Transaction on Power Systems,* DOI:10.1109/TPWRS.2018.2888907.

[30] M. Jereminov, D. Bromberg, A. Pandey, M. Wagner, L. Pileggi, “Adjoint Power Flow Analysis for Evaluating Feasibility”, *IEEE Trans. on Smart Grids,* arXiv: 1809.01569, 2018

[31] A. Pandey, “Robust Steady-State Analysis of Power Grid using Equivalent Circuit Formulation with Circuit Simulation Methods,” Doctoral Thesis, Carnegie Mellon University, August 2018.

[32] A. Pandey, M. Jereminov, M. R. Wagner, G. Hug and L. Pileggi, "Robust Convergence of Power Flow using Tx Stepping Method with Equivalent Circuit Formulation" in *2018 (PSCC), Dublin* 2018.

[33] M. Jereminov, A. Terzakis, M. Wagner, A. Pandey, L. Pileggi, "Robust and Efficient Power Flow Convergence with G-min Stepping Homotopy Method," in Proc. IEEE Conference on Environment, Electrical Engineering and I&CPS Europe, Genoa, Italy, June 2019.

[34] S.W. Director, R. Rohrer, "The Generalized Adjoint Network and Network Sensitivities", *IEEE Trans. on Circuit Theory*, vol. 16-3, 1969.

[35] S.W. Director, R, Rohrer, "Automated Network Design-The Frequency Domain Case", *IEEE Trans. on Circuit Theory*, vol. 16, no3, August 1969.

[36] S W. Director and RA. Rohrer, "Interreciprocity and its Implications," Proc. International Symposium Network Theory, Belgrade, September 1968, pp. 11-30.

[37] Quadrennial Energy Review: Energy Transmission, Storage, and Distribution Infrastructure, April 2015.

[38] "The disaster that could follow from a flash in the sky," Economist, July 13, 2017.

[39] R. Byrd, J. Gilbert and J. Nocedal, A trust region method based on interior point techniques for nonlinear programming, *Math. Programming*, 89, 149-185, 2000.

[40] L. Chen, D. Goldfarb, Interior-point L2-penalty methods for nonlinear programming with strong global convergence properties, *Math. Programming*, 108(1), 1-36, 2006.

[41] R. Byrd, R.H., Mary E. Hribar, and Jorge Nocedal, "An Interior Point Algorithm for Large-Scale Nonlinear Programming," *SIAM Journal on Optimization*, Vol 9, No. 4, pp. 877–900, 1999.

[42] R. A. Waltz, J. L. Morales, J. Nocedal, and D. Orban, "An interior algorithm for nonlinear optimization that combines line search and trust region steps," *Mathematical Programming*, Vol 107, No. 3, pp. 391–408, 2006.

[43] J. Ogrodzki, Circuit Simulation Methods and Algorithms, CRC Press, 1994.

[44] V. Ostovic, "A simplified approach to magnetic equivalent-circuit modeling of induction machines," in *IEEE Transactions on Industry Applications*, vol. 24, no. 2, pp. 308-316, March-April 1988. doi: 10.1109/28.287.

[45] R. M. T. Fleming, C. M. Maes, M. A. Saunders, Y. Ye, B. Ø. Palsson, "A variational principle for computing nonequilibrium fluxes and potentials in genome-scale biochemical networks", Technical Report SOL 2011-1, Preprint submitted to Elsevier.

[46] J. Wyatt, "Network Representation of Reaction-Diffusion systems far from Equilibrium," Computer Programs in Biomedicine (8), 1978, 180-195, Elsevier.

[47] T. L. Quarles, "Analysis of Performance and Convergence Issues with Circuit Simulation," Memorandum No.ERL-M89/42, University of California, Berkeley, April 1989.

[48] R.C. Melville, Lj. Trajkovic, C. Fang, L.T. Watson, "Artificial parameter homotopy methods for the dc operating point problem," *IEEE Transactions on CAD of ICS*, vol. 12, pp. 861-877, June 1993.

[49] R. J. Gilmore, M. B. Steer, "Nonlinear circuit analysis using the method of harmonic balance—A review of the art. Part I. Introductory concepts". *Int. J. Microw. Mill. -Wave Comput.-Aided Eng*. 1: 22–37, 1991.

[50] K.S. Kundert, A. Sangiovanni – Vincentelli, "Simulation of Nonlinear Circuits in the Frequency Domain", *IEEE Transactions on CAD*, Vol. CAD – 5, No.4, pp.521 – 535, October 1986

[51] E. B. Saff, A. D. Snider, L. N. Trefethen, "*Fundamentals of Complex Analysis for Mathematics, Science and Engineering*," 2nd Edition, Prentice Hall, Englewood Cliffs, NY 07632.

[52] M. E. Van Valkenburg, "*Introduction to Modern Network Synthesis*," John Wiley & Sons, Inc. Herndon, VA, 1960.

[53] L. Chua, C. Desoer, E. Kuh, "*Linear and Nonlinear Circuits*," McGraw–Hill Companies, 1987.

[54] I. Griva, D. F. Shanno, R. J. Vanderbei, H. Y. Benson, "Global convergence of a primal-dual interior-point method for nonlinear programming," *Algorithmic Operations Research*, *3*(1). Retrieved from https://journals.lib.unb.ca/index.php/AOR/article/view/5665.

[55] R. Hirsh, "*Power Loss – The Origins of Deregulation and Restructuring the American Electric Utility System*," The MIT Press, Cambridge, MA, 1999.

[56] W. F. Tinney and C. E. Hart, "Power flow solutions by Newton's method," *IEEE Trans. on PAS*, Vol. 86, No. 11, pp. 1449-1460, 1967.

[57] H. W. Dommel, W. F. Tinney, and W. L. Powell, "Further developments in Newton's method for power system applications," in Proc. IEEE Winter Power Meeting Conf., New York, NY, USA, Jan. 1970, Paper 70 CP 161.

[58] W. Murray, T. T. De Rubira, and A. Wigington, "Improving the robustness of Newton-based power flow methods to cope with poor initial conditions," North American Power Symposium (NAPS), 2013.

[59] A. G. Exposito, E. R. Ramos, "Reliable Load Flow Technique for Radial Distribution Networks," *IEEE Transactions on Power Systems*, Vol. 14, No. 3, August 1999.

[60] A. F. Glimn, G. W. Stagg, "Automatic Calculation of Load Flows," AIEE Summer General Meeting, Montreal, Canada, June 1957.

[61] J. B. Ward, H. W. Hale, "Digital Computer Solution of Power Flow Problem," AIEE Winter General Meeting, NY, USA, June 1956.

[62] H. H. Happ, "*Piecewise Methods and Applications to Power Systems*," John Wiley and Sons, New York. 1980.

[63] Tinney W F, Walker J W. Direct solutions of sparse network equations by optimally ordered triangular factorization. *Proc, IEEE* 55:1801-9, 1967.

[64] Sato N, Tinney W F. Techniques for exploiting the sparsity of the network admittance matrix. *IEEE Trans. Power App. Syst*. 82:944-50, 1963.

[65] A. Semlyen, F. de Leon, "Quasi-Newton Power Flow using partial Jacobian updates," in *IEEE Transactions on Power Systems*, Vol. 16, No. 3, August 2001.

[66] C. Josz, et.al, “AC Power Flow Data in MATPOWER and QCQP Format: iTesla RTE Snapshots and PEGASE”. ArXiv e-prints, March 2016.

[67] A. B. Birchfield, et.al., “Power Flow Convergence and Reactive Power Planning in Creation of Large Synthetic Grids”, *IEEE Trans. on Power Systems*, 2018.

[68] R. Zimmerman, C. Murillo-Sanchez, R. Thomas, “MATPOWER: Steady-state operations, planning and analysis tools for power systems research and education”, *IEEE Trans. on Power Systems*, vol. 26, no.1, Feb 2011.

[69] V. H. Quintana, N.Müller, “Studies of load flow methods in polar and rectangular coordinates,” Electric Power Systems Research Volume 20, Issue 3, March 1991, Pages 225-235.

[70] P. A. N. Garcia, J. L. R. Pereria, S. Carneiro Jr., M. P. Vinagre, F. V. Gomes, “Improvements in the Representation of PV Buses on Three-Phase Distribution Power Flow,” *IEEE Transactions on Power Systems*, Vol. 19, No. 2, April 2004.

[71] J. Katzenelson, "An algorithm for solving nonlinear resistor networks," in *The Bell System Technical Journal*, vol. 44, no. 8, pp. 1605-1620, Oct. 1965.

[72] T J. Overbye, “A power flow measure for unsolvable cases”, *IEEE Transactions on Power Systems*, vol. 9, no. 3, pp. 1359-1356, 1994.

[73] Y. Wang, et.al., “Analysis of ill-conditioned power flow problems using voltage stability methodology”, IEEET&D, Vol. 148-5, September 2001.

[74] Transmission System Planning Performance Requirements, NREC Standard TPL-001-4, 2015

[75] P. Kundur, N.J. Balu, and M.G. Lauby, “*Power system stability and control*”. New York: McGraw-Hill, 1994, vol.7.

[76] https://gocompetition.energy.gov/sites/default/files/SCOPF_Problem_Formulation__Challenge_1_20190412.pdf

[77] Y. Kataoka, “A smooth power flow model of electric power system with generator reactive power limits taken into consideration,” Proc. - IEEE Int. Symp. Circuits Syst., no. 3, pp. 5286–5289, 2005.

[78] Z. Jinquan, J. Xiaodong, Z. Boming,” Study on PV-PQ Bus Type Switching Logic in Power Flow Computation,” *Proceedings of the CSEE*, Vol. 25, No. 1, pp. 54-59, 2005.

[79] M.B. Cain, R. P. O’Neill, and A. Castillo, “History of optimal power flow and formulations, OPF Paper 1” Tech. Rep., US FERC, Dec. 2012.

[80] J. Lavaei and S. H. Low, “Zero duality gap in optimal power flow problem,” *IEEE Transactions on Power Systems*, 2011.

[81] S. Sojoudi and J. Lavaei, “Physics of power networks makes hard optimization problems easy to solve,” IEEE PES General Meeting, 2012.

[82] R. Madani, et.al., “Convex relaxation for optimal power flow problem: Mesh networks,” *IEEE Trans. Power Syst*., vol. 30-1, Jan. 2015.

[83] J. Carpentier, “Contribution to the economic dispatch problem,” *Bulletin de la Societe Francaise des Electriciens*, 8 (1962), pp. 431–447.

[84] H.W. Dommel and W.F. Tinney, “Optimal power flow solutions,” *IEEE Trans. on Power Apparatus and Systems*, Vol. 87, No. 10, October 1968.

[85] https://gocompetition.energy.gov/challenges/22/datasets

[86] M. Jereminov, A. Jovicic, M. Wagner, G. Hug, L. Pileggi, “Equivalent Circuit Programming for Estimating the State of a Power System,” in Proc. IEEE PowerTech Milan, June 2019.

[87] M. R. Wagner, M. Jereminov, A. Pandey, and L. Pileggi, “A Probabilistic Approach to Power System State Estimation using a Linear Algorithm,” in 2019 IEEE Conference on Environment and Electrical Engineering and I&CPS Europe, 2019.

[88] A. Jovicic, M. Jereminov, L. Pileggi, G. Hug, “A Linear Formulation for Power System State Estimation including RTU and PMU Measurements,” IEEE PES Innovative Smart Grid Technologies Europe Conference, 2019.